UNIVERSITY OF PANNONIA

System supervision and abnormality detection through multivariate statistical methods

by

Bálint Levente Tarcsay

DOI:10.18136/PE.2024.900

A thesis submitted in fulfillment for the
degree of Doctor of Philosophy

in the
Chemical Engineering and Material Sciences Doctoral School

August 2024

Kivonat

A disszertáció a hibafelderítés és elkülönítés korszerű technikáival foglalkozik, elsősorban az adatalapú, többváltozós statisztikai folyamatfelügyeleti módszerekre összpontosítva. Megoldásokat javasolok a hibafelismerési keretrendszer aktuális kérdéseinek megválaszolására, beleértve a folyamatkockázat hibafelismerésbe történő beépítését és a hibafelismerési módszerek fejlesztését elosztott paraméterű rendszerek esetében.

Az ipari fejlődés fontos része a technológiák biztonságos és pénzügyileg előnyös működésének biztosítása, ami megbízható hibaelemzési és riasztási rendszerek létrehozásával elősegíthető. A dolgok internetének (IoT) korában a hibafelismerési rendszerek többnyire a posteriori folyamatmodelleket vagy adat alapú technikákat használnak a rendellenességek felismerésére. A hibafelismerési rendszereknek úgy kell működniük, hogy lehetővé tegyék a nem biztonságos, a folyamatnak nem megfelelő üzemállapotok azonnali észlelését, ugyanakkor különbséget kell tudniuk tenni a kisebb mértékű hibák, az adatokban lévő zaj és zavarások között, hogy ne terheljék túl a rendszereket kezelő személyzetet felesleges riasztásokkal. Doktori kutatásom során vizsgáltam a hibaelemzés statisztikai eljárásokon alapuló módszereit, nyers folyamatadatok felhasználásával. Az említett módszerek alkalmazhatóságának vizsgálata különböző esettanulmányok keretében történt, amelyek a hibafelismerés és azonosítás szakirodalmából ismert összehasonlítási alapként szolgáló mintapéldákon, valamint valós műveleti egységeken mutatják be a javasolt módszereket.

Míg számos központi jellegű kihívást a hibák felismerésének, elkülönítésének és helyreállításának módszertanával kapcsolatban már megoldottak ezzel párhuzamosan rengeteg új kutatási terület nyílt meg. A fejlesztések iránya áthelyeződött a különböző hagyományos megközelítéseket ötvöző új hibafelderítési technikák kifejlesztésére, a számításigényes és széles körben alkalmazható modellek felhasználására elosztott paraméterű rendszerek felügyeletére, illetve a kockázatelemzés módszereinek beépítésére a hibafelderítési folyamatba a felesleges riasztások számának csökkentése céljából. Disszertációm során célom volt különböző irodalmi módszerek és a személyesen kidolgozott algoritmusok kombinálása révén egy átfogó módszertan létrehozása, a hibafelismerés jelen kihívásainak részleges megoldása céljából.

Abstract

This dissertation revolves around addressing the current state-of-the-art techniques for fault detection (FD) and isolation (FDI) mainly focusing on data-based, multivariate statistical process monitoring methods. New techniques were proposed to answer current issues in the FD framework including the integration of process risk into FD and FD for distributed parameter systems (DPS).

A vital part of technological advancement is ensuring the safe and financially beneficial operation of industrial technologies that can be achieved by creating reliable fault diagnosis and alarm systems. In the age of the internet of things (IoT) FD systems mostly utilize a posteriori process models or process data-based schemes for abnormality detection. FD systems must work in a manner which enables prompt detection of unsafe, not process conformant operating states but must also be sensitively tuned to distinguish between minor faults and noise in the data as to not overwhelm operators with alarm floods. During my doctorate research project I have explored the possible methods for fault diagnostics based on statistical techniques using raw process data. The application of said methods will be conducted in frame of various case studies featuring known benchmark problems of the fault detection and isolation literature as well as real life operation units. While many critical problems relating to the fault detection, isolation and recovery methodology have already been tackled a great amount of new research ground became open for exploration. The development of novel fault detection techniques which combine different traditional approaches, the applicability of computationally more expensive models for supervision of distributed parameter processes, the integration of risk analysis into the fault detection process are all intriguing and critical questions for the future of industrial process safety.

My goal is to combine various literary methods and personally developed approaches and create an overarching methodology for the sensitive and robust FD and FDI methodologies for various dynamic industrial processes which may face multiple technological abnormalities.

Abstrakt

In dieser Dissertation geht es um den aktuellen Stand der Technik der Fehlererkennung und isolierung durch datenbasierten, multivariaten statistischen Prozessüberwachungsmethoden. Es wurden neue Techniken vorgeschlagen, um aktuelle Fragen im Rahmen der Fehlererkennung zu beantworten, einschließlich der Integration des Prozessrisikos in die Fehlererkennung und die Fehlererkennung für verteilte Parametersysteme.

Ein wesentlicher Bestandteil des technologischen Fortschritts ist die Gewährleistung eines sicheren und finanziell vorteilhaften Betriebs von Industrietechnologien, was durch die Schaffung zuverlässiger Fehlerdiagnose- und Alarmsysteme erreicht werden kann. Im Zeitalter des Internets der Dinge (IoT) nutzen Fehlererkennungs Systeme meist a posteriori Prozessmodelle oder prozessdatenbasierte Schemata zur Anomalienerkennung. Fehlererkennungs Systeme müssen so arbeiten, dass sie unsichere, nicht prozesskonforme Betriebszustände rechtzeitig erkennen, aber auch sensibel zwischen kleinen Fehlern und Rauschen in den Daten unterscheiden können, um die Bediener nicht mit einer Alarmflut zu überfordern. Im Rahmen meiner Dissertation habe ich mögliche Methoden zur Fehlerdiagnose auf der Basis statistischer Verfahren unter Verwendung von Prozessrohdaten untersucht. Die Anwendung dieser Methoden wird durch verschiedener Fallstudien mit bekannten Benchmark-Problemen aus der Literatur zur Fehlererkennung und Isolierung sowie mit realen Betriebseinheiten durchgeführt.

Während viele kritische Probleme der Fehlererkennung und Isolierung bereits in Angriff genommen wurden wurde eine große Anzahl neuer Forschungsgebiete erschlossen. Die Entwicklung von neuartiger Fehlererkennungsverfahren, die verschiedene traditionelle Ansätze kombinieren, die Anwendbarkeit rechenintensiverer Modelle für die Überwachung von Prozessen mit verteilten Parametern und die Integration der Risikoanalyse in den Fehlererkennungsprozess sind allesamt faszinierende und kritische Fragen für die Zukunft der industriellen Prozesssicherheit. Mein Ziel ist es, verschiedene literarische Methoden und selbst entwickelte Algorithmen zu kombinieren und eine übergreifende Methodik für die empfindlichen und robusten Fehlererkennung und Isolations Methoden zu schaffen für verschiedene dynamische industrielle Prozesse, die mit mehreren technologischen Anomalien konfrontiert sein könnten.

Acknowledgements

Here I would like to acknowledge the help of all those without whom I would not have succeeded in finishing this dissertation.

First of all I wish to express my gratitude towards the members of the Department of Process Engineering for their continued support and valuable input during my doctorate journey.

I would like to especially thank my two supervisors, dr. Ágnes Bárkányi and dr. Sándor Németh for their guidance during my doctorate years. A special thanks goes to dr. Tibor Chován who supported me as my supervisor for the first two years and after his retirement remained a constant source of inspiration and advice during my final years of study.

I would also like to offer my gratitude and express my love and thankfulness to my family and friends who supported me on this journey. A special thanks goes to my aunt for giving me the most simple and relevant advice for my life and for my PhD journey.

" In life you won't make it anywhere without perseverance."

Contents

List of Figures

List of Tables

Abbreviations

AEM	Abnormal Event Management
AI	Artificial Intelligence
ANN	Artificial Neural Network
BN	Bayesian Network
CFD	Computational Fluid Dynamics
CM	Compartment Model
CPF	Conditional Probability Function
CPT	Conditional Probability Table
CSTR	Continuous Stirred Reactor
DAG	Directed Acyclic Graph
DFMEA	Design Failure Mode and Effect Analysis
DIST	Distributor
DKPCA	Dynamic Kernel Principal Component Analysis
DKPLS	Dynamic Kernel Partial Least Squares
DPCA	Dynamic Principal Component Analysis
DPS	Distributed Parameter System
DRA	Dynamic Risk Assessment
EC	Elementary Cell
ET	Event Tree
ETA	Event Tree Analysis
EVD	Eigenvalue Decomposition
FAR	False Alarm Rate
FD	Fault Detection
FDI	Fault Detection and Isolation
FDIR	Fault Detection, Isolation and Recovery

FFMEA	Functional Failure Mode and Effect Analysis
FMEA	Failure Mode and Effect Analysis
FMECA	Failure Mode, Effect and Criticality Analysis
FN	False Negative rate
FP	False Positive rate
FT	Fault Tree
FTA	Fault Tree Analysis
GMA	Geometric Moving Average
GMM	Gaussian Mixture Model
HAZOP	Hazard and Operability Study
IoT	Internet of Things
KPCA	Kernel Principal Component Analysis
LHHW	Langmuir-Hinshelwood-Hougen-Watson
LOHC	Liquid Organic Hydrogen Carrier
MAR	Missed Alarm Rate
MB	Methylene blue ($C_{16}H_{18}ClN_3S$)
MCH	Metylcyclohexane
MIX	Mixer
MLE	Maximum Likelihood Estimation
MLP	Multilayer Perceptron
MSPCA	Multiscale Principal Component Analysis
MSPM	Multivariate Statistical Process Monitoring
NIPALS	Nonlinear Iterative Partial Least Squares
ODE	Ordinary Differential Equation
PC	Principal Component
PCA	Principal Component Analysis
PDE	Partial Differential Equation
PDF	Probability Density Function
PFMEA	Product Failure Mode and Effect Analysis
PFR	Plug Flow Reactor
PLS	Partial Least Squares
RDP	Ramer-Douglas-Peucker algorithm
Re	Reynolds Number

RPN	Risk Priority Number
RTD	Residence Time Distribution
SDG	Signed Digraph
SFMEA	Software FMEA
SPE	Squared Prediction Error
SPM	Statistical Process Monitoring
SVD	Singular Value Decomposition
TIS	Tanks in Series
TN	True Negative rate
TOL	Toluene
TP	True Positive rate

Symbols

A	parameter matrix of state-space model (state-state), equality constraint in chapter 5
a	number of retained principal components, fuzzy membership function parameter in chapter 5
B	parameter matrix of state-space model (input-state)
b	fuzzy membership function parameter
C	parameter matrix of state-space model (state-output)
$C(t)$	concentration response function $[mol\ m^{-3}]$
c	concentration $[mol\ m^{-3}]$
c_p	heat capacity $[J\ kg^{-1}K^{-1}]$
D	parameter matrix of state-space model (input-output)
D_i	diffusion coefficient of component i, $[m^2\ s^{-1}]$
d	distance metric
d_α	deviate score belonging to confidence level α
E	prediction error matrix
$E(t)$	residence time density function
F	F-distribution
$\mathbf{F}$	force vector $[N]$
$F(t)$	residence time distribution function
F_1	classifier harmonic precision and recall score
F_i	reduced reference fault trajectories
f_i	i-th fault signal
G_F	parameter matrix of state-space model accounting for faults (fault-state)
g	fuzzy discriminant function
H	set of possible couplings between end points of curves
$H(t)$	Heaviside function
H_F	parameter matrix of state-space model accounting for faults (fault-output)

h_i	polynomial coefficient of Q statistic, $i = 1,..,3$
I	unity matrix
$\mathbf{I}$	momentum vector $[kg\ ms^{-1}]$
k	residual number
L	Luenberger observer gain matrix
LI	linkage between curves
l	lag number
l_i	liquid level $[m]$, $i = 1,...,3$
M	system input transfer function
M_F	system fault transfer function
MAF_1	macroaveraged F_1 score
m	number of process input features
$\dot{m}$	mass flow $[kg\ s^{-1}]$
N	total object number
n	number of samples in a data set
O	order of complexity for algorithms
o	number of process states
P	eigenvector matrix
p	number of process output features
pa	set of parents of a node
Q	squared prediction error
q	number of additive process faults
q_i	volumetric flow rate $[m^3\ s^{-1}]$, $i = 1,..,3$
R_c	classifier recall score for class c
R_i	reaction source term for the i-th component
r	number of linear relationships within dataset
rr	reaction rate $[(m^3 mol^{-1})^n \cdot s^{-1}]$
S	arbitrary set of objects
s	total number of process features
t	time variable $[s]$
T	principal component matrix except in chapter 4 where it is temperature $[K]$
T^2	Hotelling statistic
Tr	trajectory

u	system input signal
V, W	residual generator matrix
v	velocity $[m\ s^{-1}]$
w	controller setpoint signal
X	process data matrix
$\tilde{X}$	centered process data matrix
x	system state signal, longitudinal coordinate $[m]$ in chapter 5
$\mathbf{x}$	system feature vectore
y	system output signal, lateral coordinate $[m]$ in chapter 5
$\hat{y}$	predicted system output signal
Z	covariance matrix
α	confidence level in all chapters except chapter 5, where it is distribution rate
β	vector direction
Γ	number of linguistic labels
γ	vector magnitude
Δ_H	reaction heat $[J\ mol^{-1}]$
δ_{dF}	discrete Fréchet distance
$\delta(t)$	Dirac delta function
ϵ	relative mass balance error in chpater 5, error margin for RPD algorithm in chapter 3
η	kinematic viscosity $[m^2\ s^{-1}]$
θ	variance to be retained
Λ	matrix of eigenvalues
λ_i	i-th eigenvalue of matrix
μ	residual signal
Ξ	set of fuzzy rules
π	number of rules
ρ	material density $[kg\ m^{-3}]$
σ	set of points of curves
Υ	distribution rate
Φ	membership function
ϕ	time shift operator
ψ	eigenvector

Chapter 1

Introduction

In this dissertation the author will be focusing on creating a thorough overview of industrially applicable fault detection (FD) and isolation (FDI) techniques, with special focus on multivariate statistical process monitoring methods and tackling new scientific challenges presented within the FD literature. The dissertation contains three main thesis points which address contemporary challenges in the FD framework, these are:

- Development of novel and robust data-based FDI methods for nonlinear dynamic systems
- Inclusion of risk estimation and risk analysis into FD to reduce the number of superfluous alarms
- Addressing the FD problem in distributed parameter systems (DPS) using semi-mechanistic models

Parallel to the continuous increase in quality and quantity expectations of clientele in the last few decades, industrial systems have dramatically increased in complexity to comply with the ever rising demands of the market. This surge in technological intricacy however results in more possibilities for malfunctions and faults to arise. Due to the ever-increasing severity and probability of arising process faults, Abnormal Event Management (AEM) has gained increasing research interest and focus in recent years. AEM encompasses the strategy for timely detection of faults, the identification of possible causes and the execution of appropriate actions to return the process to a normal operating state [3].

A practical realization of AEM is the Fault Detection, Isolation and Recovery (FDIR) framework which focuses on the methods for detection of process abnormalities, pinpointing their origins and taking the appropriate measures to resolve certain problems. Generally, however, the scope of algorithms focused on assisting operators with resolving process abnormalities only focus on fault detection (FD) or fault detection and isolation (FDI). Should a process abnormality be present, the alarm system would notify the operating personnel through visual, auditory, etc. signals. Then the operators could proceed with the tasks of fault isolation and recovery. However, nowadays total automatization of FDIR became the goal with implementation of systems capable of isolating faults, tracking fault spreading patterns and enacting appropriate responses for recovery. This surging research interest can be seen from the change in the annual number of scientific publications related to the topic. This is showcased in Fig. 1.1 which is created from data extracted from the Web of Science using the search keyword "Fault Detection and Isolation" [1].

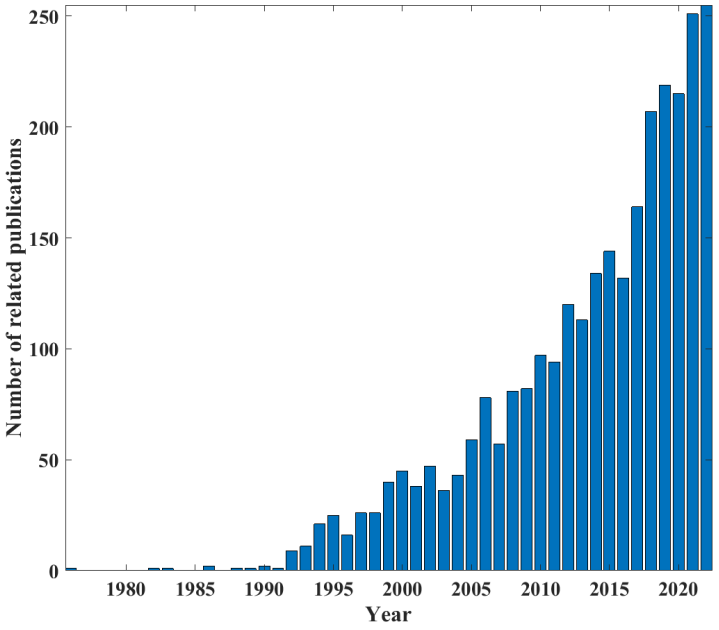

FIGURE 1.1: Number of annual publications related to "Fault Detection and Isolation" over the years [1]

However, despite the intense research interest the practical application of properly working, data or model-based FD and FDI solutions in industrial applications is still scarce. Fig. 1.2 shows the change of published patents related to the keywords "Fault Detection and Isolation" and "Chemical Engineering" between 1990 and 2020 extracted from Google Patents [2].

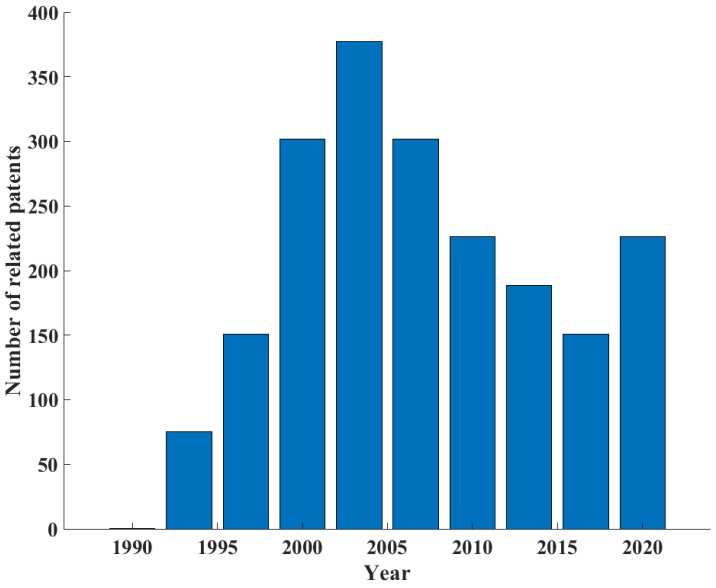

FIGURE 1.2: Number of patents related to "Fault Detection and Isolation" over the years [2]

It can be noted that the number of patents does not follow the steadily increasing trend of scientific publications. It is also important to mention that most of these patents originate from universities, with the University of California and the Massachusetts Institute of Technology being the main contributors of the showcased patent numbers [2]. This points to the fact that further research into FD and FDI with specific focus on the development of methods for practical applications is a field yet to be properly explored.

Taking just the traditional task of FD into account, it is still obvious that the design and implementation of a properly functioning framework is a crucial step in ensuring the functionality of any safety system and therefore a great research focus. This is especially prominent with the increasing focus on process safety and environmental protection, which aims to eliminate industrial accidents such as the Bhopal accident [4] or the Texas oil refinery explosion [5]. Sadly, despite the great advancements in the safety sector, the number of industrial accidents is still significant up until the 2010s [6]. The most important step to further enhance process safety is to utilize the supervision capabilities of modern distributed control systems (DCS) and the concept of IoT to establish and develop reliable, real-time, automated methods of fault detection and isolation [7]. This constant research interest as well as the chemical industry's demand for increasing process safety motivates the focus on fault detection and isolation in this dissertation.

The dissertation opens with a review of modern research trends in FD and FDI, categorization of existing techniques and critical evaluation and comparison of said approaches. Thereafter, the thesis points are explored sequentially, with a clear review of the current state-of-art for each research area. The author analyzes the bottlenecks within the currently existing techniques and proposes his own approaches to answer some arising issues. The main idea and mathematical background of the techniques are explored, and the applicability of the methods is showcased through numerical case studies using both benchmark problems of the FD literature and data collected from real-life industrial systems. In each case, a critical comparison between the methods found within the FD literature and the proposed method is performed to provide a realistic view of the contribution.

Chapter 2

Literature review

In the FD and FDI literature, a process fault is defined as a departure from an acceptable range of the expected value of a certain process variable. The underlying causes of this abnormality, are called the basic events or the root causes. Possible fault types and their root causes are shown in Fig. 2.1 where $u \in \mathbf{R}^{n \times m}$ is the signal of m observed process input variables, $y \in \mathbf{R}^{n \times p}$ is the signal of p observed process output variables and $w \in \mathbf{R}^{n \times p}$ is the set point signal of the output variables for n observed samples.

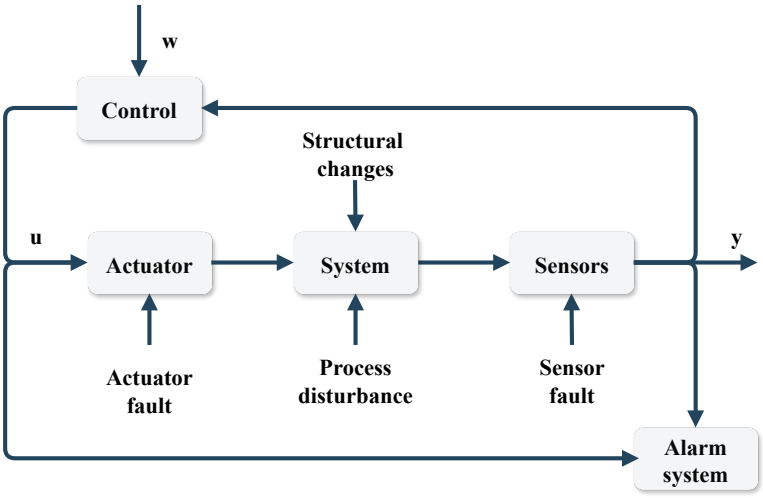

FIGURE 2.1: Fault types and their root causes [3]

Faults in industrial processes can generally be categorized into two types, which are additive and multiplicative faults, respectively. The distinction between additive or multiplicative behavior is always defined by the system which is being supervised, and often arbitrary [3].

Additive faults true to their name represent faults that cause additional inputs into the system (input or output sensor and actuator signal drift, plant faults for example leaking pipes that cause less volumetric flow to enter a reactor than expected, etc.) [3]. Multiplicative faults on the other hand stem from sources that cause the behavior of the system itself to change (structural changes in the system including fouling in heat exchangers, catalyst deactivation, etc.) and thus alter the behavior and dynamics of the system. Besides faults disturbances can also be present (bias, modeling error, etc.) which display the same behavior as faults (additive or multiplicative tendency) but from the perspective of fault detection we wish to minimize their influence because they hold no safety or economic consequences and lead to false alarms.

In order for an FD system to recognize the presence of any type of fault, a surplus of information is required. This surplus information for example can come in the form of a reference mathematical model which describes the process behavior under normal operating conditions. Through the use of the reference model, the expected system behavior can be predicted and compared to the real system behavior. The discrepancies between the two are referred to as residual signals [3]. Such residual signals can also be generated and subsequently analyzed through data-based methods. Statistical techniques, for example, may be used to provide an expected value and standard deviation for process variables under normal operating conditions. Deviations of individual samples from the expected values of normal historic values can be used similarly in a residual fashion to indicate the presence of abnormal process events [8].

The obtained residuals can then be compared to a certain standard to evaluate whether the difference is significant enough to actually give out an alarm signal. This can be most simply achieved by comparing the magnitude of the residual signal to a predefined error threshold, which takes for example process noise into account [9].

During the design phase of the safety system, choosing the proper FD strategy based on the complexity of the system, available data, etc. is vital to ensure timely fault detection and robustness [3]. After establishing an FD strategy for a given system, optimization of the alarm threshold takes priority. The necessary alarm variables have to be selected first, and alarm thresholds need to be defined based on safety, economic and utility viewpoints. Simultaneously the minimization of false alarms or FAR (an alarm when no actual fault is present),

nuisance alarms (alarms which are redundant since another alarms already indicated a process fault) and missed alarms or MAR also has to be taken into consideration when tuning FD thresholds. The first two can lead to alarm floods that overwhelm operators, and the latter can result in potentially hazardous situations going unnoticed. In case of reliable fault detection, fault isolation is the next step, which is the analysis of the detected faults and the classification of the recognized faults to pinpoint their root causes.

Selecting the applied mathematical approach for the supervision of any given technological system is crucial for proper fault detection. The type of mathematical method employed determines many of the FD system's most important qualities such as fault sensitivity, reaction speed and robustness. Fault sensitivity being the systems' ability to detect faults of a reasonably small margin. Reaction speed demands that the FD system should detect any abnormalities with a reasonably small time delay after the occurrence of said abnormality. Lastly, robustness is arguably the most important of the three, which is the systems' ability to work reliably and with minimal FAR even in face of measurement noise, disturbances, and modeling errors [10].

Three distinct mathematical approaches for FD and FDI can be discerned based on the type of knowledge used to perform the detection. These are the model-based methods which utilize quantitative knowledge [3], qualitative knowledge [9] or knowledge extracted from process history [8] as shown in Fig. 2.2.

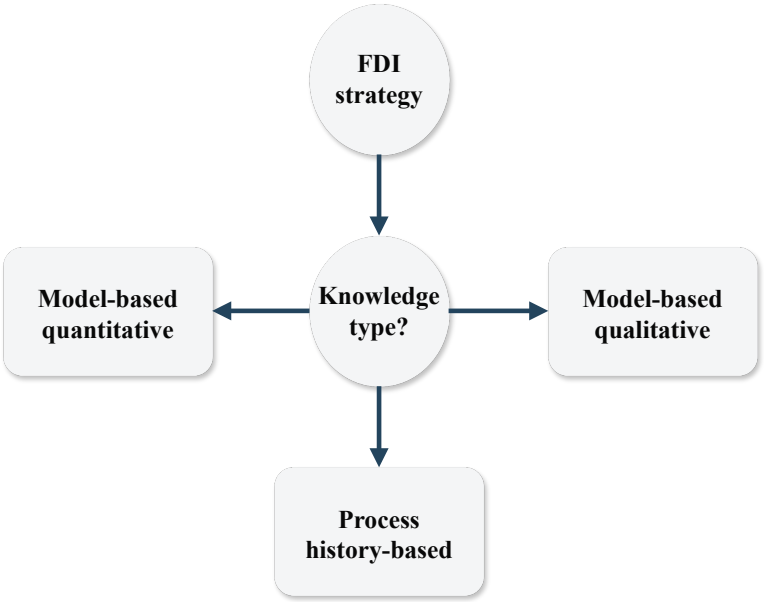

FIGURE 2.2: Different types of knowledge used to establish FD and FDI methods [3]

The first type is called the quantitative model-based approach. During this approach, knowledge of the system comes in the form of mathematical functions which describe the relationship between the input and output of the object in question. Among this group we can distinguish models which use a priori knowledge, which is based on physical laws that govern the system, or a posteriori models which use empirical relationships to determine the relationship between the system inputs and outputs. A priori models have the advantage of extreme robustness but require large amounts of knowledge about the system and thorough modeling, which in case of complex objects can not always be achieved. In contrast, a posteriori models (state-space models, input-output models, etc.) require relatively little knowledge about the physical workings of the system and modeling effort but can be lacking in robustness [10].

Qualitative models, in contrast, utilize qualitative functions and expert knowledge to establish relationships within the process [9].

Lastly, process history-based models mostly do not utilize any prior knowledge about the system but use large amounts of historical process data and transform it into a posteriori knowledge by either statistical or non-statistical inference methods [8].

The most common techniques utilized by the different knowledge-based approaches are displayed hierarchically in Fig. 2.3.

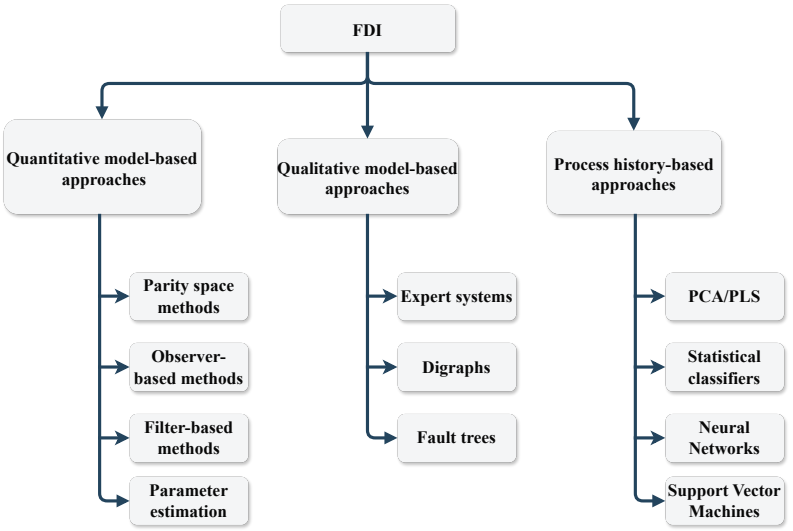

FIGURE 2.3: FDI approaches and their most commonly applied techniques [3]

Comparatively, however, while the modeling philosophies differ and different types of knowledge are utilized in each case the general steps of data acquisition and utilization are similar. The diagnostic pattern of each system follows a route between transformation spaces that convert different types of data into a basis for decision-making, which is shown in Fig. 2.4.

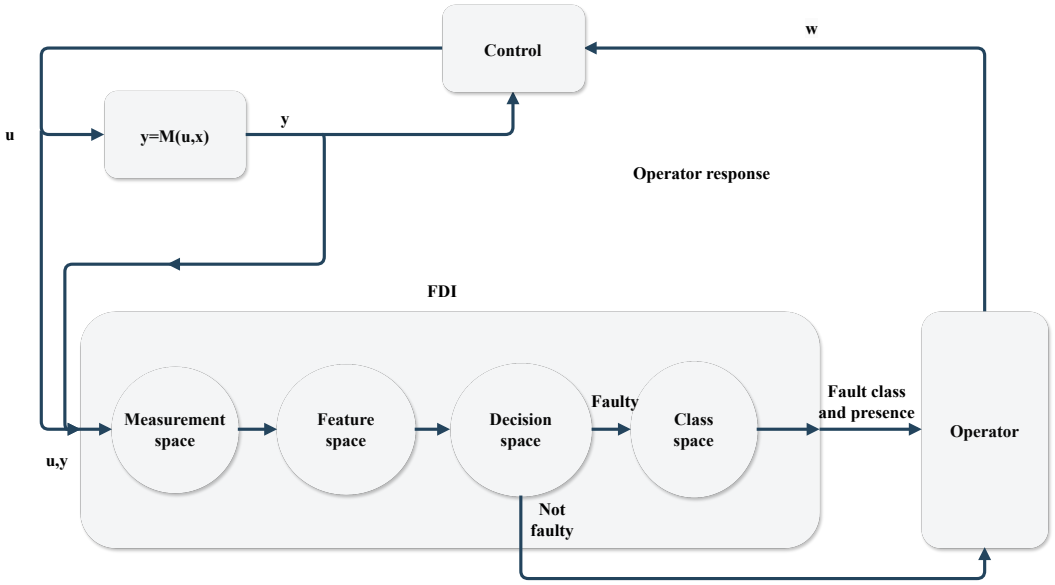

FIGURE 2.4: General scheme of FDI [9]

First the measurement space is entered where through the usage of sensors process data about the operation is acquired. This data is used as the input of the diagnostic system (u, y) as shown in Fig. 2.4. This stage is the data acquisition portion of the diagnostic system [3].

The measured values are then transformed onto the feature space, where they become features of the system's operating conditions by using process knowledge to evaluate their values (comparison to the mathematical model or process statistics). The transformation between the measurement and feature spaces can be aided by either feature selection or feature extraction techniques [3]. Next the variables of the feature space are transformed onto the decision space usually utilizing some objective function, this objective function is compared to a given threshold or other type of discriminant function (alarm generation). This is the FD portion of the FDI process. Finally, the variables of the decision space (abnormal or standard operation) are used to generate the variables of the class space. The class space separates the various fault types into categories, depending on which unit of the system became faulty, what caused the malfunction, etc. The transformation from decision to class space can

be achieved by pattern recognition algorithms, template matching or symbolic reasoning in most cases, this encompasses the isolation step of FDI.

2.1 Quantitative model-based fault detection and isolation

In quantitative model-based methods, fault detection and isolation are usually performed using the same algorithm and are inherently integrated. The mathematical model will serve as a reference to the expected behavior of the observed object under certain operating conditions. If no faults and noise are present, then the real system's response to the same input under matching operating conditions should be identical to the model's responses. Differences between the expected and actual behavior are called residuals, the surplus information of the model is known as analytical redundancy. The general scheme of the FD process using quantitative model-based techniques in industrial systems is shown in Fig. 2.5.

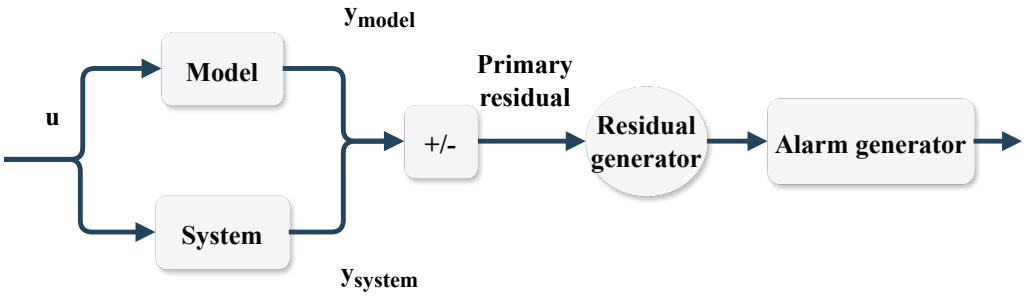

FIGURE 2.5: Analytical redundancy through process models, residual generation scheme [3]

As mentioned previously, quantitative models are based on mathematical functions employed to estimate relationships between input and output variables of a system. While many modeling approaches meet this expectation in fault diagnosis, mostly black-box (a posteriori) including general input-output and state-space models have been employed. Other types of models including first principle (a priori) and frequency response models have also been considered. The problem with the latter models, especially first principle models (based on mass and energy equilibrium calculations according to physical laws, state equations in chemical engineering practice) is the difficulty in employing them in on-line fault diagnosis due to extensive calculation load and the amount of knowledge needed to develop said models especially for complex systems [10].

In chemical engineering practice traditional black-box modeling used for fault diagnosis assumes linearized plant behavior around a certain operating point and works mostly using discrete models due to the discrete nature of sampled process data (continuous models can also be developed based on the discrete models) [11].

The model-based methods for fault detection have garnered increased interest over the recent decades with the increasing strength of calculation power of computers and the evolution of control techniques. The three general approaches for model-based FD are as follows (Fig. 2.3):

- Parity space methods
- Observer-based methods
- Parameter estimation methods

In the following a general outline of the parity space and observer-based techniques, their key ideas, current state-of-art and current research issues are addressed. Parameter estimation while noted to be a distinct approach for FDI is not often employed and its use is mostly reserved for detecting multiplicative faults in quasi-linear systems.

2.1.1 Parity space methods

Parity space techniques are mostly employed for actuator and sensor fault detection problems, where additive faults are considered. The relations between actuator inputs and sensor outputs for normal operating conditions are defined through the process model [12].

The general idea of the parity space FD can be defined as follows. Let $\mathbf{y} \in \mathbf{R}^{n\times p}$ be the measured output values of the real observed physical system and $\hat{\mathbf{y}} \in \mathbf{R}^{n\times p}$ be the expected system outputs for n observations calculated from the system inputs $\mathbf{u} \in \mathbf{R}^{n\times m}$ and the mathematical model $\mathbf{M}$ of the process. The primary residual is the difference between the measured and calculated values, which in most cases is not enough to exactly detect anomalies. The residual vector ($\mu \in \mathbf{R}^{n\times k}$) is obtained through the linear transformation ($\mathbf{V} \in \mathbf{R}^{k\times p}$) of the primary residuals as seen in Eq. 2.1.

$$\mu = \mathbf{V}(\mathbf{y} - \hat{\mathbf{y}}) \tag{2.1}$$

The choice of **V**, also known as the residual generator, must satisfy a number of conditions:

- **V** must satisfy $\mathbf{r} = \mathbf{V}(\mathbf{y} - \hat{\mathbf{y}}) = \mathbf{0}$ if there is no fault present, meaning that residuals should only respond to process faults
- **V** must result in a set of residuals which show particular patterns for the presence of different process faults, so faults may be distinguishable and isolation may take place
- **V** must be chosen such that the residual values be independent of the current state of the system and preferably be robust towards process noise and modeling errors

The method was originally heralded by the works of Chow and Willsky, who used linear state-space models to develop a parity space FDI scheme while observing the process over a finite time window [13]. Inspired by their work, many researchers have worked with the parity space approach and showcased its use for FDI, the most notable of the 1990s and early 2000s being Gertler and Ding [10, 11].

The general form of the discrete time state-space model assumed by Chow and Wilsky for the derivation of the method can be seen in Eq. 2.2 with state vector $\mathbf{x} \in \mathbf{R}^{n \times o}$ and parameter matrices $\mathbf{A} \in \mathbf{R}^{o \times o}$, $\mathbf{B} \in \mathbf{R}^{o \times m}$, $\mathbf{C} \in \mathbf{R}^{p \times o}$ where $t = 2, ..., n$.

$$\begin{aligned} \mathbf{x}(t) &= \mathbf{A}\mathbf{x}(t-1) + \mathbf{B}\mathbf{u}(t-1) \\ \hat{\mathbf{y}}(t) &= \mathbf{C}\mathbf{x}(t) \end{aligned} \tag{2.2}$$

In order to provide a compact way for formulating the relationships between current and past states and outputs, the shift operator ϕ is introduced which is indicative of the order of time delay between current and previous values. Rewriting Eq. 2.2 with the use of the shift operator and expressing the current state analytically through the current input, we obtain Eq. 2.3 and Eq. 2.4 where $\mathbf{I} \in \mathbf{R}^{o \times o}$ is a unity matrix.

$$\begin{aligned} \mathbf{x}(t) &= \phi_1 \mathbf{A}\mathbf{x}(t) + \phi_1 \mathbf{B}\mathbf{u}(t) \\ \hat{\mathbf{y}}(t) &= \mathbf{C}\mathbf{x}(t) \end{aligned} \tag{2.3}$$

$$\mathbf{x}(t) = \left(\mathbf{I} - \phi_1 \mathbf{A}\right)^{-1} \phi_1 \mathbf{B}\mathbf{u}(t) \tag{2.4}$$

Using Eq. 2.4 we can express an analytical form for the model, as a transfer function which provides the expected system output as a function of a defined system input sequence. This is shown in Eq. 2.5.

$$\hat{\mathbf{y}}(t) = \mathbf{C}\left(\mathbf{I} - \phi_1 \mathbf{A}\right)^{-1} \phi_1 \mathbf{B}\mathbf{u}(t) = \mathbf{M}(\phi)\mathbf{u}(t) \tag{2.5}$$

The proposed equations describe state-space and input-output models for fault free cases. In cases where faults are present, those are modelled as additional terms in the equations. Besides faults disturbances can also be present (bias, modeling error, etc.) which display the same behavior as faults (additive or multiplicative tendency) but from the perspective of fault detection we wish to minimize their influence because they hold no safety or economic consequences and lead to false alarms. In case of additive faults, their representation in the previously shown generalized formulation can be expressed by Eq. 2.6, where $\mathbf{M_F}(\phi)$ is the transfer function of possible fault signals and $\mathbf{f} \in \mathbf{R}^{n \times q}$ is the vector of q distinct additive faults considered in the system.

$$\hat{\mathbf{y}}(t) = \mathbf{M}(\phi)\mathbf{u}(t) + \mathbf{M_F}(\phi)\mathbf{f}(t) \tag{2.6}$$

It follows naturally that in fault free scenarios, the calculated and observed system output should be equal if no modeling errors and disturbances are present. Thus, the residual generator equations shown in Eq. 2.1 can be written in the form seen in Eq. 2.7.

$$\mu(t) = \mathbf{V}\left(\mathbf{y}(t) - \hat{\mathbf{y}}(t)\right) = \mathbf{V}\mathbf{M_F}(\phi)\mathbf{f}(t) \tag{2.7}$$

This shows that the residual generator $\mathbf{V}$ simply applies a linear transform to the system's responses of the individual additive fault signals. Designing the residual generator as previously noted means creating the proper parameter matrix $\mathbf{V}$ to evaluate the effect of process abnormalities and maximize the possibility for decoupling different fault types and noise. This can be achieved by creating so-called enhanced residuals. Enhanced residuals carry within them a pattern characteristic of the type and origin of the fault that created them, therefore the residual pattern enables fault isolation.

Enhancement has two distinct approaches and analytical solutions for residual generator design. The first subset creates structured residuals, this method produces different residual patterns, all of which respond to different fault types within the process and are insensitive to all other process abnormalities. This way, the residual pattern can be used to isolate the type of fault present. The rules for different residual sets are usually obtained by taking the separate elements of the residual vector (corresponding to the observed process variables) and evaluating them based on cluster analysis, Euclidean distance, etc. and using simple threshold functions to make decisions based on the values of the variables [10]. Comparison with a database for error codes can lead to clear fault isolation. The codes will of course all be dependent on the residual generator matrix employed. Thus, the matrix $\mathbf{V}$ must be chosen in a manner that allows for the generation of distinguishable and non-zero binary error codes for all fault cases [14].

The other employed technique is the generation of directional residuals. Directional residuals are designed to be vectors which follow a fault specific propagation direction ($\beta \in \mathbf{R}^{1\times k}$) and magnitude ($\gamma$) in the residual vector space. This condition for the residual response to a specific j-th fault, such that, $j = 1, ..., q$ can thus be expressed in the form of Eq. 2.8.

$$\mu(t|\mathbf{f}_j) = \beta_j \gamma_j \mathbf{f}_j(t) = \mathbf{V}_j \mathbf{S}_\mathbf{F}(\phi)\mathbf{f}_j(t) \tag{2.8}$$

Special cases are residual sets where each residual is only responsive to a specific type of fault, these are called basis residuals and are in nature both structured and directional [10].

While the original approach was favorable, it had certain limitations. The analytic solution for the design of an optimal residual generator was not always feasible depending on the number of inputs, outputs, fault signals and system states. Feasibility conditions for different residual generation patterns depend on the observability of system outputs, as well as the nature of the fault transfer function. Additionally, as the derivation shows, the method was developed for systems which could be accurately described by linear time-invariant models [14]. Modern research trends aim to answer these issues by providing different approaches for residual vector generation optimization and extending the methods to nonlinear systems.

Nonlinearity in parity space FDI schemes can be resolved in three main ways which include the direct generation of nonlinear parity relations in a manner similar to the previously

shown derivation, linearization of system behavior about its current state [15] or model approximation techniques. The second approach offers generally less robustness and weaker performance compared to directly derived nonlinear parity relations or parity relations based on accurate model approximations, but as a trade off their derivation and application is fairly simple and straightforward.

Direct analytical derivation of nonlinear parity relations can only be conducted in special cases when the nonlinear system model is fairly simple (such as a pH neutralization model [15] or the model of a simplified fluid cell [16]). However, in more complex cases it may be entirely infeasible to achieve these relations because of observability issues or due to lack of smoothness in the state or output functions [17].

For more complex cases specialized techniques have been developed for different classes of nonlinear models and their parity relation derivation problems which often include model approximation techniques. A popular approach includes the segmentation of system behavior into particular zones and approximation of the original system using a set of these hybrid systems which correspond to different operation regimes or modes of the original [18]. The switching between these modes can be inherently well described by fuzzy logic, which is why the use of Takagi-Sugeno models [19] to describe nonlinear systems with complex behavior as networks of simpler hybrid systems has become a well researched area in recent years [20]. The use of Takagi-Sugeno models to segment system behavior into local modes which exhibit linear behavior is well researched, the parity relations for local modes are easier to obtain analytically and offer robust FDI performance if properly established [20] for a wide class of nonlinear systems [21].

2.1.2 Observer-based methods

Observer-based techniques utilize filters, most commonly the Kalman filter for stochastic processes and the Luenberger observer for deterministic processes, to estimate system outputs and states based on a subset of available measurements and a known state-space model of the system [22]. While the parity space approach uses a constraint on the residual generator $\mathbf{V}$ which eliminates the system state from the FDI problem entirely and uses only input and output data observers actively estimate the current system state which is therefore implicitly included in the FDI procedure [10].

An initial guess for the system state vector is provided and iteratively the weighted output estimation error is used to update the state estimate and provide proper system characterization. In FDI, however, the focus is on observing the discrepancies between the estimated and actual output values as a means for abnormality detection similar to the parity relation technique rather than the state [12]. In case of a residual generator implementation through a Luenberger observer the state-space description of the system is used in the form of the system of equations seen in Eq. 2.9, where $\mathbf{L}$ is the Luenberger observer gain matrix which updates the state estimate based on the primary residual vector.

$$\begin{aligned} \mathbf{x}(t) &= \phi_1 \mathbf{A}\mathbf{x}(t) + \phi_1 \mathbf{B}\mathbf{u}(t) + \mathbf{L}\left(\mathbf{y}(t) - \mathbf{C}\mathbf{x}(t)\right) \\ \hat{\mathbf{y}}(t) &= \mathbf{C}\mathbf{x}(t) \end{aligned} \tag{2.9}$$

After applying the steps to generate the relationship between the input and output of the state-space model shown in Eq. 2.5 we can express the primary residual as a function of the measured input and output as seen in Eq. 2.10 and Eq. 2.11.

$$\mathbf{y}(t) - \hat{\mathbf{y}}(t) = \left[\mathbf{I} + \mathbf{C}\left(\mathbf{I}\phi_1 - \mathbf{A}\right)^{-1}\mathbf{L}\right]^{-1}\left[\mathbf{y}(t) - \mathbf{C}\left(\mathbf{I}\phi_1 - \mathbf{A}\right)\mathbf{B}\mathbf{u}(t)\right] \tag{2.10}$$

$$\mathbf{y}(t) - \hat{\mathbf{y}}(t) = \left[\mathbf{I} + \mathbf{C}\left(\mathbf{I}\phi_1 - \mathbf{A}\right)^{-1}\mathbf{L}\right]^{-1}\left[\mathbf{y}(t) - \mathbf{M}\mathbf{u}(t)\right] \tag{2.11}$$

Similarly to the parity space approach, the primary residual which is obtained from the input-output relations is subjected to a linear transformation, denoted here as $\mathbf{W} \in \mathbf{R}^{k \times p}$ for residual generation seen in Eq. 2.12.

$$\mu(t) = \mathbf{W}\left(\mathbf{y}(t) - \hat{\mathbf{y}}(t)\right) = \mathbf{W}\left(\left[\mathbf{I} + \mathbf{C}\left(\mathbf{I}\phi_1 - \mathbf{A}\right)^{-1}\mathbf{L}\right]^{-1}\left[\mathbf{y}(t) - \mathbf{M}\mathbf{u}(t)\right]\right) \tag{2.12}$$

In order to establish analytical solutions to the design problem, a linear, discrete state-space model is presented that includes the effects of additive faults which affect both the state and output variables. The general form of the expected model is seen in Eq. 2.13.

$$\begin{aligned} \mathbf{x}(t) &= \phi_1 \mathbf{A}\mathbf{x}(t) + \phi_1 \mathbf{B}\mathbf{u}(t) + \phi_1 \mathbf{G}_F \mathbf{f}(t) \\ \hat{\mathbf{y}}(t) &= \mathbf{C}\mathbf{x}(t) + \phi_1 \mathbf{H}_F \mathbf{f}(t) \end{aligned} \tag{2.13}$$

The model takes the same general fault types and matrices into consideration as the input-output relation model but complements them with the parameter matrices $\mathbf{G}_F \in \mathbf{R}^{o\times q}$ and $\mathbf{H}_F \in \mathbf{R}^{p\times q}$ to account for the influence of abnormalities on the state of the system as well. Using Eq. 2.10, 2.11 and 2.12 to express the residuals directly as functions of faults, we obtain Eq. 2.14.

$$\mu(t) = \mathbf{W}\left[\mathbf{C}\left(\mathbf{I}\phi_1 - \mathbf{A} + \mathbf{LC}\right)^{-1}(\mathbf{G}_F - \mathbf{LH}_F) + \mathbf{H}_F\right]\mathbf{f}(t) \tag{2.14}$$

The generator design involves the solution of the equation for matrices **L** and **W** such that the design specifications of the residual are met, and the observer is stable. Analytical solutions for this equation are almost never obtainable, thus plentiful of approximation methods for the solution have been devised [10].

Comparing equations Eq. 2.7 and 2.14 shows that a direct correlation can be established between the parity relation design method and the observer-based design method shown in equation Eq. 2.15 [11].

$$\mathbf{V} = \mathbf{W}\left[\mathbf{I} + \mathbf{C}\left(\mathbf{I}\phi_1 - \mathbf{A}\right)^{-1}\mathbf{L}\right]^{-1} \tag{2.15}$$

This form facilitates the design of observer-based residual generators through accomplishing the initial design by using parity relations and then using the defined parameter matrix to estimate matrices **W** and **L** [14]. Nonetheless, the implementation of residual generators, especially for industrial processes which are most often nonlinear, is still a challenge. While as mentioned earlier linearization around an operating point can be achieved but in any case where the operation becomes transient (start up, shutdown, operating point change) the applied residual generators become largely dysfunctional due to the huge shift in the system model.

The observer-based methods for fault detection have garnered increased interest over the recent decades with the increasing strength of calculation power of computers and the evolution of control techniques. Many of the improvements are centered around increasing the sensitivity or robustness of observer-based FDI techniques, especially in the face of modeling uncertainty. A notable research trend is the employment of techniques rooted in control theory to design optimal observers for FDI. The use of H_∞ techniques is especially prominent,

which can be used to design observers with increased robustness and tolerance to disturbance and noise factors [23]. Their prominent use in FDI lies in minimizing the effects of modeling errors in observer-based fault detection [24]. The cost function of the optimization usually involves the FDI sensitivity or robustness of the observer [25]. Works which utilize the H_∞ design strategy for observer-based FDI are less common in chemical engineering practice but are often applied for the supervision of automobiles [26], aircraft [27] and other mechatronic systems. Since many modeling uncertainties can be present in vehicles, increasing the robustness of fault detection for this application is vital [28].

Besides research to increase robustness and sensitivity of observer-based FDI, another major research focus lies similarly to parity space techniques in the extension of observer design for nonlinear systems [29]. Whether we observe the general Luenberger observer in Eq. 2.9 or the Kalman filter techniques both assume linear system dynamics and even then the observer design is not a trivial task due to potential stability issues [10]. As is the case with the parity space approaches general analytic solutions for designing observers for nonlinear systems of any type are not available readily, rather the research focus in the last decades lied in observing different specific classes of nonlinear systems and designing type specific observer design strategies for them [30]. The most common works involve designing observers for nonlinear systems which satisfy the Lipschitz condition [31], systems with sector bounded nonlinearities [32] and interconnected nonlinear systems [33]. However, just as previously with parity space methods it can be noted that hybrid techniques which involve qualitative methods, most commonly fuzzy logic to handle nonlinearities are often utilized for observer design [34].

2.2 Qualitative model-based fault detection and isolation

Qualitative and process history-based methods have become researched in FDI to rise up the issues of quantitative model-based techniques. The lack of an explicit a priori process model, the uncertainty of a posteriori process models and the difficulty of establishing robust and sensitive residual generators especially for nonlinear systems and generally the high level of mathematical knowledge needed to create proper residual generators all obstruct the applicability of model-based methods in real world FDI procedures. As a contrast to this qualitative and process history-based methods utilize statistical methods and expert knowledge in a framework which can be generalized to most systems without the need for high level

mathematical knowledge and with the proper adjustments and tuning can work reliably for nonlinear systems [9].

In case of qualitative model-based FDI strategies, the a priori knowledge about the behavior of the system is based not on mathematical functions but on qualitative functions which represent the different behaviors and relationships of process units. Qualitative models can be divided based on the type of knowledge used to create them into the subcategories of casual models and abstraction hierarchies. The former employs a freely chosen model structure to describe the system and its relationships, while the latter uses decomposition to obtain a structured set of subsystems which can be used to describe the behavior of the entire system [35].

From the perspective of search strategy, models utilizing topographic and symptomatic search can be differentiated. Topographic search utilizes templates of normal process operation to recursively analyze the system and detect any deviation from the prescribed behavior. Symptomatic search on the other hand is specifically concerned with identifying possible deviations and faults without the observation of the behavior of the entirety of the system [9].

The qualitative models utilized for FD and FDI can be divided into two major categories shown in Fig. 2.6 which are rule-based and qualitative physics-based methods [36].

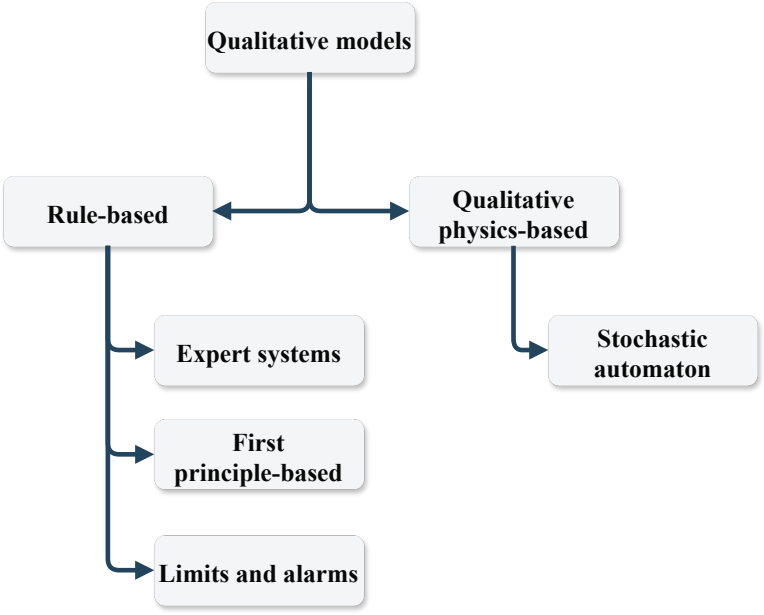

FIGURE 2.6: Common techniques of qualitative FDI found in literature [36]

Knowledge-based expert systems were among the first qualitative models to describe and supervise system behavior. By employing if-then-else rules, most commonly in a framework of abductive reasoning for various cases which could arise during the operation of the process, abnormal process behavior could be detected and possible cases for the fault source identified. The rules were established based on the knowledge of professionals who had experience working with the supervised system. The drawback of this method was that the expert system had no real knowledge of the underlying processes and thus could not handle novel problems and fault scenarios which were not previously registered in the data bank [36]. Expert systems can however not solely be based on abductive reasoning but also on inductive and default reasoning. With abductive reasoning being the generation of multiple hypotheses to explain a certain event, default reasoning being a logical process where the deducted logical explanations are constantly updated when new process knowledge becomes available and inductive reasoning being the process of generalizing or specializing certain experiences into categories and concepts [9].

One of the first examples of expert systems used for fault detection can be seen in the analysis of a ship's engine, where symbolic logic was used to create an online diagnostic system capable of recognizing process abnormalities [37]. An interaction between the operator and the process diagnostic method surveys the system and inspects variables which are outside their normal defined states. Later on, a set of rules created by a system expert is used to analyze the variables. If and then logic is employed to recognize and isolate faults with characteristic fault patterns. The structure of the fault checking often follows the logic of a fault tree, leading from the superficial symptoms to the root causes. These rules had initially been used to identify the occurring abnormalities, classify them as faults or disturbances, pinpoint their locations and showcase rules for the handling of said abnormalities.

Later on, attempts were made to organize the rules of expert systems into hierarchical structures based on the tasks in a technological process to intensify FDI potential through the organized framework. Application cases in this instance often extended to more complex chemical industrial systems and processes, such as ethylene distillation [38]

Later on, many takes have been adapted for the formulating of expert systems based on different types of available process data and knowledge. In case of abundant a priori knowledge, hierarchical decomposition was often used to analyze different systems and establish diagnostic models. A general benchmark problem for this approach in the chemical industry is

the continuous-stirred reactor (CSTR) unit, in which casual search can be used to observe the propagation of faults within the diagnostic system from the process abnormality (causality) to the fault (root cause)[39].

A novel research trend involves the combination of expert systems with various data-based techniques for systems where a priori process knowledge is scarce or entirely unavailable. Among these approaches, a significant research area is the fusion of expert systems and artificial neural networks [40]. In the primary attempts, the neural networks were used as primary filters to diagnose faulty components within technologies. The expert system subsequently diagnoses the results of the first scan and verifies the fault or directs the attention of the operators to alternative possible causes [40]. Another type of hybrid expert system algorithm supplements rule-based expert systems with stochastic knowledge to evaluate the most likely causes of process abnormalities, thus effectively transforming the expert systems into so-called belief or Bayesian networks [41].

In case of first principle-based causal models, the main employed structures for fault diagnosis consist of digraphs and fault trees. Fault trees are model structures which allow for the assessment of the impact and propagation path of faults based on the root causes by using “and”, “or”, “xor” conditions in the node graph structure to take the propagation paths for different circumstances into account. The creation of fault trees is conducted by assessing top level events, system abnormalities and hazard which are caused by root causes and expanding upon them until primary events are found which don’t have to be explained any further. The fault tree is usually dissected into cut sets. These are groups of primary events which when occur simultaneously generate a characteristic top level process abnormality. The fault tree may additionally be combined with data-based knowledge, for example information about the probability of primary events, to estimate the probability of top level hazards [9].

Digraphs are graphs with arcs between nodes which describe certain process states, in case of signed digraphs (SDG) the arcs represent the cause and effect relationships between certain process states. This representation can be used to view the relationships between the system components or states as part of a cause and effect relationship framework. In case of a faulty system, the digraphs may represent the faults as external nodes which have no inputs but provide an output which affects the other nodes (states, components, etc.) of the system. Thus, using the SDG obtained from quantitative a priori or expert knowledge of the system,

various ways of fault propagation patterns can be identified and used to trace process abnormalities back to their source [9].

There are many cases when SDGs can show much more effective FDI capabilities than other qualitative techniques, thus in recent years research focus shifted towards SDG-based FDI [42]. This is especially true for the supervision of complex systems such as electronic vehicles, fuel cells and nuclear plants. In case studies of such systems it was found after comparing the effectiveness of consistency-based qualitative fault diagnosis and first principle model-based SDGs that through the use of SDGs it was possible to eliminate inconsistent or not physically feasible patterns which often caused a high FAR and MAR when employing other techniques [42].

Various hybrid models were also proposed by transforming bond graphs into SDGs using both quantitative and qualitative knowledge of a proposed system and using it for the detection of both single and multiple faults within a chosen technological unit. Investigations like this used fuel cells as benchmark problems and the results showed that FDI became much more simplified due to the qualitative model, since a quantitative description of the system using mathematical models would have been exceedingly more complex [43].

Techniques for FDI of interconnected systems using SDGs have also been researched. For example, the online fault diagnosis and inference of nuclear power plants based on was conducted by compressing the rules of the SDG into a rule matrix, which was utilized for fault detection and diagnosis purposes. With the aid of an additional status matrix which allowed for online inference through the SDG faults and their propagation paths could be identified online [44].

Finally, qualitative physics is a methodology which derives qualitative rules to describe a certain system based on quantitative models, differential equations, etc. of said unit. This is done through the use of confluence equations, which are qualitative representations of the quantitative system model [45]. In these equations, qualitative algebra and rules can be established to describe how each system variable may change with time. Since these methods are derived from quantitative descriptions of the system behavior they are often much more robust than other qualitative methods which use expert knowledge, empirical rules, etc. [9]. Interesting extensions of these quantitative models discuss the creation of an AI capable of qualitative reasoning that could automatically handle the fault detection, isolation and response of modeled systems. Research done for FDI of wind turbines for example shows how

to utilize the knowledge obtained through qualitative physics to adjust the operating parameters of the system for different situations and enable low maintenance operations even in faulty cases to prevent total shutdowns through the use of AI [45].

While the qualitative techniques of FDI rooted solely in expert knowledge enjoyed wide research attention in the 1990s and early 2000s with the advent of the Industry 4.0 concept and the gradually increasing access to big data, process history also known as data-based methods have greatly taken over FDI research [8].

2.3 Process history-based fault detection and isolation

In contrast to the previously showcased quantitative and qualitative fault detection methods, traditional techniques based on process history operate with no specific a priori knowledge about the system. These methods utilize large amounts of previously assembled process operation data and transform it into knowledge about the investigated unit [8]. Determination of variables that hold key features regarding the process is performed through means of feature selection or feature extraction techniques. Through these techniques, quantitative or qualitative knowledge about the system can be gathered by analyzing the acquired data. Then some sort of classification is performed to separate faulty and normal process data based on the previously assembled features [8]. The most generally applied and researched methods for FD and FDI include deep learning techniques (artificial neural networks), stochastic classifiers and multivariate statistical methods. In the following subsections I will expand upon these methods, highlighting their uses, research topics and bottlenecks.

2.3.1 Neural networks

Over the last 30 years, considerable research has been provided about the uses of artificial neural networks (ANN) for the purposes of FDI. The reason for this being that ANNs are structures particularly applicable for pattern recognition, signal processing, signal classification and function approximation problems [8]. A neural network is a general mathematical paradigm whose function is based on the central nervous system of sentient beings. Various approaches for the building of such networks have been proposed over the years but despite their apparent variance these models all share the same fundamental building blocks. These

are called neurons, which are interconnected in a specific network structure. The neuron consists of two parts. The net function takes the weighted values of the input signals and an additional term. This is the input of the activation function within the neuron, which in turn determines the output of the neuron. The most prominently applied activation functions employed in the literature are the sigmoid, hyperbolic tangent, inverse tangent, threshold, Gaussian radial basis and linear activation functions [46].

The initial perceptron model was proposed for the classification of various binary data samples [47]. In this model, weighted input of the neuron is compared to a predefined threshold and is evaluated in regard to it to attach a class label to samples. In this case, the weights of the input were optimized to detect templates of certain targets and give the ANN the ability to differentiate the observed object from other entities with different inputs. The training of the network was conducted by having the network analyze standard samples and compare them to the input data. If the network did not clearly recognize the objects, then the weights were adjusted by a margin determined through a learning factor selected by the user. In case of data which can be linearly separated into classes based on the input features, it was shown that the ANN training process will converge within a finite amount of training steps [47]. The biggest deficiency of the simple perceptron model in application to real world data is the requirement of data which can be separated linearly.

In case of the Multilayer Perceptron (MLP) model, multiple layers of neurons are integrated into hidden layers. The activation functions of the various neurons are continuously differentiable nonlinear functions, in most cases like the previously mentioned sigmoid function. This structure allows only acyclic connections between the various neurons in the system, and only successive layers of neurons are directly connected [48]. In order to train the network for recognizing specific patterns, one of the fundamental techniques is the error backpropagation method [48].

Beyond the basic neural networks, many alternative versions have been explored to adapt the ANN framework to various scientific problems. Radial basis networks which utilize radial basis functions as activation functions, kernel function based learning algorithms, committee machines, dynamic and self-organizing neural networks etc. offer a wide variety of methods for the solution of differently formulated problems [48].

The main use of the neural network model was classically for classification and data analysis

problems, which is why it has found a significant home in the FDI literature [48]. Neural networks became especially prominent in the FDI problem of chemical process, which due to their nonlinearity and often hard to characterize process dynamics can be difficult to handle with analytic redundancy-based FDI methods. Another great strength of ANNs in chemical process FDI is its ability to recognize the presence of multiple simultaneous faults, which is exceedingly difficult using quantitative model-based techniques. Case studies showed that in case of single faults, failures due to multiple causes could be effectively differentiated. The main problem in such applications is the proper training of the ANN to maximize its fault detection capabilities through the testing of different network topologies with a varying number of hidden layers. Generally, an increase in the number of hidden layers and training data available greatly increases the fault detection capabilities and the convergence of the networks [49]. Comparisons between various topologies have been investigated in various case studies. One such study surveyed the FDI performance of various network topologies for centrifugal pumping rotary system by using two distinct neural networks [50].

2.3.2 Stochastic classifiers

Stochastic methods of FD and FDI methods employ pattern recognition algorithms to determine groups of possible process states, among them normal and abnormal operating conditions. The normal and abnormal process states are characterized by their probability density functions (PDF). Changes in the means and variances of the observed parameters can be inferred as being possible sources of process abnormalities, which can be used for detection purposes [8].

Major techniques employed in this type of FDI can be categorized into Bayesian and non-Bayesian procedures, with the former including Bayes networks, and the latter listing methods like limit checking, geometric moving average, filtered derivative, etc. methods. Generally, any stochastic method for abnormal change detection employs the sampling of process data over defined time intervals and using probabilistic methods to construct a decision function capable of identifying whether a change in the process behavior took place [51]. These functions are compared to a defined threshold, which can be chosen empirically or through the framework of threshold optimization [8]. Most stochastic methods of change detection in single variable systems usually rely on the logarithm of the likelihood ratio (log-likelihood ratio) as an index to evaluate whether the system is in a normal or abnormal state

[51]. Additionally, the Kullback information is employed for change detection, which provides an estimate for the detectability of the change in the process [51].

The best known of the non-Bayesian change detection algorithms is the simple limit checking approach. In this method, a process variable is inspected over a timeframe and used to construct a decision function. The decision function is the sum of the log-likelihood of the inspected variable at a given time. The decision function is evaluated compared to a predefined threshold. If the decision function is below the set threshold normal process operation is assumed, should it however cross the threshold the presence of process abnormalities are hypothesized. A specific solution to the limit checking approach in case of variables with a normal distribution function is the Shewhart control chart. This solution provides an analytical approach to threshold setting and change detection in said cases [52].

As with all other previously explored cases, due to the dynamic behavior of systems and possible nonlinearity, the behavior of units changes with the operating point. Training static stochastic models for a given operating point can lead to significant increase of FAR and MAR when operating conditions change. To circumvent this, stochastic methods have been updated to follow the changing behavior of the unit and adapt to it during FDI [53].

From the 1960s up until the 2000s, the geometric moving average (GMA) control charts use exponentially changing parameters to weigh the log-likelihood ratio of process data gathered at different time periods to calculate a decision function and evaluate it compared to a chosen threshold. The idea is to have the old data's weight decrease exponentially and to emphasize the weight of fresh process data [53]. Finite moving average control charts utilize similar methods but instead of an exponential forgetting parameter they utilize a moving time window and only use the data within the window to evaluate the decision function [51].

Recently, the use of so-called filtered derivative algorithms has become popular for FDI. In this method, the derivative of log-likelihood ratios of process variables are calculated. The change of the values indicates the deviation of the process from the normal state and is used to formulate the decision function. The calculation of derivatives, however, can be difficult in cases where process noise is present. Noisy signals do not have smooth derivative functions, the abrupt changes can be the cause of increased FAR and MAR. Therefore, some sort of filtering procedure is always employed before evaluating the derivative signals and the construction of the decision function [54].

In case of Bayesian algorithms, the detection of a change is assumed when the a posteriori probability of a change exceeds a predefined threshold. Bayesian models assume that the a priori distribution of process state change times is known. Using the additional knowledge about the conditional probability of process state transitions, a Markov chain can be used to describe the possible probabilities for the system in different time periods. Using these assumptions, a recursive formula for the updating of process state transition probabilities can be written as a function of sampling time, which is the evaluated decision function [51].

While the above-mentioned techniques are powerful and provide modeling options for statistical process monitoring (SPM) but their inherent flaw is that they were developed for univariate process control and monitoring assuming independence between the process variables. In case of multivariate processes, the correlations between variables could lead to misleading results when any of these traditional SPM methods are employed. To circumvent this problem, multivariate versions of the charting methods like the ones described previously were also developed [55].

2.3.3 Multivariate statistical process monitoring techniques

Multivariate statistical process monitoring (MSPM) methods have become increasingly important in data-based fault detection. These techniques differ from the traditional charting methods in their approach to process monitoring. Principal component analysis (PCA) and partial least square (PLS) regression are the original and most notably applied techniques. Their general key idea is to compress huge sets of correlated process variables into smaller, uncorrelated batches of variables without losing vital information. This way, a lower dimensional representation of the process can be established and used to evaluate process behavior [8].

PCA was perfected by Hotelling and became a standard statistical method for system supervision since its development [56]. During the course of PCA the process variables are evaluated, in case of correlated variables their covariance matrices are transformed to give orthogonal decompositions of the original covariance matrices. During this process, the directions of the orthogonal decomposition follow a path in the original phase space that explains the maximum variation of the process data. Thus, a large group of correlated process variables may be condensed into a set of few uncorrelated key variables which are responsible for most of

the variation in the process data [8]. This procedure is showcased in Fig. 2.7 for a data set with three variables [57].

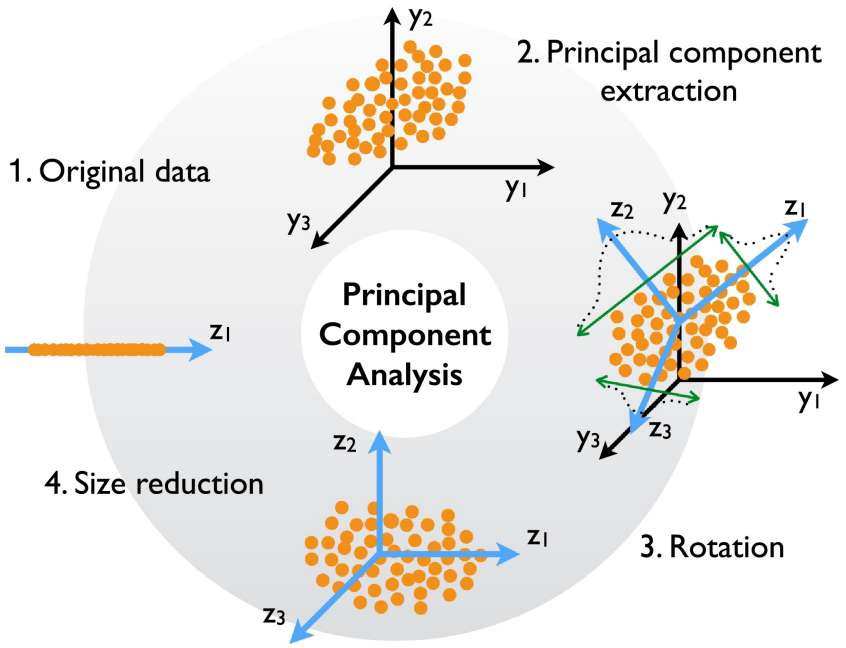

FIGURE 2.7: Procedure of PCA explained [57]

Consider a data set describing behavior of a process, denoted by $\mathbf{X} \in \mathbb{R}^{n \times s}$ with n observations and $s = m + p$ observed process variables. For PCA, the columns of $\mathbf{X}$ are centered and scaled to have a mean of zero and unit variance. The centered and scaled $\mathbf{X}$ matrix shall be denoted as $\tilde{\mathbf{X}}$. The linear transformation to obtain the set of latent variables, known as principal components (PC) from the centered data set can be obtained in various ways. Possible methods are through the eigenvalue decomposition (EVD) or the singular value decomposition (SVD) of the covariance matrix of $\tilde{\mathbf{X}}$. Alternatively, iterative methods such as the Nonlinear Iterative Partial Least Squares (NIPALS) algorithm may also be utilized.

In the following, we will discuss the EVD-based algorithm for obtaining the PCs. For the transformation, the sample covariance matrix $\mathbf{Z} \in \mathbb{R}^{s \times s}$ of $\tilde{\mathbf{X}}$ must be obtained. Due to the centering procedure, $\mathbf{Z}$ may be calculated according to Eq. 2.16.

$$\mathbf{Z} = \frac{1}{n-1} \tilde{\mathbf{X}}^T \tilde{\mathbf{X}} \tag{2.16}$$

Following this, we obtain the EVD of the covariance matrix $\mathbf{Z}$ according to Eq. 2.17, where $\mathbf{P} \in \mathbb{R}^{\mathbf{s} \times \mathbf{s}}$ is a matrix containing the eigenvectors of $\mathbf{Z}$, while $\Lambda \in \mathbb{R}^{\mathbf{s} \times \mathbf{s}}$ is a diagonal matrix containing the eigenvalues of $\mathbf{Z}$.

$$\mathbf{Z} = \mathbf{P}\Lambda\mathbf{P}^T \tag{2.17}$$

It can be shown that the eigenvectors of $\mathbf{Z}$ point to the directions of maximum variance within the space of the original data set. The degree of variation explained in the direction of each eigenvector is proportional to the absolute value of its corresponding eigenvalue. By ordering the eigenvectors based on the absolute value of their corresponding eigenvalues in descending order, we obtain the matrix $\tilde{\mathbf{P}}$. The percentage of retained variance within each eigenvector $\left(\tilde{\psi}_i, i = 1,\ldots,s\right)$ compared to the original data set may be calculated. After this, the amount of cumulative variance to be retained (θ) may be chosen based on the scree plot of the calculated eigenvalues. The optimal number of PCs to be retained (a) can be calculated according to Eq. 2.18 provided that $\sum_{i=1}^{p} \tilde{\psi}_i \geq \theta$ holds true.

$$a = \arg\min_i \left(\sum_{i=1}^{s} \tilde{\psi}_i - \theta \right)^2 \tag{2.18}$$

After calculating the number of PCs to be retained, the matrix $\tilde{\mathbf{P}}$ can be adjusted to contain only the necessary eigenvectors. This new matrix will be referred to as $\tilde{\mathbf{P}}_\mathbf{a} \in \mathbb{R}^{\mathbf{s}\times\mathbf{a}}$. The PCA transformation is then realized in the form of Eq. 2.19 with $\mathbf{T} \in \mathbb{R}^{n\times a}$, where optimally, $a \ll s$ holds true.

$$\mathbf{T} = \tilde{\mathbf{X}}\tilde{\mathbf{P}}_\mathbf{a} \tag{2.19}$$

The reduced data set can retain most of the original variance coded within the data by choosing a high value of θ. If chosen properly, the remaining $s - a$ eigenvectors account for the variation due to noise within the original data set. The PCA data decomposition model thus takes the form shown in Eq. 2.20, where the matrix $\mathbf{E} \in \mathbb{R}^{n\times s}$ is the prediction error.

$$\tilde{\mathbf{X}} = \mathbf{T}\tilde{\mathbf{P}}_\mathbf{a}^T + \mathbf{E} \tag{2.20}$$

After dimensionality reduction, control statistics such as Hotelling's T^2 statistic or the Q-statistic can be used for system supervision [56]. The T^2 statistic measures a sample's variance within the expectancy of the model and detects samples with great deviation as outliers. On the other hand, the Q-statistic, also known as Squared Prediction Error (SPE), provides a

measure for the prediction error of the PCA model for a given data point and classifies data points which do not follow the model as outliers regardless of their variance [58]. The difference between the two is showcased using Fig. 2.8. The displayed surface is the linear model describing the relationships between initial and PCA variables. Vertical deviations indicate data points which do not follow the fitted model, while horizontal deviations show data which while following the established model greatly deviate from the previous operating conditions [58].

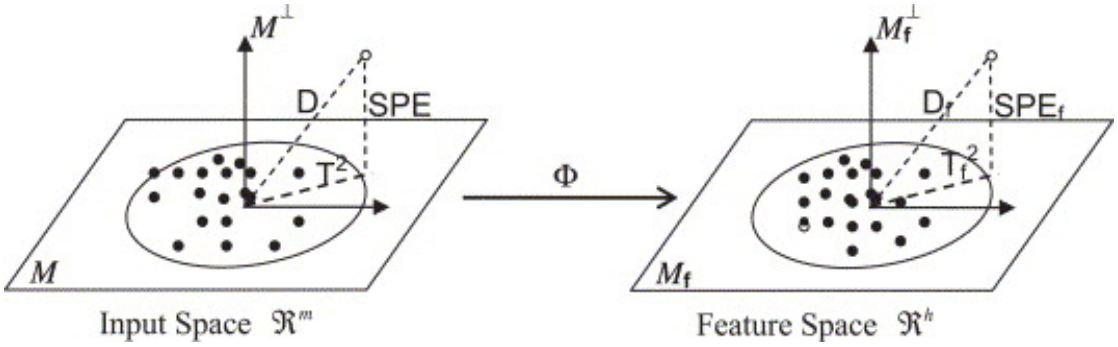

FIGURE 2.8: T^2 and Q statistic shown in the PC phase space [58]

The T^2 statistic for a given i-th sample can be calculated according to Eq. 2.21 using the calculated principal components.

$$T_i^2 = \mathbf{T}_i \Lambda^{-1} \mathbf{T}_i \tag{2.21}$$

Assuming that the PCs are normally distributed, an upper control limit can be established for the T^2 statistic for a given confidence level, α which can be used to filter abnormal outlier points [59]. In that case the control limit T_α^2 may be calculated according to Eq. 2.22 where F is the F-distribution [60].

$$T_\alpha^2 = \frac{a(n+1)(n-1)}{n(n-a)} F(\alpha, a, (n-a)) \tag{2.22}$$

The Q-statistic for a i-th data point can be calculated according to Equation 2.23, where $\mathbf{I} \in \mathbb{R}^{s \times s}$ is a unit matrix with appropriate dimensions [59].

$$Q_i = \left(\tilde{\mathbf{X}}_i - \mathbf{T}\tilde{\mathbf{P}}_\mathbf{a}^T\right)^T \left(\tilde{\mathbf{X}}_i - \mathbf{T}\tilde{\mathbf{P}}_\mathbf{a}^T\right) = \tilde{\mathbf{X}}_i^T \left(\mathbf{I} - \tilde{\mathbf{P}}_\mathbf{a}\tilde{\mathbf{P}}_\mathbf{a}^T\right)\tilde{\mathbf{X}}_i = \mathbf{E}_i^T \mathbf{E}_i \tag{2.23}$$

A control metric for the Q-statistic has been proposed by Jackson and Mudholkar [59]. For a given confidence level, α the control limit Q_α is calculated according to Equation 2.24.

$$Q_\alpha = \theta_1 \left[1 + \frac{d_\alpha \sqrt{2\theta_2 h_0^2}}{\theta_1} + \frac{\theta_2 h_0 (h_0 - 1)}{\theta_1^2} \right]^{\frac{1}{h_0}} \tag{2.24}$$

In Eq. 2.24, d_α is the deviate belonging to the upper $1-\alpha$ percentile of the standard normal distribution, while θ_i and h_0 are metrics derived from polynomial sums of the $s-a$ eigenvalues of the covariance matrix of the data. If the value of Q exceeds the defined control limit, the associated data point can be regarded as an outlier of the statistic. For observing processes where operation points gradually change over time, generally a moving window approach is used to add new measurement data to the observation matrix $\mathbf{X}$ and used to evaluate the principal components of the system [60].

While PCA is a powerful tool for the detection of process changes, it has the shortcoming that is only applicable to examine the properties of the supervised system it is applied to. PLS on the other hand is a method that is useful for using the data of the process variables to estimate the behavior of an additional group of data linked to the system, which in case of industrial technologies is most often product quality. PLS is a technique used to accurately estimate the relationship between two datasets and simultaneously reduce their dimensionality. During PLS instead of principal components, the uncorrelated process variables that describe the relationship between the two data sets and also account for most of the variance in the process data are called latent variables. These latent variables can be used not only to inspect the state of the system but also provide an estimation of how changes within the system variables will affect product quality [8].

The first instances of PLS modeling can be related to the works of Herman Ole Andreas Wold, who developed the technique as a means to analyze data from social sciences [61]. In his later works PLS found uses in natural sciences as well, mainly chemometrics, using the linear regression model Wold made predictions about the biological activity of various organic components based on variables describing their structure, acidity, etc. [62].

PCA and PLS-based FD has been extensively applied in industrial scale systems due to the ever-increasing amount of available process data and relatively easy mathematical techniques compared to other methods. The greater challenges facing the framework are the application

of PCA and PLS to nonlinear, dynamic system supervision [8]. Since both methods analyze cross-correlation between variables but do not take autocorrelation into account, they are inherently weak for FD in dynamic industrial systems where time series data is available. Their linear nature also makes their use for nonlinear system supervision difficult, resulting in increased FAR and MAR. Finally, both methods are effective at FD but isolation methods are not intrinsic to either method, as is the case for example for quantitative model-based FDI techniques [8].

In case of the isolation problem, many approaches have been proposed in the literature, but none emerged as definitively effective for PCA [63]. One of the first proposed solutions was the use of partial PCA which performed PCA on a subset of available process variables related to specific faults for isolation purposes, creating fault specific responses within the PC phase space similar to the parity space framework [64]. Later on, isolation enhanced PCA was invented which utilized a similar framework as partial PCA creating fault specific residual responses but also supplemented the technique with various statistical tests to analyze the residual responses [65]. In later works, rather than the residual-based approach, purely statistical tests such as the generalized likelihood ratio estimate were utilized to identify the detected faults and distinguish them from each other based on a priori knowledge for both linear [66] and nonlinear [67] benchmark problems.

The issue of autocorrelation was mainly addressed through the introduction of various dynamic PCA (DPCA) algorithms, which augment the base method with steps to account for dynamic changes in the data [68]. The most simple approach is the augmentation of the initial data matrix with lagged versions of the process variables to indirectly include autocorrelation into the PCA procedure [69].

The DPCA algorithm has two critical hyperparameters, these are l the number of added lag terms in the dataset and a the number of chosen principal components. In general PCA applications without considering dynamic data, various methods have been proposed for evaluating PCs, the most simple being the use of a scree plot to determine the cumulative retained variance of the original dataset within the PCs as per Eq. 2.18. Generally, the ankle of the scree plot is chosen as the desired variance level [70]. Alternatively the Q-statistic may be observed during cross-validation process to evaluate the prediction capabilities of the PCA model, the number of PCs is chosen to minimize the reconstruction error. It must however be noted that the procedure of cross-validation is not as elementary in the case of PCA as

it is with regression techniques and therefore various approaches have been proposed and compared in the literature to formulate the best cross-validation techniques for PCA model evaluation [71].

In case of DPCA however, the first and foremost parameter to be determined is the number of employed lag terms for the model used to convert the autocorrelation between data into cross-correlation [72]. In the original paper for the DPCA algorithm, the solution to the lag estimation problem is provided in Algorithm 1 [56]. In case of DPCA the algorithm proposed in the original paper is most commonly utilized for the estimation of l and a, the PC number is generally determined through observation of the ankle of the scree plot in accordance with Eq. 2.18.

Algorithm 1 Steps for choosing number of lags in DPCA [56]

1: Start
2: Set l to 0
3: Create the data matrix $\mathbf{X} = [\mathbf{X}(t), \mathbf{X}(t-1), ..., \mathbf{X}(t-l)]$, $\mathbf{X} \in \mathbb{R}^{(n-l)\times s(l+1)}$
4: perform standard PCA and calculate all PCs as per Eq. 2.16 to Eq. 2.20
5: Set $j = n \cdot (l+1)$ and $r(l) = 0$
6: Determine if the j-th component represents a linear relationship based on autocorrelation and cross-correlation functions or scree plot analysis, if yes proceed, if no move to step 7.
7: Set j=j-1 and r(l)=r(l+1), repeat 5
8: Calculate the new number of relationships $r_{new}(l) = r(l) - \sum_{i=0}^{l-1}(l-i+1)r_{new}(i)$
9: If $r_{new} \leq 0$, go to step 10, otherwise proceed
10: Set $l = l+1$, go to step 2
11: Stop

Later on, the DPCA approach was extended to handle nonlinearities [73] in the process variables as well as fault isolation issues [74]. Some modified PCA algorithms also combined the PCA algorithm with adapting threshold calculation procedures such as exponentially weighted moving average filters to adaptively update their thresholds and minimize FAR in cases of dynamic process operations [75]. Multiscale principal component analysis was also a proposed solution (MSPCA) which combined the traditional PCA technique with wavelet methods. PCA was utilized to extract cross-correlation between data, while the wavelet transform eliminated autocorrelation [76].

The handling of nonlinearities in PCA was most commonly performed through the use of appropriate kernel functions, which resulted in the development of kernel PCA (KPCA). These techniques were much easier applicable to the fault detection problems of non-linear chemical systems with great reduction in FAR and MAR compared to quantitative model-based techniques. Regardless, despite their robustness they still lacked a traditionally simple way for fault isolation techniques such as wavelet transforms or multiscale methods already developed for linear PCA [58].

In case of PLS similar research trends could be observed as with PCA, the handling of nonlinearities, isolation techniques and application of said methods for dynamic system supervision are in the focus of academic investigation [77].

An interesting hybrid method is the use of PLS to supervise the quantitative model of a given process for detection of multiplicative faults. Rather than observing input-output data and making predictions about fault impact, the PLS was used to supervise a model of the process. By using the PLS in this way, changes in the underlying sub-processes were detected which were linked to parametric abnormalities in the unit, thus establishing a link to the quantitative model-based approaches [78].

Kernel function-based PLS was also developed for the supervision of nonlinear processes. Some studies included forgetting factors in the model and continuously reevaluated the PLS based on the process data, thus creating a dynamic kernel PLS (DKPLS) for FDI of nonlinear dynamic systems [79]. The combination of kernel techniques and methods to include autocorrelation and system dynamics into supervision algorithms was also investigated in case of PCA dubbed dynamic kernel PCA (DKPCA) [80]

2.4 Bottlenecks of fault detection and isolation, contemporary trends and issues, research motivation

After analyzing the FD and FDI literature it can be clearly seen that the spectrum of approaches is diverse and the evolution of applied techniques can be clearly traced and distinguished with quantitative model-based approaches dominating in the early stages of FD and FDI and process history-based techniques gradually overtaking them with the spread of big data.

To highlight current trends a clustering result is presented in which keywords of 5000 publications from 2000 to 2020, related to the keyword "fault detection" have been collected from the Web of Science, analyzed and clustered based on their co-occurrence frequency, this can be seen in Fig. 2.9.

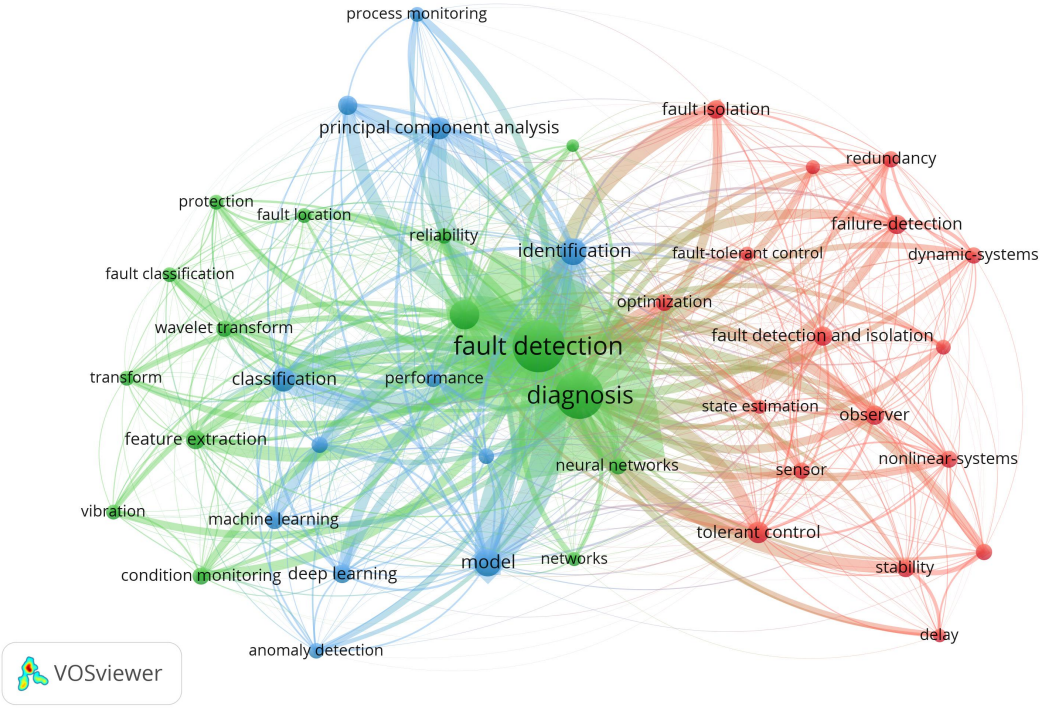

FIGURE 2.9: Clustering of keywords related to "fault detection"

The results only include keywords which appeared at least 70 times within the 5000 publications and show that FD is strongly dominated by process history-based methods, especially MSPM research. Three main clusters could be distinguished, these are colored differently, with the size of various keywords indicating their frequency during the search. Link width and distance between individual keywords indicates their co-occurrence frequency during the clustering. The three main clusters can be grouped into keywords related to analytical redundancy-based FD methods (red), process history-based FD methods (blue) and general miscellaneous keywords and supplementary techniques (green). In case of process history-based applications, "PCA" is the most impactful method related keyword, closely followed by "deep learning" and the general "machine learning" expressions. In the analytical, redundancy-based group observers and state estimation take the leading role, with a stronger emphasis on "fault-tolerant control" than FD.

From the results, it can also be inferred that FD and FDI strongly move towards data-based techniques, with analytical redundancy methods trailing behind and qualitative FD methods having fallen off. To further clarify the trends, the change in the number of publications relating to different approaches of FD have been reviewed over the years on Web of Science. Fig. 2.10 shows the change in number of annual publications related to each fault detection technique over the time period between 2000 and 2020. To conduct the research, "Fault Detection" plus the specific method have been applied as keywords. The related entries have been analyzed and plotted.

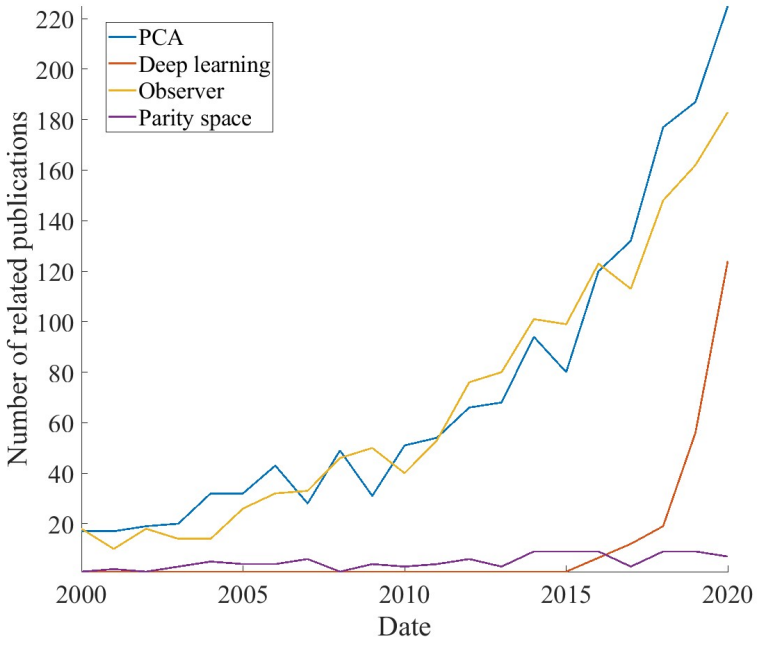

FIGURE 2.10: Number of annual publications with keywords related to specific techniques and fault detection

Fig. 2.10 shows that the number of publications for both observer-based methods and PCA have been increasing, it is notable that deep learning methods have been gaining a steep rise in popularity over the last years. Based on these findings, MSPM techniques, especially PCA, have been chosen as the focus of further study and development due to both great research interest and practical applicability for FD and potentially FDI [81].

Based on the literary review, three main areas of research focus have been proposed to supplement the current FD and FDI framework related techniques, which are listed as follows:

- Developing further fault isolation solutions for MSPM techniques, with focus on PCA (discussed in Chapter 3)
- Integration of risks associated with different process abnormalities to minimize the number of superfluous alarms and prevent alarm floods (discussed in Chapter 4)
- Developing MSPM-based techniques for supervision and FD in distributed parameter systems (DPS) (discussed in Chapter 5)

The first point was proposed because it was noted that while most MSPM techniques and especially PLS and PCA have strong FD capabilities, they inherently lack ways in which effective fault isolation can be performed with them [63]. Alternative methods which heavily rely on the previously established parity space framework have been proposed [65] and further developed [66]. However, their application begs the question of why parity space techniques can not be employed in the first case when the residual generation framework is almost identical to those employed in parity space methods. Additionally, extension of these methods to nonlinear systems is not perfectly resolved either [63].

The second issue, the integration of risk into the FD and FDI framework, has become a research topic in the 2010s when the problem of alarm optimization started gaining importance in the FDI research community [82]. Due to noise and disturbances model-based FDI techniques were especially prone to false alarms, this increasing FAR would encumber operators especially when due to fault propagation alarm floods would occur [83]. Research has proposed the integration of a priori knowledge about process faults and their associated risks into FDI and eliminating alarms caused by faults which hold little to no risk to the process and do not impact production quality [82].

The third issue is the FD problem in distributed parameter systems (DPS). The FD and FDI framework were mostly designed assuming concentrated parameter systems where process variables only show temporal dependence and are not dependent on spatial coordinates. This can be seen especially when observing model-based methods of FD such as parity space and observer techniques, which all assume that the system can be described through the general state-space framework [10]. Methods have been proposed for FD and FDI in DPS, but most of these rely on modified parity space or observer schemes. Their application due to their mathematical complexity is difficult in practice, and they were designed for supervising systems with process variables changes along a single spatial coordinate and time, not taking

3D spatial detection into account [84]. Therefore, it is required to implement reliable, data-based methods for DPS supervision. Yet, this sparks further research questions about optimal sensor localization and means of acquiring reliable data for training said methods.

Based on these questions, three research items have been explored and discussed in the remainder of the dissertation.

Chapter 3

Fault isolation using principal component analysis and trajectory distance metrics

In this chapter, I will review fault isolation methods in PCA and propose a method based on trajectory similarity metrics for fault isolation in dynamic systems [85]. After a literary review of the current isolation techniques for PCA, the proposed method is introduced and showcased using an FDI benchmark problem. Subsequently, detection and isolation capabilities of the method are studied and evaluated in comparison with other, traditional FDI approaches.

3.1 Isolation techniques for principal component analysis proposed in the fault detection and isolation literature

As was mentioned in Chapter 2, section 2.3, PCA as a technique inherently lacks methods of fault isolation, the traditional PCA control statistics such as T^2 and Q statistic hold only FD capabilities [65].

To resolve this issue, extensions of the traditional PCA method have been proposed which have been enhanced with fault isolation capabilities. One of the first methods was an isolation enhanced PCA, which developed structured residuals from the PC scores similar to the

parity relation framework [65]. Based on these principles, later on partial PCA was proposed which differently from the previous method analyzed the PC variables and developed residual generator schemes for subsets of the total PC variables which strongly respond to specific faults for isolation purposes [64]. Later on, the reconstruction of the original variables from the PCs and subsequent structure residual generation has also been proposed relating to the PCA framework [86]. The trend of deriving parity relation-like structured residuals from PC scores for FDI using PCA continued until the end of the 2000s, when other alternative techniques had begun to dominate the problem of isolation in PCA.

Some case studies utilized PCA and derived methods such as kernel PCA and proposed isolation schemes based on classification methods in the PC subspace. They identified different fault classes which to test for and developed a prognosis by comparing the direction of new data points within the PC subspace with the known fault classes [87]. Some research proposed the use of expert-based multivariate decoupling for analyzing fault patterns in PC subspaces and developing isolation schemes based on the established expert rules [88]. Some methods utilized techniques based on contributions plots, where the various PCs have been evaluated under different fault conditions and their contribution to the overall value of the Q-statistic was utilized for fault isolation [89]. Similar contribution-based techniques have also been proposed for safety critical FDI problems, such as supervision of nuclear power plants [90].

While these methods provide efficient methods of fault isolation, they suffer from certain shortcomings. Residual-based techniques while robust and reliable suffer from the problems of traditional parity-relation methods, their extension to nonlinear systems while partially resolved is a rather complex problem as well [65]. The modern techniques of isolation such as those based on PC contribution analysis or observation of general fault evolution in the PC subspaces is promising due to its simplicity [87]. However, most of these techniques listed previously focus on identifying fully developed faults in the PC subspace and thus have more delayed fault responses [87].

Therefore, the application of data mining techniques to analyze anomalous patterns, sequences of evolution for the observed systems process variables in the PC subspace could lead to more efficient FDI with prompt isolation. These patterns are captured in trajectory data of dynamic systems, which assign a system's process variables in phase space to certain sequence stamps, which leads to a map of evolution of the system state. In a mathematical

formulation a trajectory Tr of the i-th observed entity where $i = 1,2,...,N$ is the identifier of the observed entity is expressed as $Tr_i = \{\mathbf{x}_i(1),\mathbf{x}_i(2),...,\mathbf{x}_i(n_i)\}$, where $\mathbf{x}_i(j) \in \mathbb{R}^{1\times s}$ is the vector of observed process variables related to the systems state in the j-th sequence stamp where $j = 1,2,...,n_i$, such that n_i is the total number of sequence stamps for the i-th observed trajectory. In recent years, there has been a rise in the use of trajectory similarity metrics as tools of fault isolation in the framework of FDI. Among them, the discrete Fréchet distance as a similarity metric has garnered special research interest. The discrete Fréchet distance describes the distance between two polygonal curves, which takes ordering of points along the curve into account. Its use in isolation lies in analyzing time series of system variables and pointing out similarities between real-time data and various known fault signal responses. As an example of its use, a method was proposed based on the discrete Fréchet distance to analyze current transformers and differentiate between internal and external fault currents [91]. In some applications, it was used in two-stage turnout fault diagnosis methods [92].

The application of trajectory similarity metrics for fault classification in FDI is a promising direction due to the simplicity of said methods compared to other classifiers, such as neural networks, support vector machines, etc. Trajectory similarity methods compare two trajectories and derive a metric to analyze their similarity, popular metrics for this application include the Hausdorff, Fréchet distance and dynamic time warping [93]. One of the factors which could be limiting for its application though is the large amount of observed variables within a technological system. Selecting the optimal variables for observation is highly dependent on the fault types which are taken into consideration, since observation of changes within all variables is computationally demanding and hinders online diagnosis.

It must be noted that many trajectory similarity measures can be utilized for various clustering and classification schemes related to the FD and FDI problems. The most common trajectory distance measures utilized in the literature are dynamic time warping (DTW), the longest common subsequence (LCSS), edit distance on real sequences (EDR) as well as discrete and continuous Fréchet distance. It is noted that the choice between these measures is in a way arbitrary for clustering/classification purposes and must be based on observation of data and specific application goal case-by-case. While efforts have been made to compare the performance of these measures for specific applications in comparing trajectories, such investigations are limited to comparisons based on a limited number of trajectories without deep theoretical underpinning [94]. Selecting the basis for comparison between these metrics is also a difficulty as many evaluation standards such as computational performance

(computational complexity, sensitivity to data transformations such as addition/deletion of points or resampling) or specific application performance may be taken into account [95].

To give a brief analysis and comparison of the highlighted trajectory distance measures, the following properties were taken into account:

- Metrics status of measures.
- Applicability of measures to discrete or continuous data.
- Computational efficiency of algorithms when comparing two trajectories where $n, m \in \mathbb{R}$ are the sample numbers of trajectories to be compared respectively.
- Outlier sensitivity based on use of maximum or sum of distances for similarity evaluation.
- Bounded or unbounded status of the similarity measures.
- Interpretability of distance magnitudes.

The comparison of the five most commonly used metrics based on the previously listed properties is showcased in Table 3.1 [96].

TABLE 3.1: Comparison of most commonly applied trajectory distance measures for distance evaluation of trajectories with sample numbers $n, m \in \mathbb{R}$

Performance measure	DTW	EDR	LCSS	Discrete Fréchet distance	Continuous Fréchet distance
Metric status	Not a metric	Not a metric	Not a metric	Metric	Metric
Applicable to continuous data	No	No	No	No	Yes
Computational complexity	$\mathbb{O}(n \cdot m)$	$\mathbb{O}(n \cdot m)$	$\mathbb{O}(n \cdot m)$	$\mathbb{O}(n \cdot m)$	$\mathbb{O}\left(log(n \cdot m)n \cdot m\right)$
Tolerance to outliers	Medium tolerance	High tolerance	High tolerance	Low tolerance	Low tolerance

After observation of the measures, discrete Fréchet distance was chosen based on its acceptable computational efficiency, its metric status which is advantageous for classification applications as will be utilized here and the existence of the continuous Fréchet distance variant which facilitates extension of the method to continuous trajectory data. Regardless, it must be noted that during application to different systems other measures may be explored which could have specifically better FD performance for the given system, especially when outliers or noise are present in the data.

3.2 The proposed fault isolation scheme through trajectory distance measurement

The key idea in this chapter is the use of dynamic PCA (DPCA) for detecting the presence of abnormalities within a dynamic system while simultaneously pinpointing the root causes of the anomalies through a classification technique based on the discrete Fréchet distance metric. The application of DPCA provides dimensionality reduction for the data set, which makes trajectory similarity calculations for fault isolation computationally less expensive and suitable for online fault diagnosis [85].

The algorithm uses input–output data of a dynamic process to establish a DPCA model with optimized lag number to reduce dimensionality within the data set and pinpoint outliers. The Q statistic is then employed to identify irregular data points belonging to faults. Within the PC subspace, the Fréchet distance metric is used to characterize similarity of registered abnormalities to a predetermined fault library and select the best possible match for each fault instance. The efficiency of the method has been validated using simulated data gathered from a three-tank benchmark problem. FDI capabilities have been characterized using False Alarm Rate (FAR) and Missed Alarm Rate (MAR) metrics, while classification accuracy for fault isolation has been evaluated based on the F_1 score. The results show that the method exhibits good FDI capabilities with low computational cost, easy implementation and proper robustness.

The discrete Fréchet distance (later on simply referred to as Fréchet distance) is a measure of similarity between two polygonal curves that takes into account the location and ordering of points along the curves. A way of computation for the discrete Fréchet distance between two curves with finite defined points is also known as the coupling distance [97].

For measuring the similarity between two arbitrary continuous curves, they are approximated as polygonal curves. Let the two curves to be compared be defined as sets of point $S_1 : [0, n_1] \rightarrow T_f$ and $S_2 : [0, n_2] \rightarrow T_l$. The sequence of end points for each line segment is denoted by $\sigma(S_1) = \{\mathbf{x}_{S_1,1}, \mathbf{x}_{S_1,2}, \ldots, \mathbf{x}_{S_1,n_1-1}\}$ and, $\sigma(S_2) = \{\mathbf{x}_{S_2,1}, \mathbf{x}_{S_2,2}, \ldots, \mathbf{x}_{S_2,n_2-1}\}$respectively. The set of all possible combinations between the end points of the polygonal curves (H) is defined in Eq. 3.1 [97].

$$\sigma(H) = \sigma(S_1) \times \sigma(S_2) \tag{3.1}$$

Couplings between the two curves are sequences of distinct pairs from H which respect the ordering of points in both curves. The length of a possible coupling between the two curves is denoted by, $\|LI\|$ which corresponds to the length of the longest link within the defined coupling. $\|LI\|$ is calculated according to Eq. 3.2. In the equation, the metric d stands for a chosen distance metric of the two sequences, which is most often the Euclidean distance.

$$\|LI\| = \max\, d(S_1, S_2) \tag{3.2}$$

The discrete Fréchet distance ((δ_{dF}) is defined as the minimum length of all possible couplings between the two polygonal curves, as seen in Eq. 3.3 [97].

$$\delta_{dF}(S_1, S_2) = \min\, (\max\, d(S_1, S_2)) \tag{3.3}$$

The proposed algorithm for FDI consists of two phases. These phases start with the traditional FD problem solved by PCA [72].

Phase I consists of acquiring a subset of process data about the system to be supervised under normal operating conditions. Using this data, the in-control DPCA model is established, and control limits for statistical measures are determined. In our case, this phase also includes the generation of a fault library for later isolation purposes.

Phase II consists of real-time monitoring of the system, which includes the detection and isolation of process abnormalities. In this phase, process data is analyzed and the presence of faults is determined based on the control statistic of PCA. If a fault is recognized, the trajectory of variables within the PC subspace is recorded for the out-of-control state. The observed trajectory is compared with the reference trajectories within the fault library and is matched to the fault most similar to it using a nearest neighbor classification logic. The general steps of the FDI algorithm for both phases are shown in Algorithm 2.

Algorithm 2 Steps of the DPCA and Fréchet distance-based FDI algorithm

Phase 1 – Establishing the DPCA model and fault library

procedure ESTABLISHING THE DPCA MODEL
  Calculate l based on the algorithm proposed by Ku et al. [56]
  Compute the enhanced data matrix $\mathbf{X} \in \mathbb{R}^{(n-l)\times s(l+1)}$
  Center the enhanced data matrix $\left(\tilde{\mathbf{X}}\right)$ using the process steady state
  Calculate $\mathbf{Z} = \frac{1}{n-l-1}\tilde{\mathbf{X}}^T\tilde{\mathbf{X}}$
  Calculate matrix $\tilde{\mathbf{P}}$ using EVD
  Determine a using the scree plot according to [56]
  Calculate $\tilde{\mathbf{P}}_\mathbf{a}$
end procedure
procedure ESTABLISHING THE FAULT LIBRARY
  Obtain data set $\mathbf{X}_f \in \mathbb{R}^{n\times p}$containing system abnormalities F
  Compute **PC** values for the data $\mathbf{PC} = \tilde{\mathbf{X}}_\mathbf{f}\tilde{\mathbf{P}}_\mathbf{a}$
  Compute Q-statistic for the data set and isolate out of control points $\mathbf{T}_f$
  for each fault f **do**
    Calculate $\mathbf{T}_n\left(f\right) = \frac{\mathbf{T}_f}{\max\|\mathbf{T}_f\|}$
  end for
end procedure

Phase 2 – Online supervision of the process

procedure FAULT DETECTION
  Obtain data set $\mathbf{X}_o \in \mathbb{R}^{n\times s}$ to be analyzed
  Compute **PC** values for the data $\mathbf{PC} = \tilde{\mathbf{X}}_\mathbf{o}\tilde{\mathbf{P}}_\mathbf{a}$
  Pinpoint outliers for a given confidence level using the Q-statistic
  Store data of outlier points within the PC subspace $\mathbf{T}_o$
end procedure
procedure FAULT ISOLATION
  for each recognized individual fault signal (F_o) within data set $\mathbf{T}_o$ **do**
    for each reference fault stored within the fault library $T_n\left(f\right)$ **do**
      Calculate $\delta_{dF}\left(PC_n\left(f\right), F_o\right)$
      Define the unknown fault F_o as $\arg\min_f\left(\delta_{dF}\left(T_n\left(f\right), F_o\right)\right)$
    end for
  end for
end procedure

The contribution of the work to the FDI methodology includes:

- A novel application of the Fréchet distance metric combined with DPCA to isolate process abnormalities and identify their root causes.
- Reduction of computational cost for the Fréchet distance calculations between reference and measured fault trajectories.
- A sensitive and robust FDI method with simple implementation and high accuracy that greatly fits into the Industry 4.0 framework.

The metrics and techniques which are used to tune the hyperparameters of the methods and evaluate the FDI potential of the technique are introduced in the following. After establishing the model, the false alarm rate (FAR) and missed alarm rate (MAR) metrics were used for evaluating the detection prowess of the method. To quantify the performance of the isolation algorithm based on the Fréchet distance metric, the macro-averaged F_1 score was utilized. The extensive description of the employed performance metrics and their means of calculation are described in Appendix A.

3.3 Case study and method evaluation

The FDI capabilities of the proposed method have been tested using data gathered from the a priori model of the three-tank benchmark system displayed in Figure B.1 [98]. This benchmark problem is well-known in the FDI framework, for this work, it was utilized due to the nonlinear, dynamic nature of the system as well as its relative simplicity and the abundance of FD and FDI literature which utilizes it for method testing [99, 100]. The thorough description of the benchmark problem including the measured system input and output variables, system model, and system parameters are expanded upon in Appendix B.

The training data for the DPCA method was obtained by observing system behavior around the steady-state under the conditions shown in Table B.1. The development of the steady-state conditions can be seen in Fig. 3.1. The system of differential equations seen in Eq. B.1 describing system behavior was solved using Euler's explicit method.

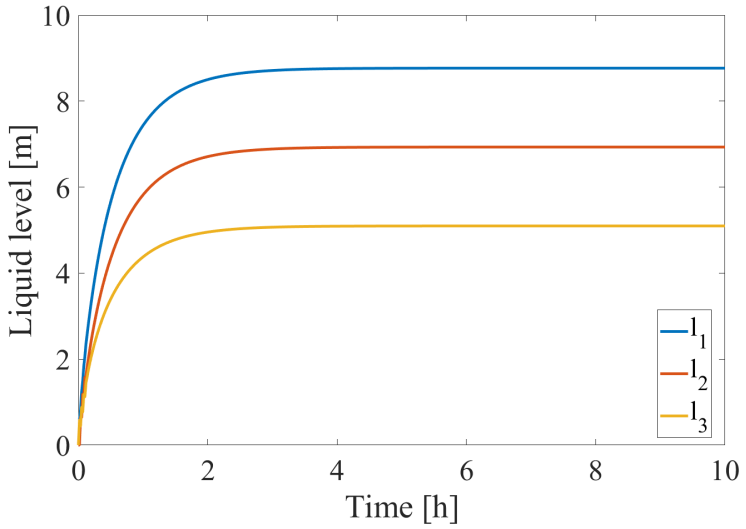

FIGURE 3.1: Steady state liquid level within the three tanks under the operating conditions of Table B.1

The system was observed in a time window of 1500 h, with a sampling time of 600 s based on the dynamics of the system. The observation period and sampling time were chosen based on the time-constant of the system, which was approximately 5 hours. During this time, 30 changes were made in the value of the input volumetric flow according to a ramp function. The percentage deviation of the inputs from their steady-state values were calculated as random variables with a normal distribution that has an expected value equal to the steady state input values and standard deviation of 0.01 times the expected value. The changes in the input volumetric flow and the liquid levels compared to their steady-state values are shown in Fig. 3.2.

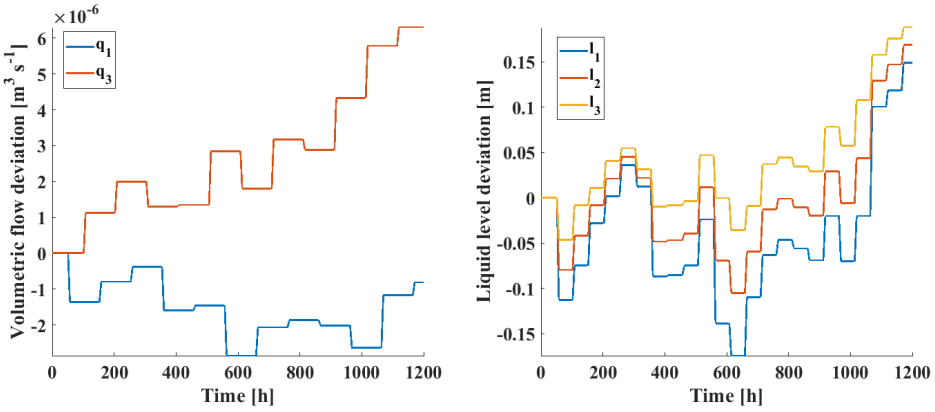

FIGURE 3.2: Changes in the inlet volumetric flows (**left**) and the liquid levels (**right**) within the tanks compared to their steady-state conditions

The DPCA model was constructed in accordance with Algorithm 1, proposed in the original article detailing DPCA [56]. The PCA transform was calculated as per Eq. 2.17 to Eq. 2.20. The lag number was tuned as well as the number of PCs, to determine linear relations a threshold was determined for the eigenvalues (λ_{min}) of the corresponding PC scores. The chosen threshold for the eigenvalues was determined using Eq. 3.4

$$\lambda_{min} = \max_{1 \leq i \leq s} \lambda_i \cdot 10^{-4} \tag{3.4}$$

During the tuning, lag values from 0 to 2 have been utilized as per Algorithm 1, for testing. The eigenvalues of the DPCA transformation as well as the threshold have been plotted for the investigated instances, the results can be seen in Fig. 3.3, in the form of a scree plot for the first four calculated PCs. As the lag number increases the numeric values of the first few eigenvalues also increase, therefore at lag 2 the third PC also becomes more significant. Based on the results, an optimal lag number of 2 was determined, and the first two PCs have been retained. The r_{new} value of new relations has been calculated during the different iterations and plotted, the results can be seen in the second subplot of Fig. 3.3. The subplot shows that the transform reveals new successive relations due to the addition of lags, the autocorrelation between data is properly contained within the PCs, however after a lag number of 2 no new relationships can be observed.

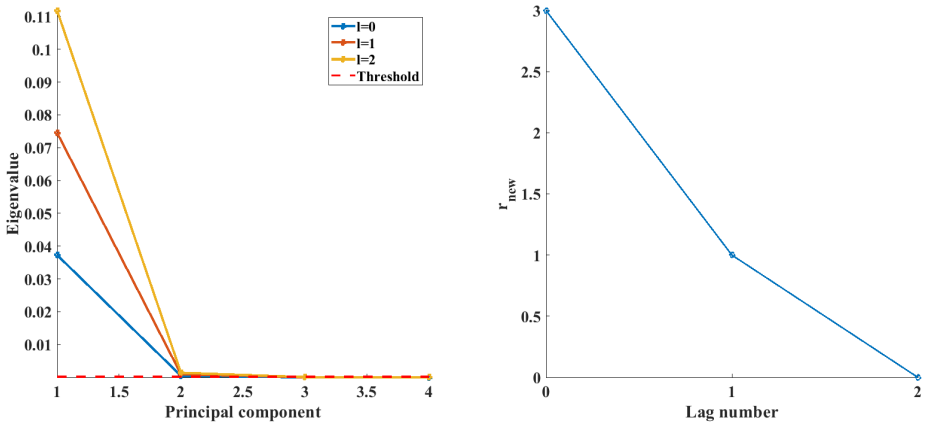

FIGURE 3.3: Eigenvalues of the PCs (**left**) as well as the number of new relations for different lag values (**right**)

The auto and cross-correlation in the discarded PCs was observed to validate the results as proposed by Ku et al. [56]. The results for the first two discarded PCs for both the original PCA transform and the chosen DPCA transform with a lag value of 2 are displayed in Fig. 3.4

and Fig. 3.5. It must be noted that for 0 lags the optimal PC number to be retained was 1, thus the correlation plots are displayed for PCs 2 to 3. When comparing Fig. 3.4 and Fig. 3.5 it shows that the DPCA transform with 2 lags significantly decreased the autocorrelation of the discarded PC scores, meaning that the dynamic tendencies of the data have been mostly captured in the transform.

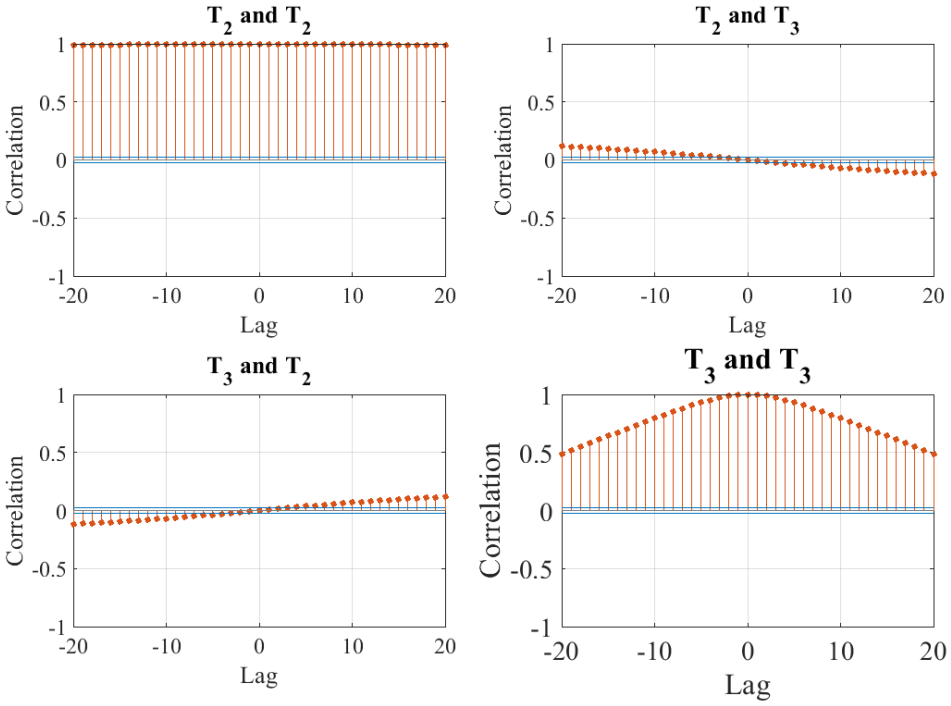

FIGURE 3.4: Correlation plots for the first two discarded PCs in basic PCA

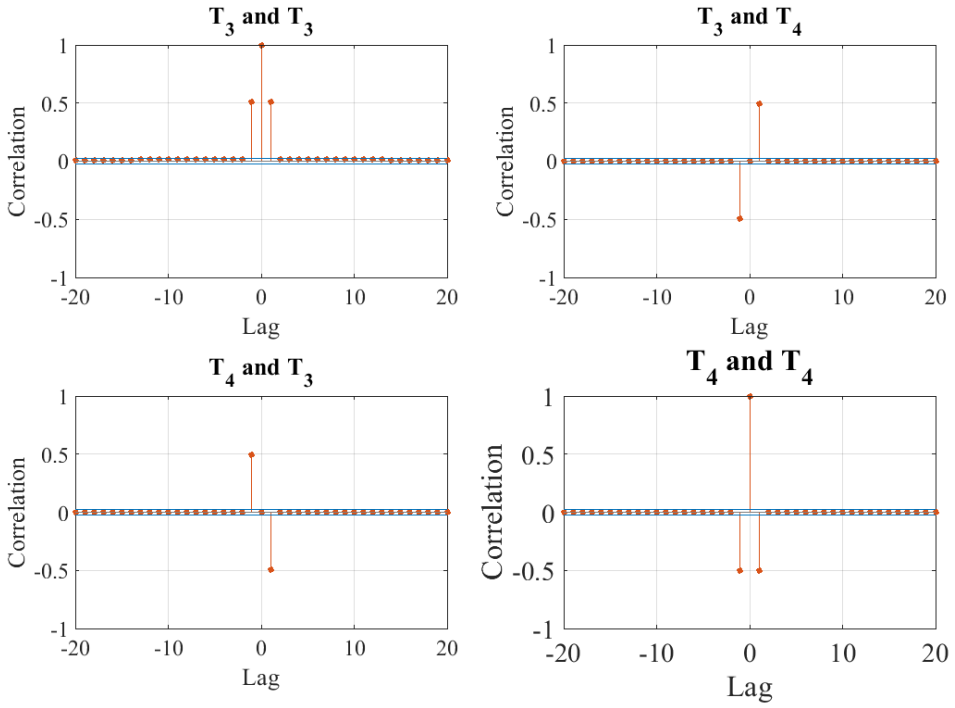

FIGURE 3.5: Correlation plots for the two three discarded PCs in DPCA, with a lag number of 2

To validate the performance of the model on the training data set, the Q-statistic was calculated and evaluated against the upper control limit calculated from Eq. 2.24 corresponding to a 95 % confidence level. The results are shown in Fig. 3.6, the low value of the Q-statistic and the fact that it nowhere exceeds the control limit indicates that the model accurately represents the process.

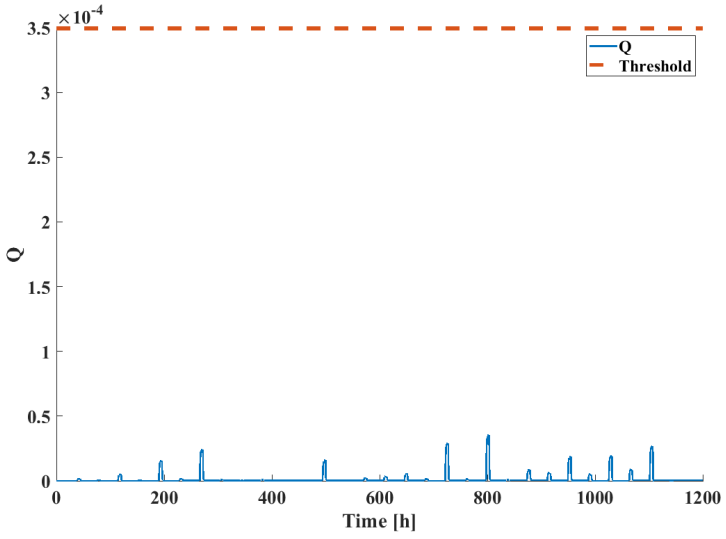

FIGURE 3.6: Q-statistic for original training data (Fig. 3.2) with the trained DPCA model

Subsequently, the faults have been introduced and their responses in the PC subspace have been registered. The six fault signals in the flow parameter and the binary signals of leakages compared to the normal steady state are seen in Fig. 3.7, subsequently the level changes compared to the established steady state are seen.

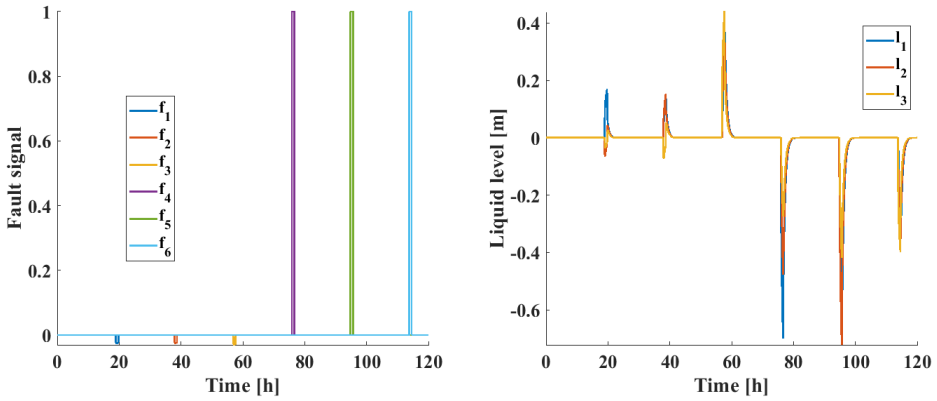

FIGURE 3.7: Fault signals (**left**) and fault response signals (**right**) within the tank compared to the normal steady state operation

Since the algorithm of Eiter and Mannila for computing the discrete Fréchet distance takes time $O(n \cdot m)$ for two polygonal curves with number of vertices n and m it is critical to minimize the number of points during the calculations lest the computational load explodes [97]. To do this various methods have been proposed in the literature, with the two main approaches being the simplification of the curves through proper approximations and elimination of superfluous points [101] or the optimization of the discrete Fréchet distance algorithm to pinpoint and compare critical points of trajectories [102].

One of the widest known solutions for the trajectory simplification problem is the Ramer-Douglas-Peucker (RDP) vertex subsampling algorithm [103]. The method simplifies isolated polylines, with the result being a sub-sequence of the original polylines vertices. We define a fault trajectory in the obtained PC subspace as $Tr_i = \{\mathbf{T}_i(1), \mathbf{T}_i(2), ..., \mathbf{T}_i(n_i)\}$, where $\mathbf{T}_i(j) \in \mathbb{R}^{a\times 1}$ is the vector of retained PCs in the j-th sequence stamp where $j = 1, 2, ..., n_i$, such that n_i is the total number of sequence stamps for the i-th observed fault trajectory, corresponding to the vertices of the polyline.

Let $e_{k,l} = [\mathbf{T}_i(k), \mathbf{T}_i(l)]$ be a straight line segment between the k-th and l-th vertices of the fault trajectory and hyperparameter $\epsilon \geq 0$. The algorithm connects the initial and final points of the polyline with the edge e_{1,n_i} and uses this as the initial approximation of the trajectory of the i-th fault, subsequently denoted as $F_i = \{e_{1,n_i}\}$. The perpendicular distance of each

remaining vertex of the original trajectory from the new edge is calculated. If the vertex that is the farthest away from the edge is at least ϵ units of distance from the closest edge, then it is added in an ordered manner to the forming polyline as a new edge. The algorithm continues with the approximations until no point on the original polyline is further as ϵ from the closest edge of the approximation, the remaining points are then discarded [103]. Since the computational time of the RDP algorithm varies between $O(n_i)$ and $O(n_i \cdot log(n_i))$ based on the employed pseudocode the total computational time of the Fréchet distance calculation can be significantly reduced through the use of the vertex subsampling algorithm.

In case of each fault trajectory, the RDP algorithm was employed to reduce the number of points used to represent the trajectories. The ϵ parameter was tuned by observing the percentage of retained points compared to the number of original data points representing the trajectory and the Fréchet distance between the original and reduced trajectories for each instance of ϵ, the results are displayed in Fig. 3.8. Based on the results, a ϵ value of 0.01 was chosen in each instance to minimize the number of retained points while achieving relatively small distances between the reduced and original trajectories.

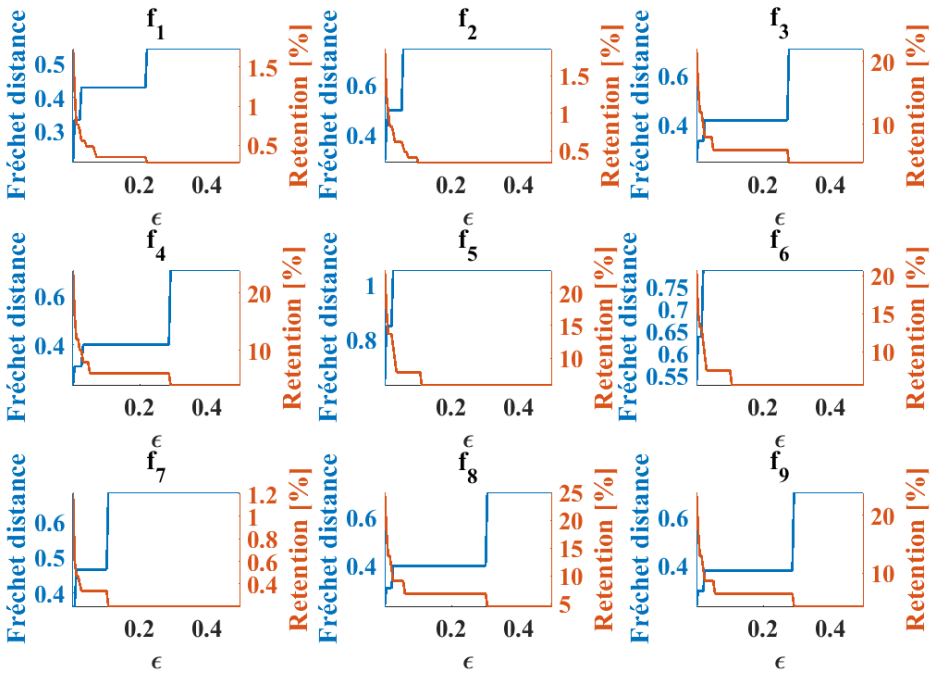

FIGURE 3.8: Retained data points and Fréchet distance for each fault trajectory after RDP

The original and reduced trajectories are displayed in the PC subspace in Fig. 3.9. It can be seen that the reduced trajectories capture the original trend accurately while reducing

the original data to 20-30 % of its original sample number. In some cases (faults 3,4,6) the α = 95% confidence bound bisected the fault signal into two parts belonging to the same fault occurrence, therefore both instances of the fault trajectory were registered and used for analysis.

To evaluate the dissimilarity of the obtained trajectories, the distance matrix of the individual trajectories was utilized, taking the discrete Fréchet distance as a basis. The results show similar tendencies as those observed in Fig. 3.9, faults 1 and 2 have similar behavior in the PC subspace, while faults 4 and 6 also have slightly hard to distinguish responses.

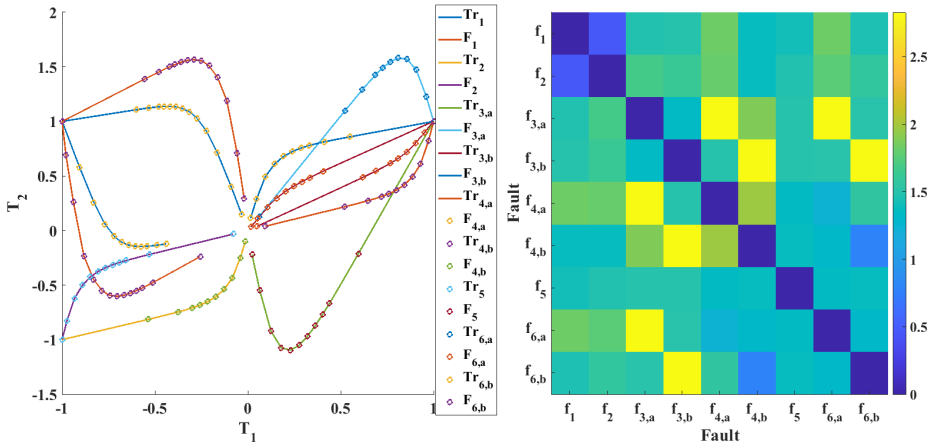

FIGURE 3.9: Reduced and original trajectory data in the 2D PC subspace (**left**) and the distance matrix of the reduced trajectory data (**right**) in the 2D PC subspace

To showcase the workings of the algorithm, a realization of the FDI process is shown for a duration of 120 hours, with a number of 10 randomly generated fault occurrences and 3 randomly generated set point changes. The changes of the input values, the fault signals, the system responses in the form of level changes and the corresponding Q statistic scores are all shown in Fig. 3.10.

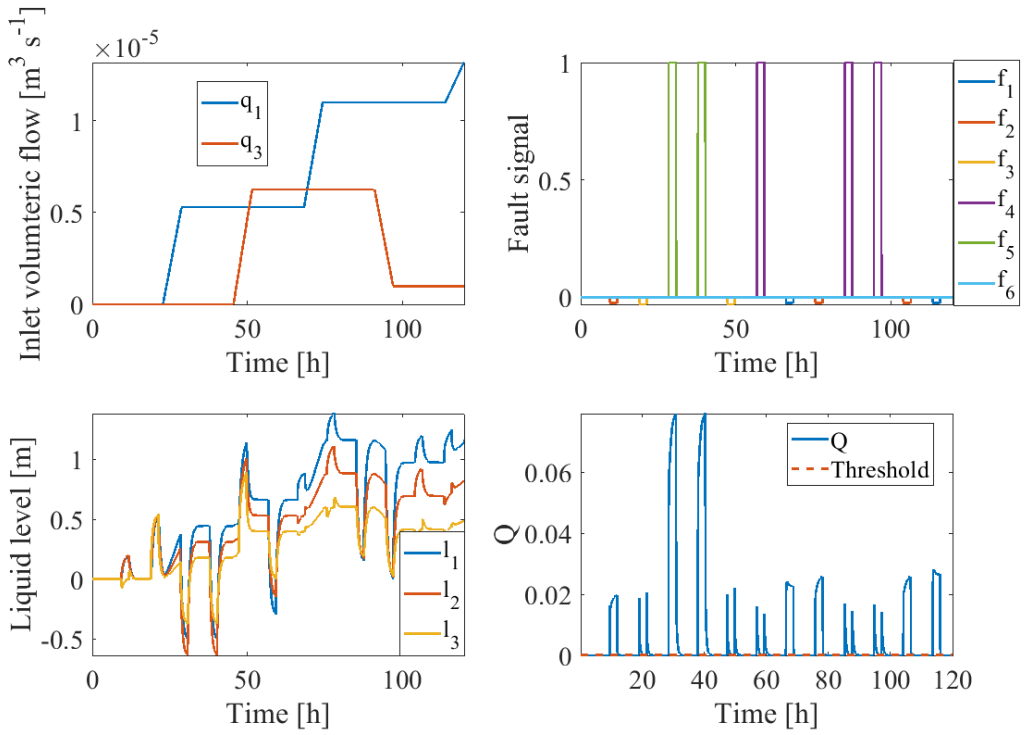

FIGURE 3.10: Process variables compared to their steady state values (volumetric flow-**upper left**, fault signals-**upper right**, liquid level-**lower left**) and monitoring statistic (**lower right**) results for the validation data

After the fault detection step was completed, the PC scores of the new faults have been compared with those contained in the fault library based on the Fréchet distance for identification. The recorded trajectories of the recorded faults are showcased (dots) after normalization and centering together with the original fault trajectories (continuous lines) recorded in the library. The identified and actual fault signals have been compared and the confusion matrix of the classification was calculated, the results are shown in Fig. 3.11. Note that while there were only 12 original fault input signals, responses of faults 3,4 and 6 count as two recognized alarms signals due to the bisection. The results show that the algorithm was capable of reliably differentiating between the various fault signals, while also recognizing each fault without false or missed alarms. The change of the recorded fault trajectories compared to those in the library is due to the change in operating point as seen in Fig. 3.10, regardless the dynamics and alignment of the changes in the PC subspace is consistent enough to recognize process abnormalities.

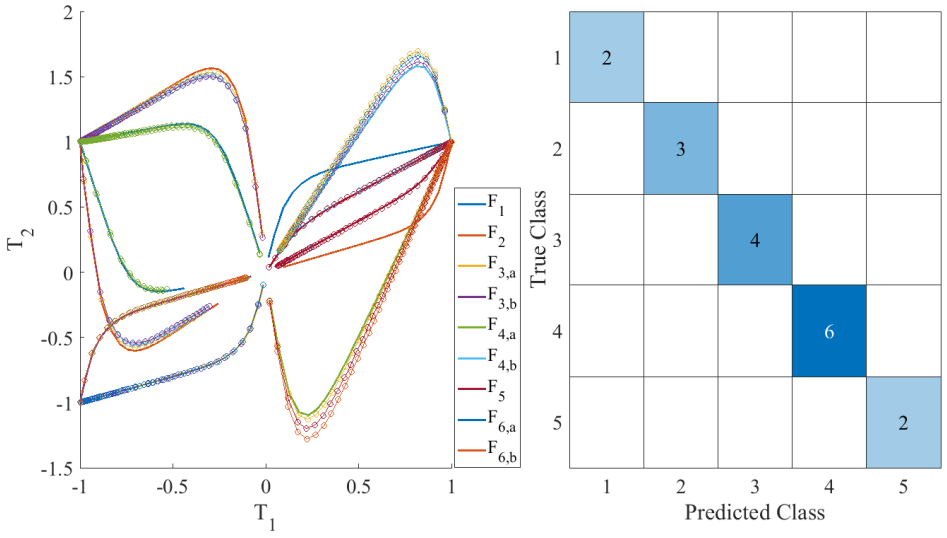

FIGURE 3.11: Recognized (dots) and prerecorded (continuous line) fault trajectories (**left**) in the 2D PC subspace and the subsequent confusion matrix (**right**) of the isolation step

To evaluate the robustness of the method, the time integrated FAR, MAR and macro averaged F_1 (MAF_1) score have been utilized according to Eq. A.1, A.2 and A.5. The metrics have been observed as functions of the set point changes of the two input variables, assuming a noise signal of Gaussian distribution affecting the measured level variables with a signal noise ratio of 30. The investigations have been made over a time interval of 1200 observation hours with 100 registered faults.

The results for the FAR and MAR metrics are shown on a heat map in Fig. 3.12.

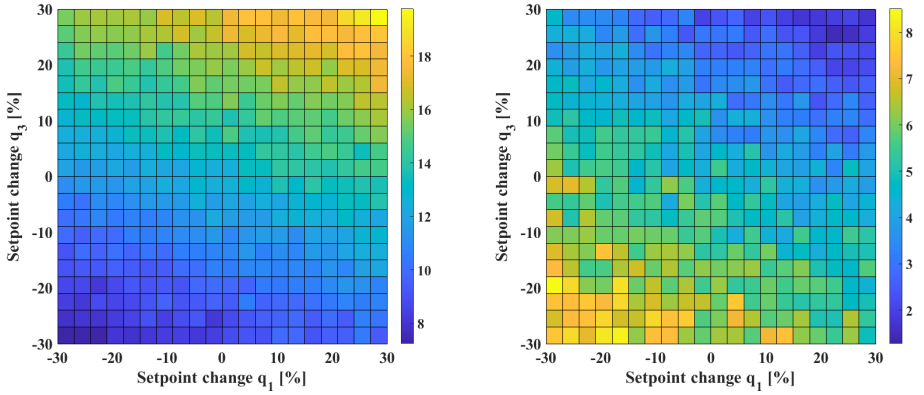

FIGURE 3.12: FAR (**left**) and MAR (**right**) metrics of the developed method as a function of set point changes compared to the steady state input values

The figure shows that, as expected, FAR and MAR are negatively correlated. When both input variables change in opposing directions, due to level equalization in the tanks, the overall

dynamics of the process do not change significantly and there is no great difference compared to steady state FAR and MAR. In cases where both input variables change in the same direction compared to the steady state conditions, either FAR and MAR steeply increase due to changing process dynamics, causing the fault response signal to be delayed (FAR increment) or decreasing in magnitude (MAR increment). When both inlet volumetric flows decrease MAR increases, the liquid levels decrease, the fault responses are smaller compared to the steady state levels as compared to higher liquid levels therefore many missed alarm responses are present. In the opposing case when inlet volumetric flow increases in both inputs the level changes due to faults are great, therefore the dynamics of the system slow down and false alarms increase.

The macro averaged F score of the isolation step is shown in Fig. 3.13 as a function of the input changes compared to their steady state values.

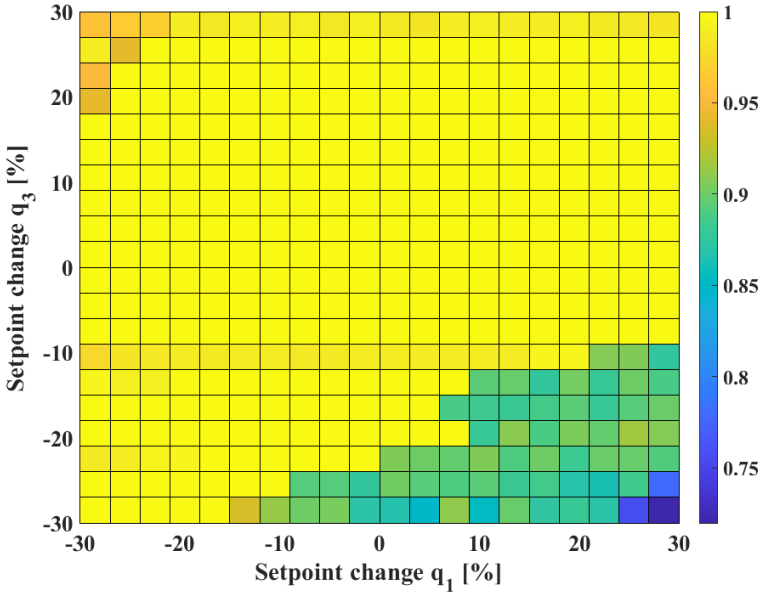

FIGURE 3.13: Macro averaged F_1 score of the fault isolation step as a function of set point changes compared to the steady state input values

The figure shows that the isolation process based on the Fréchet distance metric shows great fault isolation capabilities in a wide range around the set point (macro averaged F score close to 1) its capabilities only decreasing around the line with equation $q_3 = 0.5q_1 - 20$ and at the area close to 30 % increase in q_3 and 30 % decrease in q_1. Still, at its worst performance, the method has a macro averaged F score of around 0.75 when there is a 30 % increase in the value of q_1 and 30 % decrease in q_3 compared to their steady state input values. This

shows that the proposed isolation technique works reliably even for major set point changes, despite the nonlinear dynamics of the investigated system.

Additionally, the noise sensitivity of the technique was also evaluated. Utilizing set point changes of 5 % in both inputs q_1 and q_3 the signal-to-noise ratio (SNR) was adjusted during simulation tests to evaluate FAR, MAR and the macro averaged F_1 score of the classifier under different noise conditions. The definition of SNR for random signals is the ratio of the expected value of the set point signal, and the noise signal [104]. To perform the investigation, random noise with a Gaussian distribution was added to both measured outputs and inputs with a simulation timescale of 4800 hours and 400 fault instances. The FAR, MAR and macro averaged F_1 measures were evaluated as a function of the utilized SNR (between 10 and 100) and are displayed in Fig. 3.14 and Fig. 3.15 respectively.

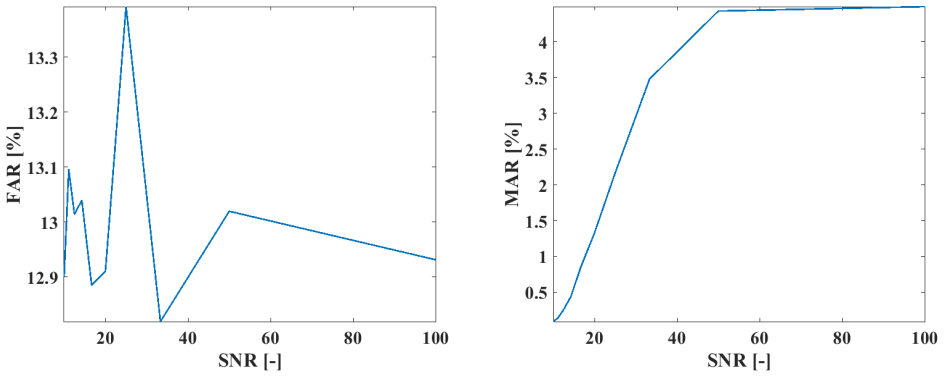

FIGURE 3.14: FAR (**left**) and MAR (**right**) metrics of the developed method as a function of different measurement signal-to-noise ratios

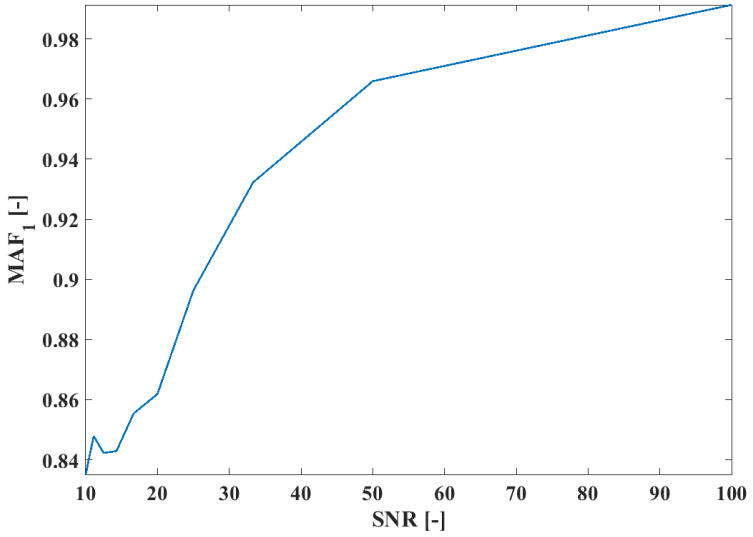

FIGURE 3.15: Macro averaged F_1 score of the fault isolation step as a function of different measurement signal-to-noise ratios

From Fig. 3.14 it can be seen that as SNR increases (the signal is more prominent compared to the noise) the MAR metric also steadily increases. This is because as the data becomes more noisy, alarms will be raised even if no faults are present (FAR) and the chance of faults being missed decreases. In case of FAR, clear trends could not be discerned at this point, but occasionally increasing FAR is noticed as SNR decreases. This is expected, as false alarms are likely to increase in number when more intense process noise is present within the data. Further investigations (up to SNR of 1) revealed that later on, FAR takes on a similar looking trend line to MAR but with opposite relation to SNR. In case of the macro averaged F_1 score, trends similar to MAR could be observed. As expected, the greater the signal-to-noise ratio, the more pure the fault trajectory data is and the easier the classification into fault classes becomes. With the decrease of SNR, the macro averaged F_1 score steadily decreases, reaching a score of 0.83 at SNR of 10, which corresponds to measurement noise which has an expected value of 10 % compared to the base signal. However, it must be noted that such extreme noise conditions are infrequent and already unacceptable for proper measuring equipment and with SNR between 50 and 100 (process noise between 1-2 % of measurement signal magnitude) the macro average F_1 score is between 0.97 and 0.998 pointing to significant isolation capabilities.

As a conclusion, it can be said that the detection and isolation method performs well for the

benchmark problem and showcased good robustness, sensitivity, and classification capabilities for the supervision of a nonlinear system despite being based on a linear PCA technique. This was explored by investigating the FAR and MAR metrics as well as the macro averaged F_1-score for the proposed scheme under a wide range of conditions. It can also be listed as an additional strength of the isolation method that it has the possibility to be extended to a variety of methods derived from PCA capable of handling various issues which would be difficult for conventional ML techniques, such as missing data during training or varying scales of data (MSPCA). The possibility of extending the method for nonlinear PCA variants is also promising for describing a wide range of dynamic processes and increasing isolation and fault detection capabilities further.

As a demerit, it must also be noted that the technique may suffer from the same issues as traditional PCA, such as its currently linear nature. The employed statistical test for FD is also a critical issue, as is the choice of the statistical confidence level, α due to the possibility of high FAR and MAR. We must also note that in this case the good isolation capabilities of the scheme could be due to the fact that dynamics of the process do not change rapidly when deviating from the set point, in systems with stronger nonlinearity the applicability of the isolation technique may become more limited.

In order to compile the possible merits and demerits of the proposed method, Table 3.2 contains a comparison of the proposed technique and standard FDI techniques found in literary sources based on general considerations for the evaluation of FDI methods. To summarize, the proposed technique presents a flexible and low computational cost alternative for FDI with proper sensitivity and robustness. Since the PCA technique may be extended to nonlinear approximations as well, handling of nonlinear systems is also a possibility. An issue may be the noise sensitivity of the method depending on the utilized statistics for the FD procedure; however, this may be circumvented through the proper optimization of statistic confidence thresholds.

TABLE 3.2: Comparison of the proposed method with other popular FDI approaches (+ indicating positive, − indicating negative qualities).

Consideration	**Model-Based Techniques**	**Neural Networks**	**Proposed Method**
Complexity	Requires deep mathematical and system knowledge to implement (−)	Easy implementation (+)	Easy implementation (+)
Requirements	Exact process model (−)	Abundance of reliable process data (−)	Abundance of reliable process data (−)
Adaptability to new faults	Easy adaptability (+)	Requires additional training to identify new fault classes (−)	Easy addition of new faults to the database after fault occurrence (+)
Computational load	Low computational cost (+)	Depending on the network structure computational cost may be high (−)	Low computational cost (+)
Design procedure	Straightforward & simple (+)	Great consideration has to be given to determine the optimal network structure (−)	Straightforward and simple (+)
Robustness against noise and disturbances	Robustness may be an issue for nonlinear systems (−)	Great robustness depending on the network structure (+)	Robustness is easy to adjust through the use of nonlinear PCA (+)
Sensitivity to faults	Great sensitivity (+)	Great sensitivity (+)	Sensitivity may be an issue based on the utilized statistic (−)

Chapter 4

Integration of risk factors into fault detection, minimization of superfluous alarm rate

In this chapter, I introduce a risk-based fault detection (FD) method for supervision of technological processes using a combination of dynamic principal component analysis (DPCA) for FD and a failure mode and effect analysis (FMEA) based Bayesian network (BN) for risk assessment [105]. The two methods work in parallel, utilizing each other's results to pinpoint the presence of abnormalities and the simultaneous estimation of risk associated with the abnormalities. Only safety-critical process states are highlighted through alarm signals, non safety-critical process states where faults are present are only shown by warnings. The method thus mitigates alarm floods by eliminating alarms for faults which hold little risk to the process performance and safety going forward.

4.1 Risk-based fault detection and alarm number reduction

In the past various techniques have been proposed for FD and their performance has been continuously enhanced since to minimize false alarm rate (FAR) and missed alarm rate (MAR) and allow for subsequent crisp fault detection using model [3], data [8] and qualitative knowledge-based [9] logic. While these techniques and specifically multivariate statistical process monitoring [55] methods among data-based techniques have adequate performance

for system supervision and great popularity in the FD community the problem with many FD methods as noted by multiple authors is the fact they usually do not take the risk associated with each fault into account [106].

Among the multivariate statistical process monitoring (MSPM) techniques the most popular, principal component analysis (PCA) based methods utilize the T^2 and Q statistics for FD and compare these metrics calculated from process data to predefined statistical thresholds to decide whether a sample can be categorized as normal or abnormal [76]. The performance of the FD method therefore is usually evaluated using only the FAR and MAR metrics. The issue with this approach is that since no risk is associated with the out-of-control process states in traditional MSPM FD alarms will be raised regardless of whether the detected abnormality is just a simple nuisance that holds no process risk or if it is a state that could cause severe damage when left unchecked [82]. Therefore, many nuisance alarms are raised which could lead to alarm floods in complex systems, especially when due to fault propagation other alarms are raised as well [83].

To circumvent these, methods have been born that take the risk of each indicated fault into account during the FD process through dynamic risk assessment (DRA), however the arsenal of techniques which utilize risk assessment in coordination with FD are still scarce [107]. Among the first instances of such methods was a technique which proposed a PCA model for the supervision of chemical processes and incorporated risk estimation using a quantitative risk assessment model. Using this technique, alarms were only raised when a fault was detected by the PCA metrics and the predicted risk exceeded a defined threshold [82]. Later on, self-organizing maps were utilized to address the FD problem of nonlinear systems. Using a probabilistic approach, faults were categorized into several classes based on severity and FD was performed while taking the risk into account as well [108]. Qualitative models have also become researched for the risk-based FD methodology, such as the use of the R-vine copula and the event tree methods for supervision of nonlinear and non-Gaussian processes [109].

The techniques for risk-based FD have become increasingly more researched and popular, as the previous examples show, but are still relatively few. While most methods propose risk estimation techniques which are in a manner related to traditional techniques of industrial risk assessment such as hazard and operability study (HAZOP) [5], event trees (ET) [110], fault trees (FT) [111] or failure mode and effect analysis (FMEA) [112] these methods are not intrinsically integrated into the framework and performed in a rigorous manner [82].

For example in the previously noted articles [82, 108, 106] the general definition of risk was formulated as a product of probability of a fault occurring which leads to an unwanted catastrophic event and the severity score assigned to each fault consequence as per Eq. 4.1, from which a dynamic risk profile for the process was calculated [113], this procedure and its basic logic is fairly similar to the calculation of risk priority numbers (RPN) in FMEA.

$$Risk(t) = Probability(t) \cdot Severity \tag{4.1}$$

The probability of fault occurrence leading to catastrophic events was fitted as a cumulative normal distribution function in these cases, with the probability of catastrophe increasing as the process variables deviate from their expected values. Severity scores were calculated based on the type of process variable deviating, with each process variable having an assigned severity parameter and the severity score being defined as a sum of the product of severity parameter and a function of the deviation of each variable from their normal value [106]. While the method proved applicable especially when combined with latent variable modeling techniques such as PCA [82] or self-organizing maps [108] where the latent variables were used for risk estimation, the approach has an issue in case of real-world industrial application.

Since the probability of fault occurrence which could lead to catastrophic results was fitted as a cumulative normal distribution function, the probability of faults leading to catastrophic events would change uniformly regardless of which variables deviated. From a general process perspective, it is obvious that the probability of fault occurrence which could lead to catastrophic results is not only dependent on the magnitude of process variable deviation from its normal state, but also on the type of process variables which deviated [113].

For example in industrial systems for safety critical process variables such as temperature or pressure often inherent safety protocols or fail-safes are in place which significantly lower the probability of catastrophic events from occurring even if due to some fault a critical process variable showed abnormal behavior [114]. Therefore, the probability of occurring safety critical events may not be properly characterized by simply observing the deviation of process variables from their normal states without taking the general construction of the system, the presence of fail-safes, inherent safety and possible fault propagation paths into account.

To overcome this issue, established risk assessment methods and models from the literature have been evaluated to propose hybrid techniques for more rigorous risk-based FD [115]. Based on previous trends the most popular methods for quantitative risk assessment are probabilistic graphic models such as dynamic event and fault trees, event sequence diagrams, Markov models [116], Monte-Carlo simulation [117], Bayesian networks, Petri nets [118] etc. to estimate the risk of certain system states under both static and dynamic conditions [119].

In recent years Bayesian networks (BN) have gained especially great popularity in the risk assessment community with many applications aiming to extend their applicability and combining them with previously established methods such as FMEA or ETs [120]. The allure of these techniques is a more rigorous way to estimate the probability of process risks than the traditional FMEA or HAZOP techniques and addressing the entirety of the system (fail-safes and components included) and taking possible failure propagation paths into account [120].

In light of this the key idea of this thesis point is to extend the framework of risk-based FD using a method based on dynamic principal component analysis (DPCA) and BN-FMEA-based risk assessment which can be used to give a more accurate estimate of process risk by taking fault propagation paths into account as well (fail-safes and inherent safety as well) when evaluating possible abnormal process states.

The authors utilize DPCA to characterize the observed process and produce indicators for the presence of process faults and risk events. After establishing the model under normal operating conditions, the presence of characteristic faults is observed and statistic indicators such as the Q statistic are calculated for the different fault scenarios. Parallel to the FD procedure a risk profile is observed for the system based on BN-FMEA. Severity scores are assigned based on the deviating principal components, detectability is evaluated using MAR metrics of the DPCA technique and probability of fault presence is evaluated using the BN.

The main contribution of our approach can be summarized in the following points.

- Development of a risk-based fault detection method which combines standardized expert knowledge (failure mode and effect analysis) with data-based techniques (Bayesian network) for risk assessment
- Mitigation of alarm floods through combination of risk assessment and fault detection

In the following, the mathematical formalization and background of the employed techniques is introduced in Section 4.2. The flowchart and general logic of the proposed algorithm is formalized is Section 4.3. Case studies for method evaluation are given in Section 4.4 including both a case study of an FD benchmark problem and a case study utilizing a dehydrogenation reactor of the liquid organic hydrogen carrier (LOHC) technology.

4.2 The proposed risk-based FD method and utilized techniques

In this section the basic techniques of FMEA and BN are introduced and formalized, subsequently the proposed technique utilizing the methods for risk-based FD is explained. The DPCA and base PCA algorithm are already introduced in Subsection 2.3.3.

4.2.1 Failure Mode and Effect Analysis

The traditional FMEA method is a "bottom-up" inductive logic-based procedure used to solve quality and reliability issues in the development stages of processes or later for risk assessment of already existing technologies [121]. Base FMEA is at the core of the method, this technique can be specified further to resolve specific issues related to safety and quality with a focus on process (Process FMEA or PFMEA), product design (Design FMEA or DFMEA), system functionality (Functional FMEA or FFMEA) and software issues (Software FMEA) [112]. The FMEA technique is based on the hierarchical decomposition of the system and identification of failure modes on the lowest possible indenture level. Subsequently, the effect of failure modes on the higher ordered subsystems is observed and iterated through them [122]. The FMEA analysis can be enhanced through a subsequent criticality evaluation of identified failure methods. The FMEA analysis should result in the following items:

- Systematic overview of possible failures
- Evaluation of failure impact on the system performance
- Identification of failure causes
- Quantitative evaluation of risks associated with each failure mode
- Specification of corrective actions for risk reduction

The FMEA procedure is initiated by consulting relevant professionals who have sufficient empirical and theoretical knowledge of the observed process. The specific topic of FMEA is established (the scope of the observed system) and system specifics such as system architecture, characteristics and functions are analyzed by the professionals. For a reliability and risk analysis, all possible system failure scenarios are evaluated. The failure modes are most commonly identified based on observed issues of similar systems, based on historical data or in case of novel processes system decomposition and analysis techniques, such as product-function analysis, function-component relationship analysis, function-structure relationship analysis, etc. during brainstorming sessions of the team of professionals. More rigorous methods such as fault tree (FTA) or event tree analysis (ETA) are also often times applied to perform the failure mode analysis [123].

After analyzing the failure modes and their propagation through the system, risk evaluation of each failure method is compiled. The risk evaluation of failure modes in FMEA can be performed in a wide manner of ways, with the most common being the application of the risk priority number (RPN) [122]. This involves either addition or multiplication of three factors associated with the failure mode, these being severity, occurrence and detectability. In order to express these scores, two main approaches are utilized, these being the expression of risk factors through fuzzy-logic, the other being the use of a 10-level integer scale to quantify each measure [121]. The RPN score using the latter solution is calculated traditionally as per Eq. 4.2.

$$RPN = Severity \cdot Occurrence \cdot Detectability \tag{4.2}$$

While the FMEA method is a great tool to ensure process quality and safety in the design stages of a system, it lacks capabilities for online diagnosis, therefore limiting its applicability for system supervision and decision-making [124]. Therefore, FMEA was often enhanced using more rigorous risk assessment techniques with a probabilistic framework to enable system diagnosis as well. A common approach is the integration of FMEA into Bayesian networks or Markov models [125].

4.2.2 Bayesian Networks

Bayesian networks (BN), are graphical models which are used for representing cause and effect relationships using Bayes' theorem of conditional probability [126].

BNs can be visually represented as directed acyclic graphs (DAG), where root nodes are root causes of a series of events linked by causality and leaf notes are the final possible consequences of the root event (an example is provided in Fig. 4.1).

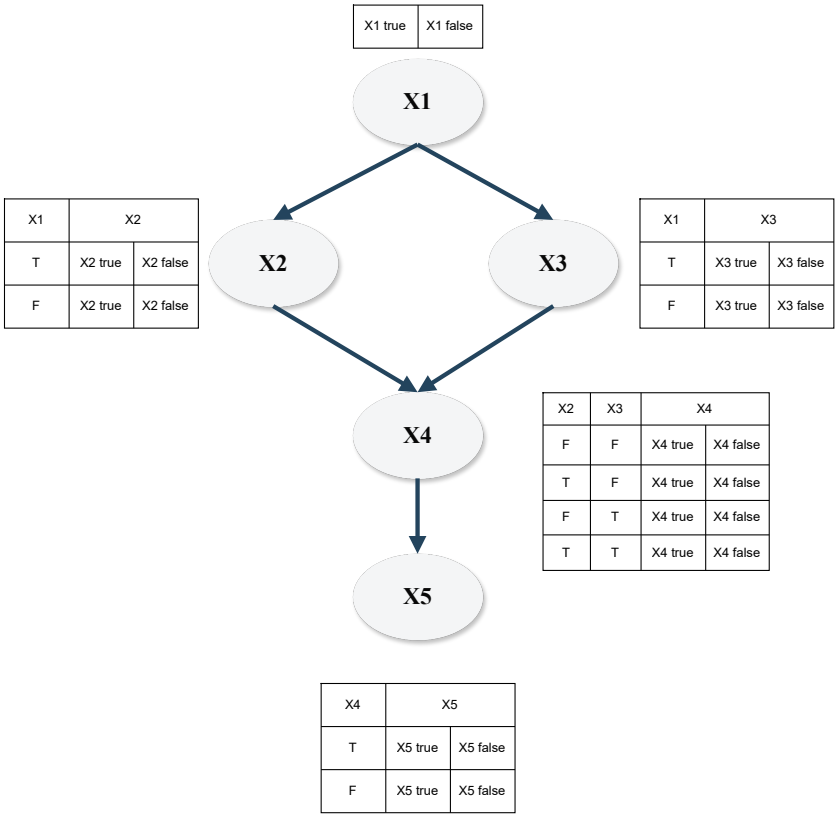

FIGURE 4.1: Example of a BN structure with 5 nodes that have binary states

The nodes of BN are linked trough conditional probability functions (CPF), in general the CPF can be a continuous or discrete probability distribution function, the former describing an infinite number of possibility values for process states for a node variable while the latter assumes only a certain amount of fixed probability values for the variable states. In the risk estimation state, the possible event states are usually discrete variables (for example "Is the i-th system component faulty? → the corresponding states can be "true" or "false"), here conditional probabilities determine each states' likeliness based on known event states within the DAG [127]. The individual CPFs of different states are summarized in conditional probability tables (CPT) describing the conditional dependence of all states of a node, given

all possible states of its parent nodes. To provide an example in Fig. 4.1 the CPTs are displayed next to each node, depicting the conditional probabilities of node states based on their parent nodes, binary states "True-T" and "False-F" are given for each node.

During the quantitative analysis of the net, the user wishes to estimate the probability of a given state of a variable in the BN through knowledge about the state of another observable variable by means of inference. For this the conditional dependence of the variables in the network has to be analyzed, we denote the CPF of a given variable x on another variable y as $CPF(x \mid y)$. For any given variable in the graph, the probability distribution of its states may be calculated using the probability distribution of its parent nodes' states through the underlying assumptions of conditional independence encoded in the graph using Eq. 4.3.

$$CPF(x_1, x_2, ..., x_i) = \prod_{j=1}^{i} CPF\left(x_j \mid pa(x_j)\right) \tag{4.3}$$

The sturcture of BN-s can be approximated using expert knowledge or data-based techniques, the same is true for the various CPFs and CPTs. In our work, the structure of the BN was based on the initial FMEA analysis of the system while the CPFs were approximated using maximum likelihood estimation [128] (where simulation data is available) and expert knowledge in cases which are not observed during the simulation.

4.3 The proposed technique for prediction of safety critical events

The outline of the proposed online supervision strategy is shown in Figure 4.2.

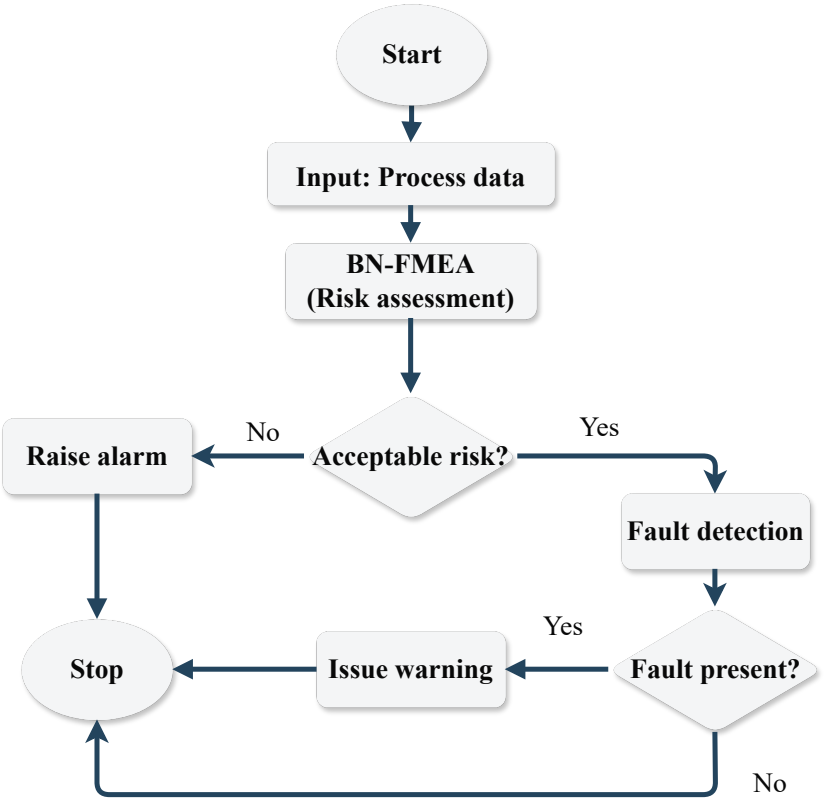

FIGURE 4.2: Flowchart of the proposed risk-based FD algorithm

To set up the procedure first, the structure of the system is evaluated through FMEA analysis. Possible failure modes are summarized, and operation data is acquired through the analysis, the resulting FMEA chart serves as a baseline for the BN structure. Generally the concept of inferring a BN from FMEA is not a novel idea, many approaches and tools have been proposed, yet the use of expert knowledge is the most basic solution to establish the subsequent BN [129]. In this work, the FMEA results are translated into BN and the CPFs are established using expert knowledge and maximum likelihood estimation using historical data where applicable. The DPCA model is established through a simulation framework, the symptoms of the BN-FMEA are associated with the process variables.

During the online supervision process, the real-time system behavior is observed, and risk assessment is performed by means of BN-FMEA and the risk level is estimated. Should the risk level exceed the acceptable range, alarms are instantly raised, while in case of no serious process risk the evaluation of the fault presence is performed. Detected faults with negligible process risks are analyzed and warnings are issued, but alarms are not raised, if no faults were present no actions are taken. As in general, due to behavioral changes within the system the FMEA analysis as well as the dependent BN model have to be updated. This could

be achieved using either the employment of dynamic FMEA techniques or regular system checkups.

4.4 Case study and method evaluation

The method is tested using data gathered from a three tank benchmark system and for a model of a dehydrogenation reactor utilized in the LOHC technology. The results are displayed in the following subsections.

In case of the three tank benchmark, the entire procedure starting from DPCA model development until the BN and FMEA establishment is thoroughly explained. In the LOHC case study the procedure is showcased, but the thorough procedure is not explained in detail as it is identical to the steps described in the three tank benchmark problem.

4.4.1 Case study of the three-tank benchmark problem

The capabilities for risk-based FD of the proposed method have been tested using data gathered from the a priori model of the already introduced three-tank benchmark system displayed in Figure B.1 displayed in Appendix B. The DPCA model for system supervision was taken from the established model in Chapter 3.

The FMEA analysis for the unit was performed with a focus on process functionality, the core was a PFMEA evaluation. Using the observed system in Fig. B.1 the six main failures used in the case studies were defined as root causes for the observable failure modes. The results of the initial PFMEA analysis for each system component are shown in Fig. 4.1. During the analysis, the following assumptions were made:

- The liquid stored in the tanks was water
- The system contains both liquid level and flow rate measurement sensors
- Failures of system components were accounted for, but no sensor failure was taken into account

The possible failures in this case are the degradation of valve flow coefficient due to fouling and leakages due to corrosion. Both issues can lead to abnormal level changes within the

tank. While valve fouling can decrease the flow rate between tanks leading to overflow, leakages result in direct material outflow from the tank. In both cases the end effect is water spill which can lead to human injury through various accidents. The evaluation of severity, observability and occurrence scores were discretized onto the traditional 10-scale FMEA, using the conditions and criteria displayed in [130].

TABLE 4.1: FMEA table of the three tank benchmark system

Fault root cause	**Function**	**Potential Failure Mode**	**Potential Cause of Failure**	**Failure Consequences**	**Process Supervision**	**Recommended Actions**	**Severity score**	**Detectability score**
Valve	Flow rate control	Decreased flow rate	Valve fouling	Overflow, Human injury	Flow rate sensor	Valve Cleaning	2	2
Tank	Liquid containment	Leakage	Corrosion	Human injury	Liquid level sensor	Tank welding	3	4

Based on the analysis, a preliminary BN was established to model the process. The graphical representation of the BN is shown in Fig. 4.3. The model was developed using the results of the FMEA analysis as well as expert knowledge and process data. The connections between the observed variables (in this case the liquid levels in the tanks) and the fault scenarios were established using historical data through process simulation of 7200 hours, with a data set containing 100 set point changes and 500 fault scenarios, including simultaneously occurring fault instances. Since each valve and leakage failure mode has the same associated severity and detectability scores, the individual valve and leakage failures ($f_1 - f_6$) were not represented. Using the historical data obtained through the simulations, the CPTs of the liquid level values associated with valve fouling and leakage scenarios were calculated using the maximum likelihood estimation algorithm (MLE) [131]. The probability of valve fouling, leakage and the conditional probability of human injury could not be estimated as no historical data was available to the authors, therefore the authors utilized expert knowledge to give estimates for the probabilities.

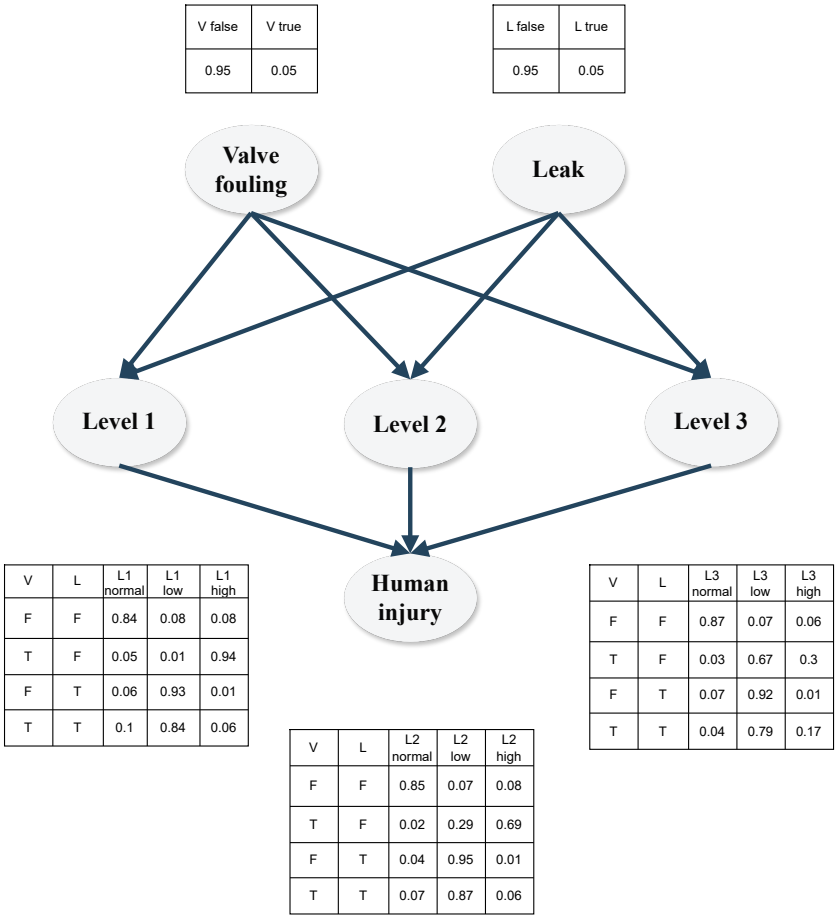

V false	V true
0.95	0.05

L false	L true
0.95	0.05

V	L	L1 normal	L1 low	L1 high
F	F	0.84	0.08	0.08
T	F	0.05	0.01	0.94
F	T	0.06	0.93	0.01
T	T	0.1	0.84	0.06

V	L	L2 normal	L2 low	L2 high
F	F	0.85	0.07	0.08
T	F	0.02	0.29	0.69
F	T	0.04	0.95	0.01
T	T	0.07	0.87	0.06

V	L	L3 normal	L3 low	L3 high
F	F	0.87	0.07	0.06
T	F	0.03	0.67	0.3
F	T	0.07	0.92	0.01
T	T	0.04	0.79	0.17

FIGURE 4.3: BN for risk assessment of the three tank system

The valve fouling and leak instances both have two possible states "False-F" and "True-T", while the liquid level states can be "Low-L", "Normal-N" or "High-H". The state of the liquid level scores was assigned using Eq. 4.4, where $mean(l_i)$ and $std(l_i)$ are the mean and standard deviation of the respective i-th liquid level over the simulation interval and $l_i(t)$ is the i-th liquid level at a given time stamp t.

$$State_{l_i}(t) = \begin{cases} L & l_i(t) < mean(l_i) - std(l_i) \\ N & \text{if } mean(l_i) - std(l_i) \leq l_i(t) \leq mean(l_i) + std(l_i) \\ H & \text{otherwise} \end{cases} \tag{4.4}$$

Subsequently, the risk profile of each failure mode could be continuously calculated as a function of time through Eq. 4.2. Since the severity and observability of both faults modes is known a priori and static, the time dependent part of the RPN score is the probability of a fault mode occurring. Using the BN, the risk of valve fouling and leakage are constantly

calculated using the process variables. Thus, for each failure mode an RPN risk profile can be observed and an acceptable RPN threshold can be given. In the following, the results of the method for the three tank system are shown through a case study with a timescale of 300 hours and 5 simulated fault scenarios.

Fig. 4.4 shows the changes in the input volumetric flow of the system as well as the values of the fault signals over the observation period. Also displayed are the changes of liquid level, compared to their steady-state values, and the values of the Q-statistic for FD.

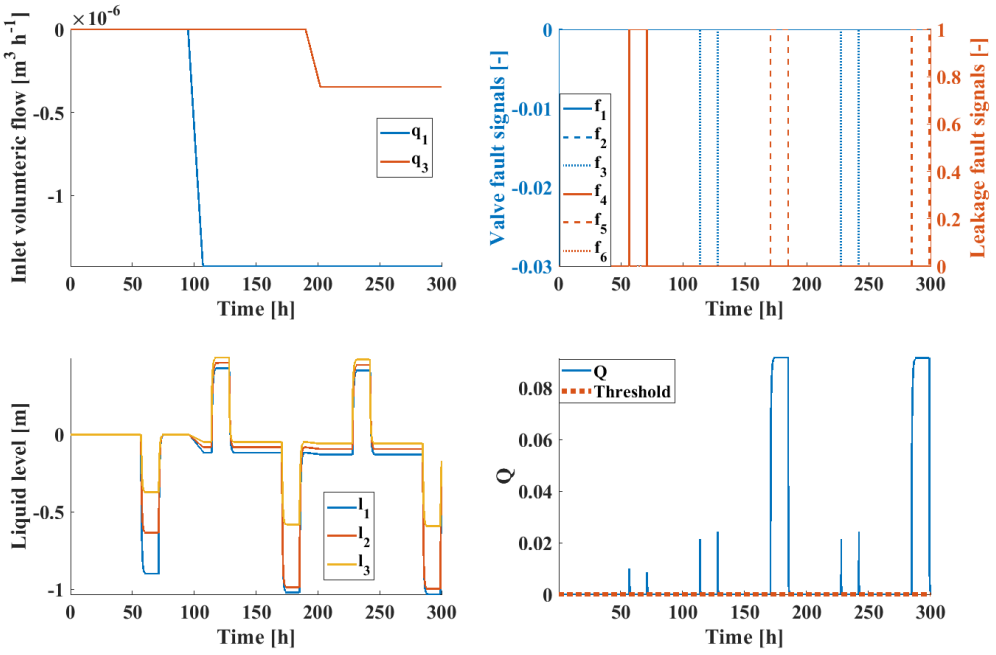

FIGURE 4.4: Results of DPCA FD in the three tank benchmark problem showcasing system variables (inlet volumetric flow-**top left**, fault signals-**top right**, liquid levels-**bottom left**) and Q-statistic scores (**bottom right**)

It can be seen that the greater values of the Q-statistic correspond well to the fault signals. The warning signals of FD, seen in Fig. 4.5, when the Q-statistic exceeds the statistic limit correspond to the fault signals.

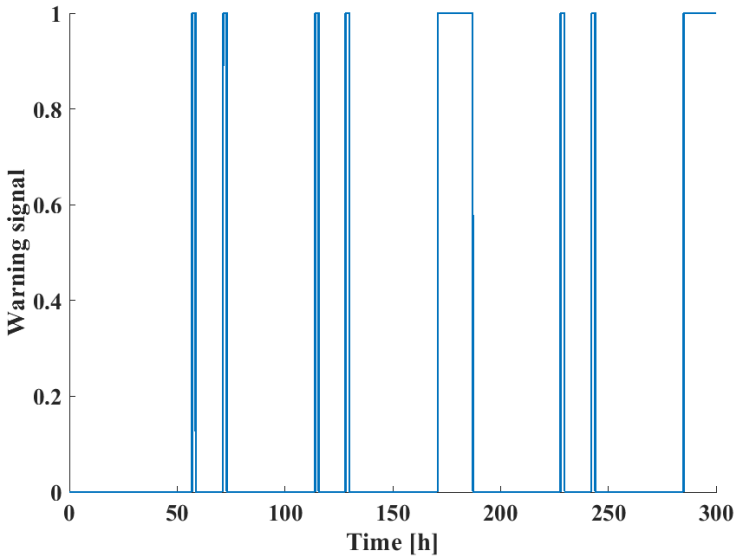

FIGURE 4.5: Warning signals of DPCA FD in the three tank benchmark problem without risk assessment

After running a simulation of 10000 hour time with 1000 randomly generated fault signals and 50 set point changes the FAR and MAR values were estimated to be 1.7 and 12.9 % respectively.

Using the values of the liquid levels, the probability of failure modes was calculated using the BN structure of Fig. 4.3. The resulting probabilities are shown as a function of time in Fig. 4.6. When comparing Fig. 4.6 with the fault signals in Fig. 4.4 it can be seen that both leakages and valve fouling can be reliable identified using the BN, in case of leakages the distinction is almost perfect, in case of valve fouling instances of leakages also result in small probability values of valve fouling but the actual valve fouling events possess significantly higher probability scores.

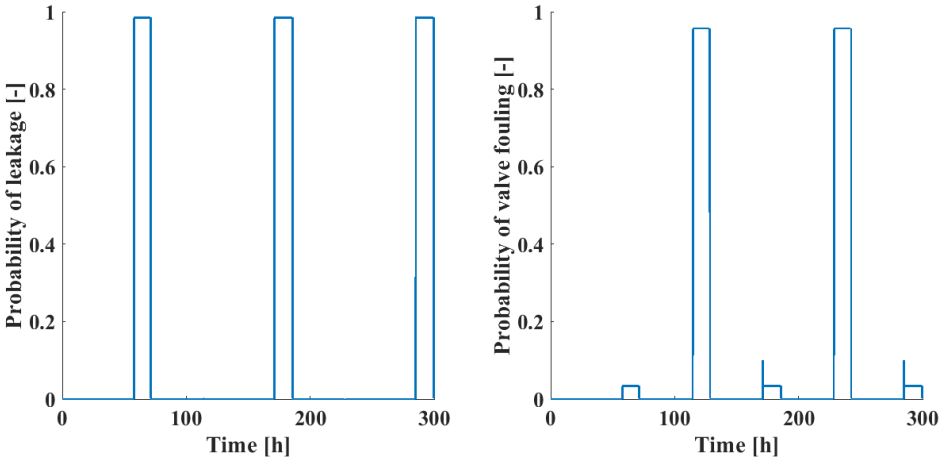

FIGURE 4.6: Probability of leakage (**left**) and valve fouling (**right**) modes in the three tank benchmark problem

The RPN scores as a function of time are shown in Fig. 4.7, for both failure modes. In case of valve fouling the low probability events which belonged to leakages induce no great differences in the final RPN score, actual valve fouling events are characterized by the maximal possible RPN for this failure mode (40). In case of leakages, the accurately identified leakage events all achieve their maximum RPN value (120). The RPN threshold for this application is also shown, it was chosen as 100.

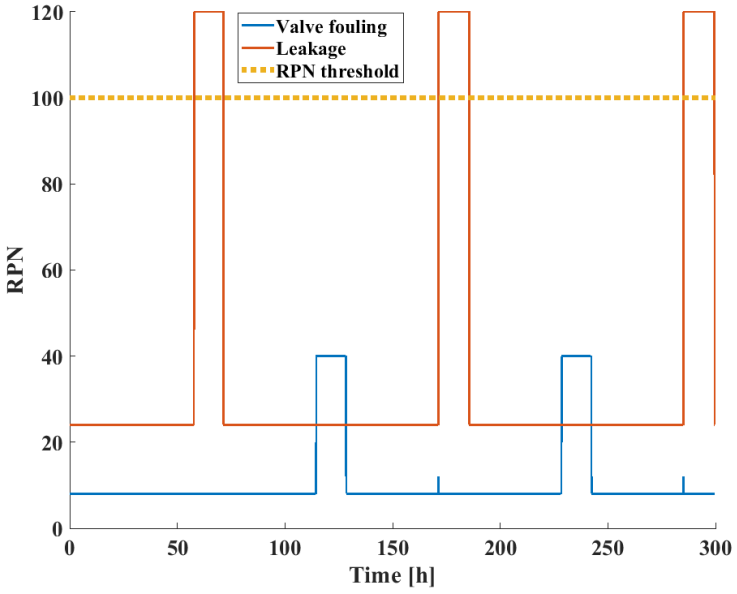

FIGURE 4.7: RPN scores of failure modes in the three tank benchmark case study

Finally, the actual alarm signals are shown in Fig. 4.8, taking both process risk and FD results into account.

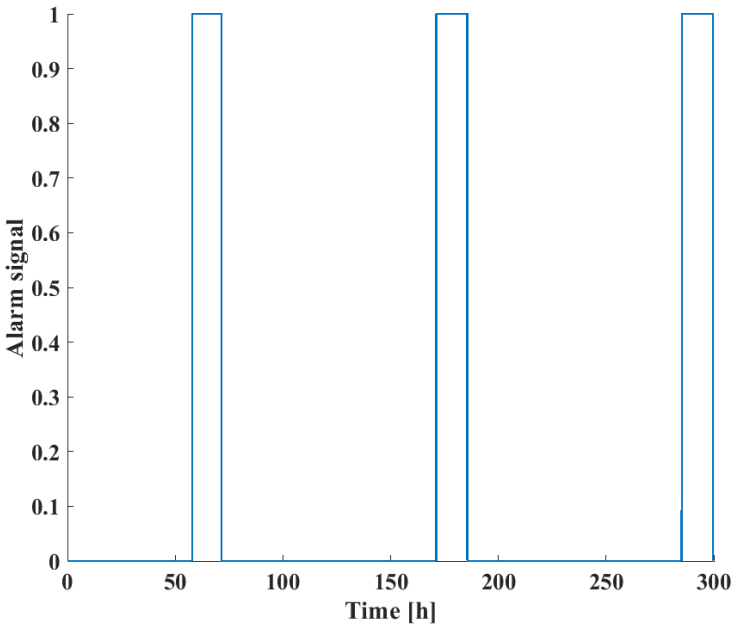

FIGURE 4.8: Alarm signals in the three tank benchmark case study, taking both process risk and FD results into account

When compared with the warning signals in Fig. 4.5 it can be seen that while all fault instances may be reliably detected using the DPCA technique the FMEA-based BN risk analysis was able to sort out safety critical events which require the immediate attention of operators and possible shutdowns of the system to prevent accidents in the technology.

4.4.2 Case study of a dehydrogenation reactor

The LOHC technology is a promising industrial process to ensure the future of the hydrogen-based economy [132]. One of the critical questions of hydrogen-based energy involves the safe and economically sustainable transport and storage of hydrogen during its lifecycle, since hydrogen is a low density and highly explosive gas [133]. Various solutions have been proposed for this problem, such as binding hydrogen to metal-hydrides or storing hydrogen as a high pressure gas or in a liquified state. As an alternative to these techniques, the LOHC process for hydrogen transport and storage involves chemically binding hydrogen during a reaction to a liquid organic carrier molecule for safe transportation which can be economically beneficial as it allows storing hydrogen at ambient conditions [132]. The transport of

hydrogen during this procedure is based on two-steps, the first involves binding of the hydrogen (hydrogenation), into the LOHC molecule, the subsequent second step is the release of hydrogen (dehydrogenation) at the site of use.

In this case study, we have studied the dehydrogenation step of an LOHC reactor with methyl cyclohexane (C_7H_{14} from now on MCH) as a carrier molecule. During the dehydrogenation step, the transported hydrogen (H_2) is removed from the carrier in a heterogeneous catalytic reaction leading to the formation of toluene (C_7H_8 from now on TOL) and H_2 [134]. The formula of the reaction is shown in Eq. 4.5.

$$C_7H_{14} \rightarrow C_7H_8 + 3H_2 \tag{4.5}$$

In this study, kinetics of the reaction were assumed to follow the Langmuir-Hinshelwood-Hougen-Watson (LHHW) kinetics, which is suitable for heterogeneous reactions in presence of a solid catalyst [135]. Parameters of the kinetic equation were identified using experimental data from a laboratory-scale plug flow dehydrogenation reactor by Dr. Lajos Nagy, an associate professor at the Department of Process Engineering [136]. During the investigations, Clariant brand EleMax H catalyst (spherical 1.8 mm diameter, platinum, and palladium on aluminium-oxide carrier) was utilized for dehydrogenation. The reaction rate (rr) was approximated using the previously mentioned LHHW kinetic model, the form of which is expressed in Eq. 4.6.

$$rr = \frac{k\left(\frac{T}{T_0}\right)^n e^{\frac{-E_a}{R}\left(\frac{1}{T}-\frac{1}{T_0}\right)} \cdot \left(k_1 \prod_{i=1}^{N} c_i^{\alpha_i} - k_2 \prod_{j=1}^{N} c_i^{\beta_j}\right)}{\left[\sum_{i=1}^{M} K_i \left(\prod_{j=1}^{N} c_j^{\nu_j}\right)\right]^m} \tag{4.6}$$

Parameters of the driving force (k_1, k_2) and adsorption phenomena (K_i) were described as functions of temperature (T) and fitted using the form seen in Eq. 4.7 for N number of components with M adsorption terms.

$$A + \frac{B}{T} + C \cdot ln(T) + DT \tag{4.7}$$

To develop a model of the system, the kinetic parameters of reaction rate were identified using experimental data gathered from a laboratory scale pilot dehydrogenation reactor. The

construction of the catalytic bed within the pilot reactor as well as catalyst loading parameters are displayed in Fig. 4.9. The figure shows the location of the catalyst as well as the heating sections of the unit ($F1-F4$) along with the temperature sensors and their positions compared to the reactor inlet in mm-s ($T1-T4$).

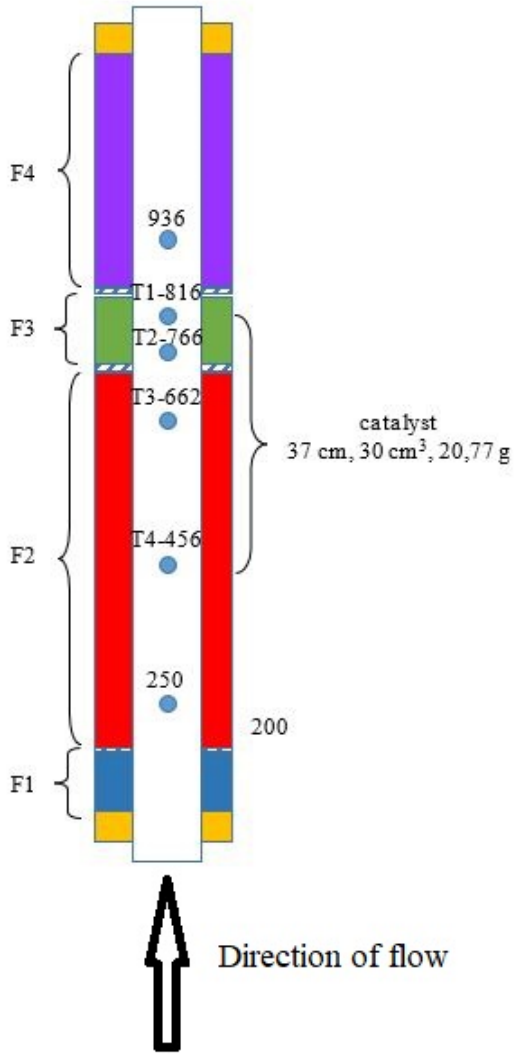

FIGURE 4.9: Layout of the pilot reactor catalytic bed

The kinetic parameters were obtained by developing a model of the plug flow reactor in Aspen Plus V11 and utilizing the LHHW kinetic described in Eq. 4.6 to calculate the steady-state conversion of methyl-cyclohexane along the catalytic bed. After combining the Aspen model with MATLAB, the kinetic parameters were found using the method of interior points by minimizing the sum of squared errors between measured and predicted conversion values. The

fitting was conducting using a total of 38 experimental cases with varying reaction temperature and pressure conditions, as well as methyl cyclohexane and hydrogen feed ratios. The measured and estimated steady-state conversion values of methyl cyclohexane are shown using a predicted vs actual plot in Fig. 4.10 along with the R^2 score of the fit.

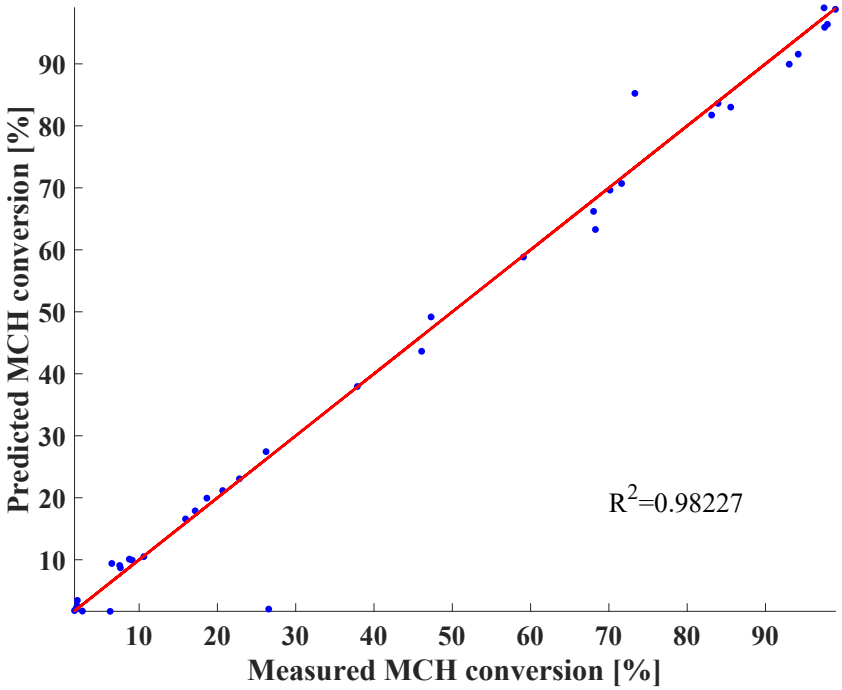

FIGURE 4.10: Measured vs estimated conversion of methyl cyclohexane of the fitted kinetic model

In our case study, we utilized the obtained kinetic model alongside a simplified structure of the dehydrogenation system for dynamic case studies. The assumed layout of the studied unit is displayed in Figure 4.11. The reactor is fed H_2 and MCH, the gas streams are mixed before entering the system in the static mixer unit (1.) in which their concentration ratio is controlled. After creating the proper mixture, the gas stream is heated in a heat exchanger (2.) to the temperature of the operating point before entering the reactor (3.). The reactor is an adiabatic plug flow reactor where the dehydrogenation process takes place, after exiting the reactor the temperature (4.) and concentration of H_2 and MCH in the outlet stream are measured using a sensor unit (5.).

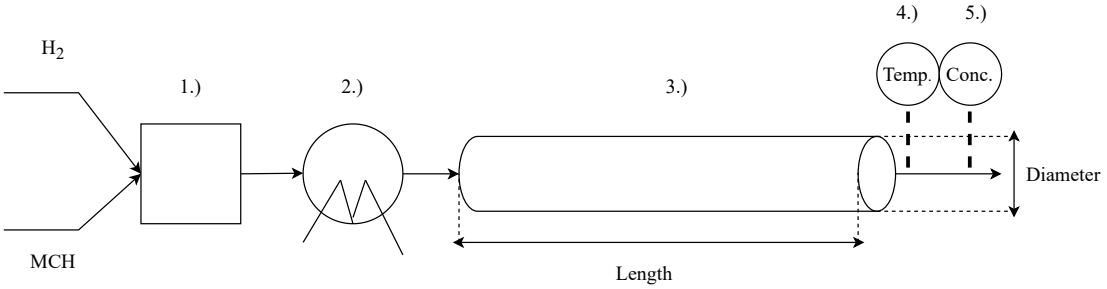

FIGURE 4.11: Simplified layout of the reactor system

The constructional parameters of the pilot reactor such as length, diameter, cross-section area and volume are shown in Table 4.2.

TABLE 4.2: Geometrical parameters of the reactor

Construction parameter	Value
Length [m]	$4.5 \cdot 10^{-1}$
Diameter [m]	$1.4 \cdot 10^{-2}$
Cross-section [m^2]	$2.3 \cdot 10^{-4}$
Volume [m^3]	$1.02 \cdot 10^{-4}$

Observed variables within the reactor were the concentration of MCH, H_2 within the feed as well as the inlet temperature T_{in}, the concentrations of the components at the outlet as well as the outlet temperature T_{out}.

Using the identified kinetic parameters, a dynamic first principle model for the system was developed. The flow regime was approximated as being an ideal plug flow. During the calculations of energy and component mass balance, convection (in the longitudinal direction) and source terms due to reaction have been accounted for. Under the above assumptions, the component mass and energy balances for the unit were given as a system of partial differential equations shown in Eq. 4.8.

$$\begin{aligned} \frac{\partial c_i}{\partial t} &= -v_x \frac{\partial c_i}{\partial x} + R_i \\ \frac{\partial T}{\partial t} &= -v_x \frac{\partial T}{\partial x} + \frac{\sum_{i=1}^{N} \Delta H_{R,i} r_i}{\rho c_p} \end{aligned} \tag{4.8}$$

In the equation c_i refers to the concentration of the i-th component, v_x is the flow velocity in the longitudinal direction within the reactor, R_i is the reaction source term for a specific component, $\Delta H_{R,i}$ refers to the reaction heat of specific reactions taking place, ρ and c_p are the density and heat capacity of the medium within the reactor.

The mathematical model of the system was solved using MATLAB R2020b, with the appropriate initial and boundary conditions. The initial (x, $t = 0$) and boundary($x = 0$, t) conditions as well as the parameters of the material within the unit are seen in Table 4.3, where q is the inlet volumetric flow rate of the feed. The heat capacity and density of the material was studied as a function of temperature, and it was found that in the investigated regime the material qualities showed no significant changes. In light of this, both density and heat capacity of the material system were assumed to be constant in regard to temperature and only changed depending on the mixture composition.

TABLE 4.3: Initial and boundary conditions as well as material parameters within the unit

Boundary conditions	Values	Initial conditions and material parameters	Values
q $[m^3\ s^{-1}]$	$5.5 \cdot 10^{-6}$	c_{MCH} $[mol\ m^{-3}]$	0
v $[m\ s^{-1}]$	$3.5 \cdot 10^{-3}$	c_{TOL} $[mol\ m^{-3}]$	0
c_{MCH} $[mol\ m^{-3}]$	12	c_{H_2} $[mol\ m^{-3}]$	0
c_{TOL} $[mol\ m^{-3}]$	0	T $[K]$	593
c_{H_2} $[mol\ m^{-3}]$	3	ρ $[kg\ m^{-3}]$	Mixture formulae
T [řC]	593	c_p $[J\ kg^{-1}K^{-1}]$	Mixture formulae

In the following, the application of the proposed method for the LOHC case study is discussed. An FMEA analysis was initiated to pinpoint safety critical failure modes of the system, during the analysis the following assumptions have been made:

- The system contains outlet temperature and concentration sensors, faults in the sensors have not been taken into account during the FMEA analysis
- A heat exchanger is present at the inlet of the unit which heats the inlet mixture to the desired temperature, no heat exchanger is present however along the length of the reactor

In the light of these assumptions, the FMEA table is shown in Fig. 4.4.

TABLE 4.4: FMEA table of the LOHC benchmark system

Fault root cause	**Function**	**Potential Failure Mode**	**Potential Cause of Failure**	**Failure Consequences**	**Process Supervision**	**Recommended Actions**	**Severity score**	**Detectability score**
Heat exchanger	Temperature control	Abnormal temperature profile	Heat exchanger fouling	Explosion, catalyst fouling	Outlet temperature sensor	Heat exchanger cleaning, process shutdown	9	2
Mixer	Inlet concentration control	Abnormal inlet concentration profile	Valve sticking	Explosion, product loss	Inlet composition sensor	Shutdown, valve change	10	4

The characteristic safety indicators of the process are the changes within the mixture temperature and the concentration of hydrogen and MCH. Thus, the risk level of the process is determined based on the deviation of these three variables. The root causes for the deviations include the failure of the process heat exchanger due to fouling which causes deviation of process temperature from its nominal values, this in turn can lead to catalyst deactivation within the reactor unit.

In case of abnormal MCH or hydrogen concentrations being simultaneously present due to mixer control failure, this could lead to possible explosions. The BN established through the FMEA analysis is shown in Fig. 4.12

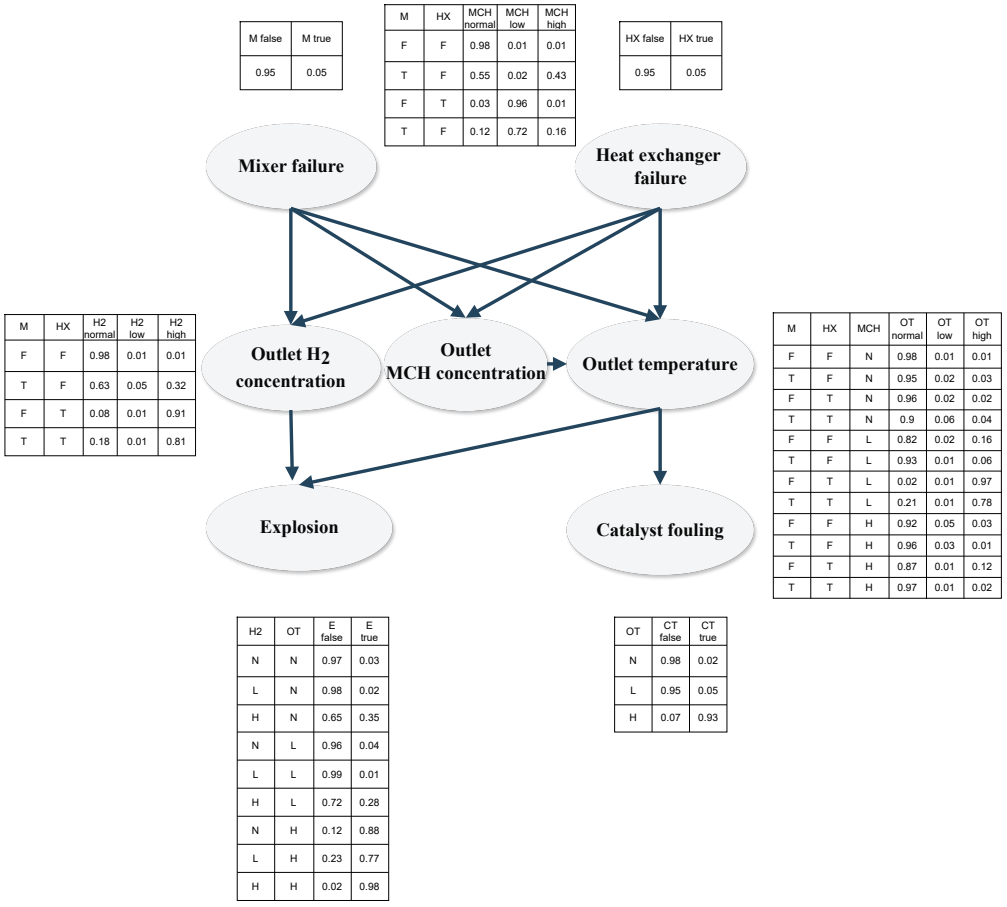

FIGURE 4.12: BN for risk assessment of the LOHC dehydrogenation reactor

Mixer failure and heat exchanger failure as well as explosion and catalyst fouling have two possible states "False-F" and "True-T" respectively, the CPT-s of these occurrences, similarly to the previous instance have been filled out using expert knowledge as no process data was initially available. In contrast to this, the relationship between the failure modes and the failure symptoms (inlet concentration and outlet temperature deviation) have been filled out using simulation case studies as before through the use of maximum likelihood estimation. The failure symptoms have three possible states "Normal-N","Low-L" and "High-H" respectively which were determined similarly as Eq. 4.4.

After training the DPCA model using observation data of the process obtained for 1000 hours using a set of 500 observed process faults and 100 set point changes, the FMEA-based BN was utilized to simultaneously detect faults and observe process risks. There are three distinct types of process faults, $f_{1,MCH}$ being the fault of the mixer causing changes within the MCH inlet concentration, f_{1,H_2} is the change in the inlet H_2 concentration due to mixer failure and f_2 is the fault of the heat exchanger resulting in abnormal outlet temperature.

The steady-state concentration and temperature profile of the stream exiting the unit is shown in Fig. 4.13 under the conditions given in the Table 4.3.

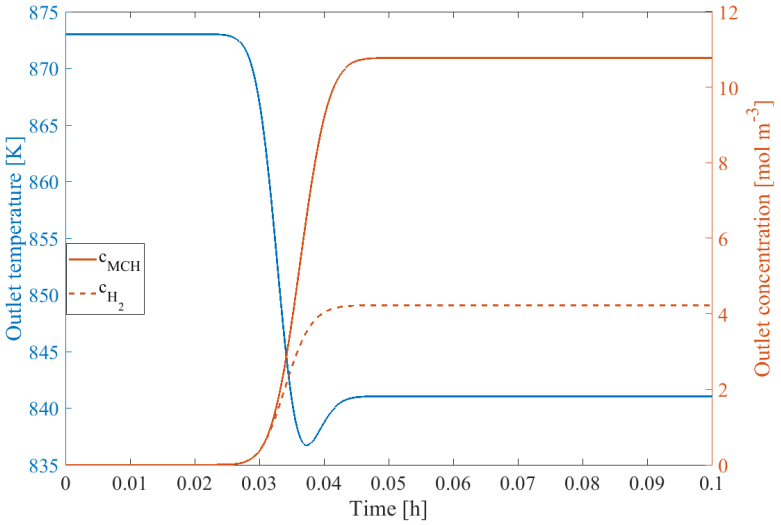

FIGURE 4.13: Steady-state operating point of the LOHC technology under the conditions in Table 4.3

The changes within the steady-state boundary conditions and the possible fault signals are shown in Fig. 4.14 under an investigation of 1 hour simulation time with 5 set point changes and 5 fault signals. It can be seen that all faults could be isolated using the Q-statistic within reason.

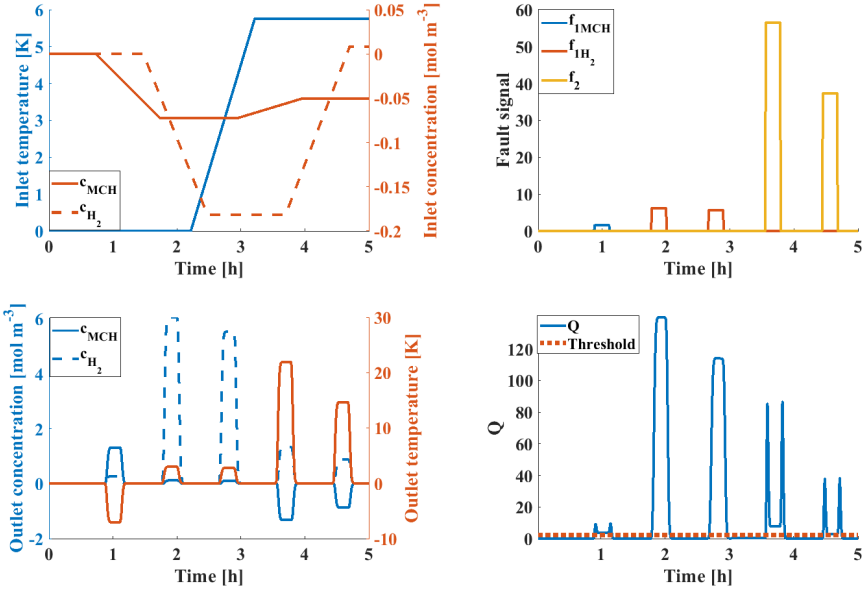

FIGURE 4.14: Fault detection procedure of the LOHC process, operating point changes (**top left**), fault signals (**top right**), system responses (**bottom left**) and Q-statistic (**bottom right**)

The warning signals due to fault presence are shown in Fig. 4.15, the warning signals correspond to the fault presence.

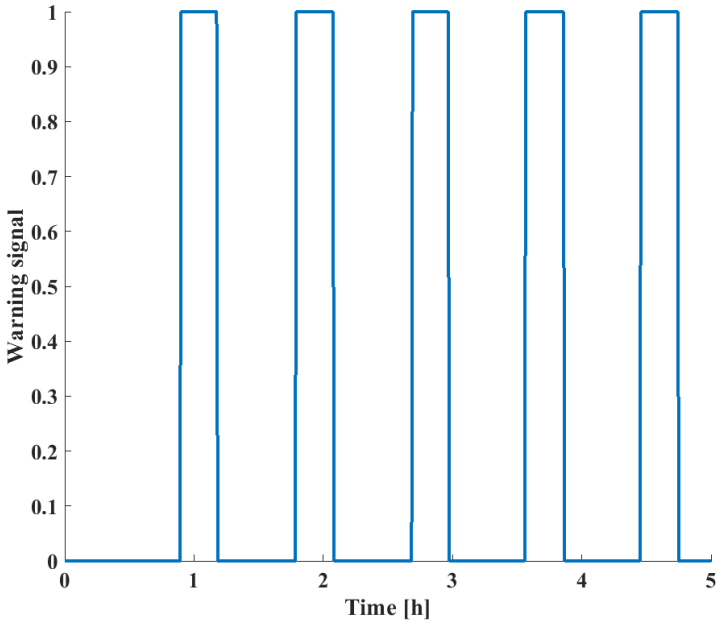

FIGURE 4.15: Warning signals given based on the DPCA FD procedure

The risk of each failure mode was calculated using the trained BN, the results for both heat exchanger and mixer failure are displayed. The probability of each failure mode as a function of time is displayed in Fig. 4.16.

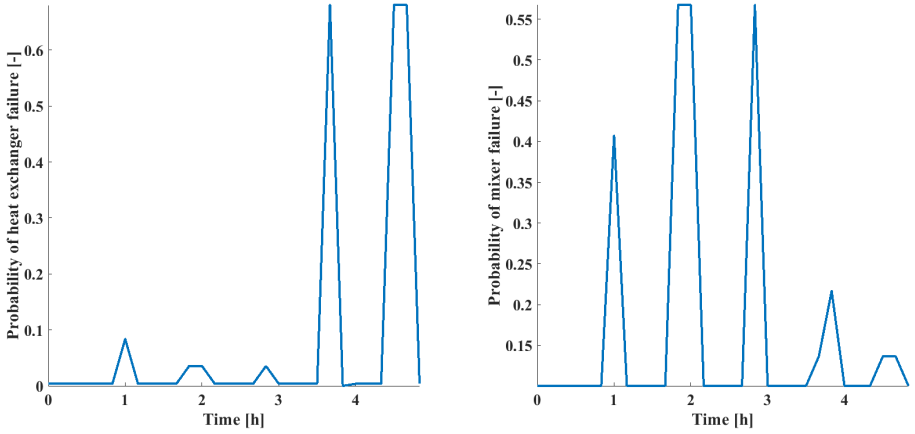

FIGURE 4.16: Probability of heat exchanger (**left**) and mixer (**right**) failure modes as a function of time

The corresponding RPN scores are shown in Fig. 4.17.

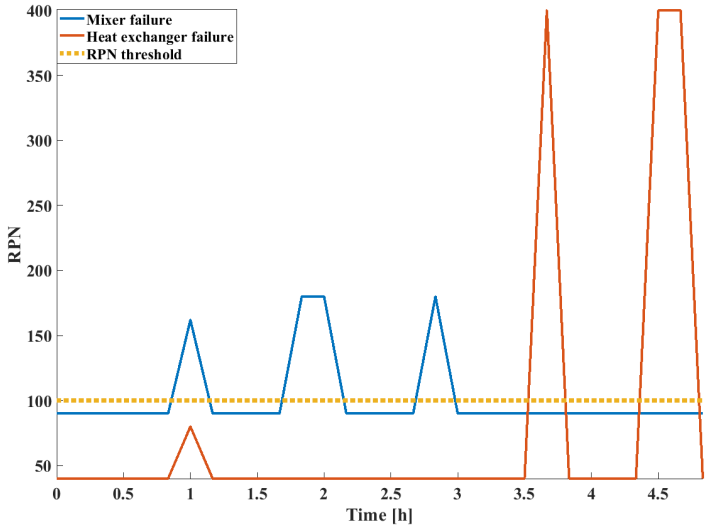

FIGURE 4.17: RPN score as a function of time

Finally, the alarm signals based on the RPN score are shown in Fig. 4.18.

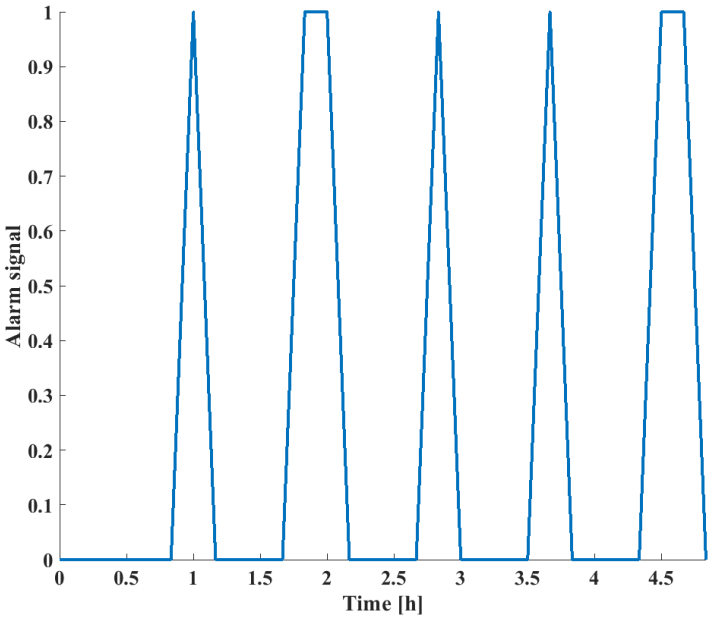

FIGURE 4.18: Alarm signals as a function of time for the LOHC reactor

Comparatively, it can be seen that the change of RPN scores of different failure modes correspond to the actual failure scenarios shown in Fig. 4.14. The RPN scores are defined by the extent of deviation of given process variables from their expected steady-state values, in this case all three process faults carried significant risks however as seen in Fig. 4.8 when

non safety-critical faults are present they are eliminated by the RPN screening. This way the FD capabilities of the system are not decreased since warnings will indicate fault presence, however alarm floods can be prevented as only critical failures are highlighted.

This was tested in the case of both studies, in both instances 10 000 fault random fault signals have been generated and the alarm and warning numbers were compared. In case of the three tank system the ratio of alarms to warnings was 0.63, with a MAR of 12.5 %, for the LOHC example the alarm to warning ratio was 0.89 with a MAR of 4.3 %. In both instances the number of alarm signals was significantly decreased, only safety-critical faults were highlighted while faults which posed no significant risks were effectively filtered out as warnings.

4.5 Conclusion

In this chapter a risk-based fault detection (FD) method which utilizes dynamic principal component analysis for FD and a Bayesian network (BN), constructed using failure mode and effect analysis (FMEA) as a risk assessment tool was introduced.

The method was used for online supervision of systems and was showcased using a three tank benchmark model and the model of a laboratory scale reactor used during the dehydrogenation step of the liquid organic hydrogen carrier (LOHC) technology.

In both cases, the method managed to effectively reduce the number of process alarms by filtering out non safety-critical process faults, thus reducing the possibility of alarm floods. The reduction of superfluous alarm signals was between 11 and 37 % respectively for the investigated case studies. Compared with previously introduced methods, the technique has the advantage of being based on standard risk assessment techniques (FMEA) which is widely available for industrial applications. Additionally, compared to previous works in risk-based FD, the method takes fault propagation paths and system architecture into account for risk assessment through the BN.

On average, the use of the technique reduced the number of raised alarms by 20-30 % in the observed case studies while being sensitive enough to pinpoint all fault presences.

Chapter 5

Reduced models for training fault detection methods of distributed parameter systems

In the third chapter, my goal was to develop models with reduced computational loads to facilitate fault detection in complex, distributed parameter systems (DPS) [137, 138, 139]. DPS are systems where spatio-temporal dynamics can be observed, meaning that variables change both as function of time and spatial coordinates within the observed system. These systems can be represented and mathematically modeled using partial differential equations (PDE) subject to initial and boundary conditions [140]. This is different from the framework of traditional FD and FDI methods, which assume systems that can be described using ordinary differential equations (ODEs) [84].

First an introduction is given on the current state and challenges regarding FD of DPS with heightened focus on data-based methods. Data-acquisition issues for training the data-based FD methods are highlighted, additionally the issue of optimal sensor placement is also mentioned. Subsequently, a method to automatically generate less computationally intensive compartment models for generating training data in DPS is introduced. The algorithm is showcased using a real-life mixing tank where residence time distribution experiments were performed. The technique was used to establish a reduced model of the system which accurately captures spatio-temporal dynamics and was used to train FD models with reduced

computational load. The FD performance of the trained method using the reduced order model was tested using data generated by the original, first principle model.

5.1 The current state of fault detection in distributed parameter systems

In the literature, various methods for FD and FDI of DPS have been introduced. In the early stages of the literature, model-based techniques have become common for such problems, mostly observer-based methods [84]. These techniques either utilized model reduction to supervise systems, reducing the DPS into interconnected ODE models and tackling the design problem in a finite dimensional space [141, 142] or tried to tackle the development of analytical solutions for observer design in an infinite dimensional space described by an approximate ODE form [84]. These two types of techniques are referred to as [143]:

- Early lumping (ODE approximation with finite dimensionality)
- Late lumping (ODE approximation with infinite dimensionality)

While both methods served well and enabled the development of robust and sensitive FD and FDI methods for nonlinear DPS, they both had issues. In case of the early lumping techniques, the FD performance was inferior compared to that of methods designing observers for the original DPS because of the finite dimension approximation of the DPS. On the other hand, designing observers while assuming infinite dimensionality of the ODE approximation as per the late lumping methods was something only applicable to a few types of select systems describable by specific types of PDEs [143]. Alternatively, approaches based on modulating functions have also gained traction. These techniques were utilized for parameter estimation in lumped parameter systems in a modified form to be applicable for the DPS FD problem [144]. Using the modulating functions, PDEs were transformed into algebraic fault detection equations, foregoing the observer design and other issues [145]. The problem present with these approaches was their analytic nature, which resulted in them being not readily applicable for systems described by more complex PDEs [146].

In the later stages of the DPS supervision problem, data-based methods have also begun dominating the field, mainly those based on MSPM approaches. The proposed approaches

utilize standard techniques such as independent component analysis [147] or partial least squares methods [148] assuming a limited amount of sensors within the process. However, as such two problems are encountered within data-based methods:

- Training data acquisition
- Sensor localization

The first issue stems from the acquisition of proper training data for the data-based techniques. Acquiring sufficient historical operation data for systems, especially systems with spatial distribution, is a difficult demand. As experimental data is often not available, first principle models of the systems are most commonly utilized to generate training data, alas this comes at a significant computational cost. Secondly, the performance (FAR,MAR, detection time delay, etc.) of the data-based method will heavily rely on the sensor location spots where the data was acquired. Sensor localization for optimal FD performance has been a topic studied before, with many methods focusing on optimization through the use of the Fischer information matrix [149]. The main goal in these studies is to configure a steady operation network of a finite number of sensors which maximize information gain within a DPS [140]. These techniques were showcased for both model and data-based techniques [150, 149] and gave promising results, however to initiate them dynamic case studies of fault evolution within the dynamic system were necessary both as a function of time and space [151].

5.2 Computational Fluid Dynamics (CFD) techniques

In chemical engineering practice, first principle models of systems which describe spatio-temporal evolution of certain parameters are usually resolved through numeric schemes, as analytic solutions are not readily available. In cases where the mass and energy conversion of fluid systems is modeled, then the set of specific numeric methods used to tackle these problems are referred to as computational fluid dynamics (CFD) techniques. CFD methods have become widespread in the last few decades for solving the material and energy balance equations of complex systems, to describe transport phenomena and to evaluate flow patterns, velocity fields and mixing in fluid systems. These numerical methods involve the

discretization of the systems of partial differential equations describing the behavior of the unit and solving them through direct or iterative computation methods [152].

CFD utilizes computer aided design to develop the geometry and bounds of a given fluid flow transport phenomenon problem, and a calculation mesh is generated to define the scale of computation. Subsequently, applicable initial and boundary conditions are provided to enable the solution of the partial differential equations describing fluid transport within the geometry. Finally, the system of partial differential equations is solved using various discretization schemes. The most prominent discretization methods in CFD include three techniques [153].

- Finite difference method
- Finite element method
- Finite volume method

Finite difference techniques utilize finite differences to approximate derivatives in the partial differential equations describing system behavior numerically and convert the problems into algebraic equations. The finite element method utilizes the previously mentioned computational mesh to achieve spatial discretization of the system. Test functions are utilized to model the local behavior of system variables, and weights associated with the test functions are found using an optimization framework by minimizing the residual associated with the solution of the differential equation. The finite volume method applies the divergence theorem to formulate flux equations by dividing the observed geometry into control volumes. This network of cells is utilized similarly to the finite element method to approximate the solution to the set of partial differential equations describing system behavior [153].

CFD techniques can be applied to address a broad range of fluid flow problems associated with various industries and disciplines such as car design, ship design, biology, oceanography, meteorology and of course the chemical engineering industry. Recent trends in CFD have mainly addressed the technical issues associated with the techniques, such as their intense computational demand. While the recent advancement in computer technology enables numerical simulation for physically and geometrically complex systems using PC clusters, the development of efficient solution and discretization methods to minimize computational load remains a critical problem [154].

5.3 Compartment models (CM) and their application in model reduction

As noted previously, the use of CFD techniques, especially for data generation to train data-based FD methods, is majorly impractical due to the great computational burden of said techniques.

An alternative to these methods is the use of Compartment Models (CM). CM emulates the behavior of complex systems by identifying individual spatial sets of the system that can be approximated using idealized models describable by ODEs, this in turn can greatly reduce the computational burden of such models compared to CFD [155]. In case of chemical technologies, the flow and transport phenomena in a system can be approximated by decomposing the system into compartments with idealized flow behavior [156]. The main question when developing a CM is how to select the appropriate number, characteristic and connections of compartments to obtain a model that accurately represents the flow patterns of the real system. CMs developed for chemical engineering systems usually employ two types of idealized compartments to approximate a velocity field in a system. These are compartments which are assumed to be perfectly stirred and homogeneous (Continuous Stirred Reactor or CSTR model) or compartments with turbulent plug flow (Plug Flow Reactor or PFR model). These compartments are linked through mixer (MIX) and distributor (DIST) models [157]. Mixer and distributor units only hold mathematical meaning, and are assumed to have zero volume.

When taking into account a lumped parameter system where one of the ideal flow types is present coupled with the convective transport of a given material species, i then the component balance model for the units is showcased in Eq. 5.1 – Eq. 5.4. The equations are written assuming that a steady-state mass balance is present within the unit.

- For unit CSTR:

$$\frac{dc_i(t)}{dt} = \frac{q_{in}}{V_{in}}\left(c_{i,in} - c_i(t)\right) \qquad q_{out} = q_{in} \tag{5.1}$$

- For unit PFR:

$$\frac{\delta c_i(t,x)}{\delta t} = -v_x \frac{\delta c_i(t,x)}{\delta x} \qquad q_{out} = q_{in} \tag{5.2}$$

- For unit MIX:

$$c_i(t) = \frac{\sum_{j=1}^{n} c_{i_j}(t) \cdot q_i}{\sum_{j=1}^{n} q_i}$$
$$q_{out} = \sum_{j=1}^{n} q_j \tag{5.3}$$

- For unit DIST:

$$\mathbf{c}_i(t) = c_{in}$$
$$\mathbf{q}_{out} = \alpha \cdot q_{in} \tag{5.4}$$

The volumetric flow (q) entering and exiting the units is also provided assuming constant temperature and dilute solutions. The models establish relationships between the volume of the unit (V), the inlet velocity (v), and the inlet and actual concentration in each idealized unit (c). Concentration is introduced as a function of time and/or Cartesian length coordinate (x). In case of the distributor unit the outlet concentration is the same as the inlet concentration, the flow rate depends on the division rate (α).

The idealized CSTR and PFR models have characteristic responses to known input signals, such as the Heaviside or step function ($H(t)$) or the Dirac-delta function ($\delta(t)$). The step response ($C(t)$) of the ideal flow models as well as the serial combination of CSTR units to the Tanks in Series (TIS) model are shown in Fig. 5.1.

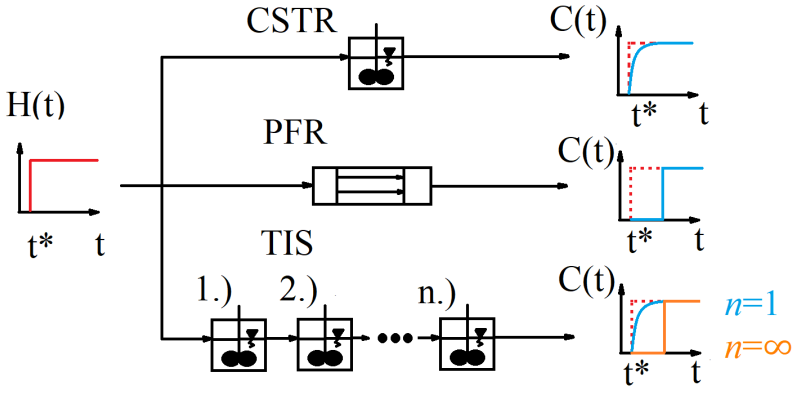

FIGURE 5.1: Idealized flow models and their response to the Heaviside input function

The response functions can be used to characterize the residence time distribution (RTD) of a chemical species within the system [158]. Therefore, obtaining the step response of the system and using the RTD function as a basis for the identification of the compartment structure and the connections between the various compartments is a popular approach [137]. Alternatively, additional approaches which use the CFD model as a basis for the estimation of the

CM structure, without experimental measure of the RTD, have also become popular in recent studies [159, 160]. However, in the early times of research on the conversion of CFD results into CM models the compartmentalization was conducted manually based on expert knowledge and visual observation of the flow field. Algorithms for the automatized identification of CM structures from CFD have been proposed in later stages of development. These methods often use frameworks where zones are defined using CFD results, such that the spatial distribution of some observed flow variable (pressure, kinetic dissipation energy, etc.) is within an acceptable threshold in a clustering manner [155, 161] or by using a hypothesis-driven logic [162].

5.4 The proposed CFD-based method for developing compartment models used for system supervision

During the course of this work the goal was to develop an algorithm capable of identifying the CM structure of a system based on results obtained from CFD methods and utilize it to train data-based FD techniques. The developed CM may be used to generate operation data for the system in a computationally efficient manner and highlight areas of special interest for sensor placement. The algorithm utilizes two steps to first identify the CM structure and then the flow rates between the individual compartments. Expectations for the algorithm were:

- Production of compartment models that can greatly mimic spatial and temporal behavior of the investigated system with reduced computational
- Generating reduced order models for training FD techniques at reduced computational cost but acceptable FD performance process

The proposed algorithm uses CFD results to establish CMs. The velocity field within a given unit is acquired through the CFD techniques. Subsequently, the investigated space is partitioned into a grid of units (from now on referred to as elementary cells (EC)). The algorithm utilizes fuzzy logic to evaluate the properties of the local velocity field within the ECs and categorizes them into one of the idealized flow types. Adjacent cells with similar flow behavior are agglomerated to form compartments with idealized behavior. The flow rate between the individual compartments is estimated through optimization by minimizing the summed

square of errors between the RTD function of the CFD and CM. The flowchart of the proposed algorithm is displayed in Fig. 5.2.

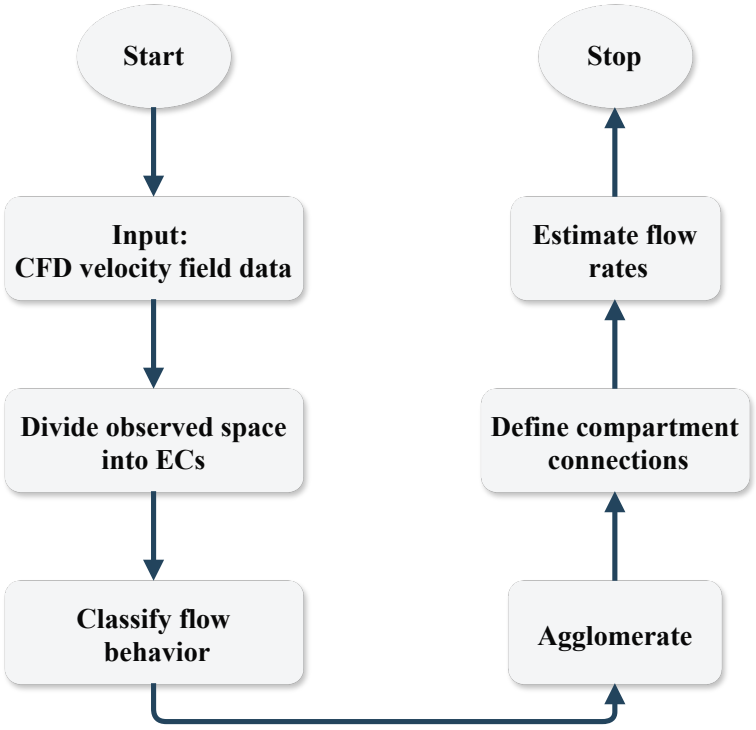

FIGURE 5.2: Flowchart of the CM development algorithm

To summarize the procedure, the compartmentalization process is conducted in six steps.

- Acquisition of a reliable steady state estimate for the velocity field of the system in question using CFD methods.
- Definition of elementary cells (EC) by diving the investigated volume.
- Evaluating the flow characteristics in the individual ECs through fuzzy logic and identifying them as CSTR, PFR or dead flow volumes.
- Agglomerating adjacent ECs with similar flow characteristics into compartments.
- Defining possible connections between compartments based on the physical geometry of the system.
- Estimating flow rates between linked compartments through optimization based on the step response function of the system.

5.4.1 Fuzzy classification

To properly characterize the local flow tendencies within the unit a fuzzy logic-based classifier was utilized[163]. The basic terms and formalization of fuzzy logic and fuzzy classification are introduced in the subsection.

Let a set of class linguistic labels be defined as $S_{cl} = \{s_{cl,1}, s_{cl,2}, ..., s_{cl,c}\}$, where $s_{c,i}$, $i = 1, ..., c$ is the label of the i-th class and $c = |S_{cl}|$ is the cardinality of the set of class labels. Additionally, we define $\mathbf{x} \in \mathbb{R}^{s\times 1}$ be a vector of numerical features about an observed object. As per the general definition of a classifier, the classifier is a mapping $\mathbf{x} \rightarrow S_{cl}$. In fuzzy classification, qualitative and linguistic rules are established to connect the state of input features with the class labels, in most common cases expressed in the form of "if-then" rules. Let Γ_j be the number of linguistic labels for the state of the j-th feature and $S_{j,i}$ be the i-th fuzzy set on the axis x_j, such that $i = 1, .., \Gamma_j$ and $j = 1, ..., s$. Let the set of rules for the classifier be denoted $\Xi = \{\xi_1, \xi_2, ..., \xi_k\}$, $k = 1, ..., \pi$. The classes and rules are linked through discriminant functions, $g_{i,k}$ which express degrees of belief in the membership of a sample with features $\mathbf{x}_j$ in a given class $s_{cl,i}$ based on the set of rules which connect the features $S_{j,k}$ and the particular class $s_{cl,i}$. This support is formulated as the quantity $z_{k,i} \in \Xi$ which shows the degree of support for the class $s_{cl,i}$ based on rule ξ_k [164].

Generally, the support for various classes is expressed numerically using membership functions which scale the support values through an order-preserving transformation in the form of $\Phi : \mathbf{R} \rightarrow [0, 1]$. Popular membership functions include sigmoid, Gaussian and ramp functions [164]. In the literature, three distinct types of fuzzy classification systems are discussed, depending on the relation between rules and consequent properties [165]. These include:

- Fuzzy rules which propose class labels as consequent of rules
- Fuzzy rules which include a class label and a certainty degree of the sample belonging to the class as a consequent
- Fuzzy rules which provide degrees of certainty for all classes in the consequent

Additionally, fuzzy inference systems may be categorized based on their types of inputs and outputs (Mamdani or Takagi-Sugeno-Kang inference systems) as well as the structure of the components of the classifier [164]. These include three elements:

- The structure of the fuzzy rule base
- The conjunction formulation of the rules, as well as the method of calculation for their consequent firing strength
- The way of calculating the output of the classifier

In terms of Takagi-Sugeno-Kang models based on the three components of the inference systems, four traditional types of inference systems can be identified, denoted as TSK_1 – TSK_4 [164].

5.5 Case study and method evaluation

The steps of the proposed method and the results derived from it will be showcased in case of a model system derived from the applications' library of a commercial CFD simulator (COMSOL Multiphysics Version 5.2a). The model was of a wastewater treatment tank which included baffles as static mixer units within. The system was constructed in real life as an experimental mixing tank device to validate the results of both CFD and CM models.

5.5.1 System construction and experimental work

During the experimental investigation, the RTD function of the system was registered. The residence time probability density function ($E(t)$) at any time instance (t^*) describes the ratio of fluid volumes whose residence time within a given system is infinitely close to t^*. Assume that q volumetric flow of tracer fluid or particle is injected into a unit of defined control volume (V) with concentration (c) according to the Dirac delta function ($\delta(t)$). Let the measured concentration response at the outlet of the system be defined as $C(t)$. In this case, the residence time probability density function may be calculated according to Eq. 5.5.

$$E(t^*) = \frac{C(t^*) \cdot q}{\int_{t=0}^{\infty} c(t) \cdot q \, dt} \tag{5.5}$$

In case of a step input, the F residence time probability distribution function (RTD) of the residence time may be calculated as the integral of the function $E(t)$ as per Eq. 5.6 or from the response function and the maximum input tracer concentration of the step input (c_0).

$$F(t^*) = \int_{t=0}^{t^*} E(t)\, dt = \frac{C(t^*)}{c_0} \tag{5.6}$$

During our experiment, we employed methylene blue ($C_{16}H_{18}ClN_3S$-from now on referred to as MB) dye as a tracer to register the step response of a laboratory-scale tank and estimate the $F(t)$ function to characterize residence time within the unit. The simplified top-, and side-view of the experimental system are shown in Fig. 5.3 with its characteristic sizes.

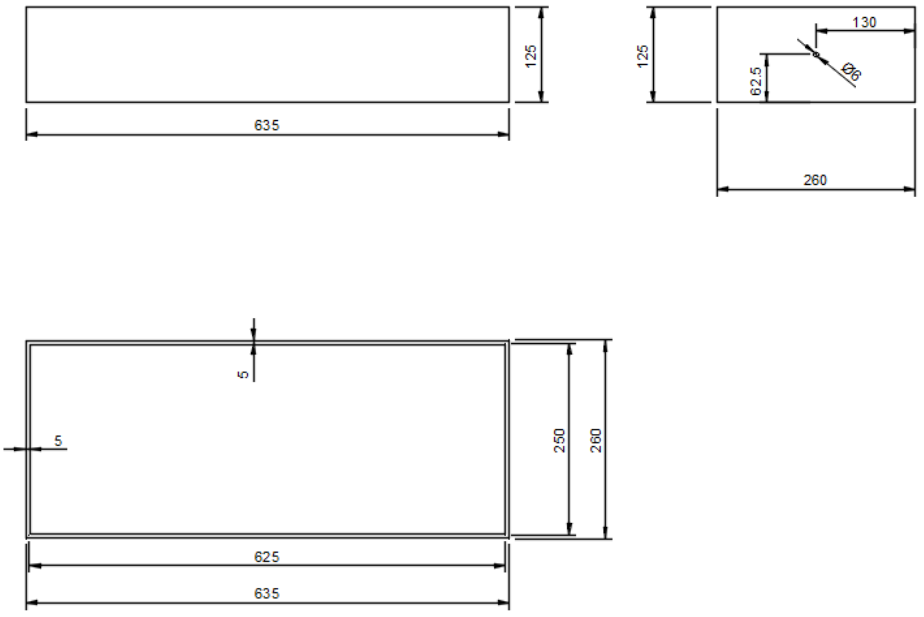

FIGURE 5.3: Geometry and construction of the investigated tank, side (**top left** and **top right**) and top (bottom left) view

The inlet of the system is positioned on the left side of the system from the top view. The inlet for liquid feed into the system can be seen on the side view at 62.5 mm height, at a 130 mm distance from the outer side of the unit. The outlet was positioned at the same latitude and altitude as the opposing (right) face of the unit when viewed from the top. There were four possible points within the tank for the insertion of baffle plates (125 mm height, 120 mm length, and 5 mm width). The reference point of the possible baffle positions (0,0) is the lower left corner point of the tank shown in Fig. 5.3. All four baffles were inserted into the tank for the purpose of investigation, their positions shown in Table 5.1.

TABLE 5.1: Baffle positions within the unit

Buffer number	Longitudinal position	Lateral position
1	125 mm	0 mm
2	250 mm	140 mm
3	375 mm	0 mm
4	500 mm	140 mm

The layout of the experimental setup used to register the RTD function within the system is shown in Fig. 5.4.

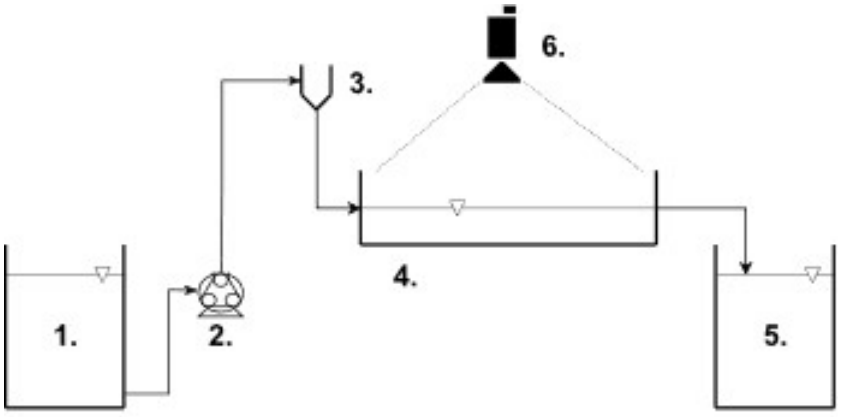

FIGURE 5.4: Experimental setup for the investigation of the RTD within the tank

During the experimental procedure, MB tracer of 0.1 $molm^{-3}$ concentration mixed from commercially available solid MB (CAS 61-73-4) and ion-exchanged water were stored in a tank (1). The tracer was fed into the system through the use of a diaphragm pump (2) at the start of the investigation, the steady state flow profile was established after a few seconds which was negligible compared to the time of concentration change. The pulsation from the pump would have resulted in the movement of the fluid surface and external mixing and back mixing within the tank, therefore a buffer unit (3) was inserted between the pump and the unit to mitigate pulsation. The tracer entered the investigated tank (4) and the effluent was stored in a tracer containment tank (5). The tank was initially filled with pure ion-exchanged water, and the change of tracer concentration was registered using a camera (6). The intensity of the blue color of the MB tracer within the tank was compared to the reference color of the pure inlet tracer and converted into tracer concentration using a calibration equation.

The temporal evolution of the tracer color intensity was registered and thus used to estimate the RTD function of the system. The experiments have been conducted within a time frame of 3 hours. The average residence time within the system calculated from the tank volume and inlet volumetric flow was one hour. The operational parameters of the experiments are shown in Table 5.2.

TABLE 5.2: Experimental conditions

Operation parameter	Value and unit
Tank volume	12.5 l
Inlet volumetric flow	12.5 lh^{-1}
Average residence time	1 h
Inlet velocity	0.17 $m\ s^{-1}$
Inlet MB concentration	0.1 $mol\ m^{-3}$

5.5.2 CFD modeling procedure and results

To complete the first step of the algorithm, the CFD model of the unit was developed. COMSOL Multiphysics version 5.2 was used to complete the momentum and component mass balance calculations within the unit assuming a $2D$ geometry, since no significant buoyancy or sedimentation effects were observed during the experiments. First to establish and validate the system model the steady-state momentum and dynamic component balance have been solved and the RTD function was obtained. During the validation of experimental findings for the calculation of the steady state liquid velocity field, the laminar Navier-Stokes equations have been employed (Reynolds number (Re) of 43 was calculated from the hydraulic diameter and average flow velocity within the tank). The form of the Navier-Stokes equations can be seen in Eq. 5.7.

$$\rho\left(\nabla\mathbf{v}\right) = \nabla\left[-\rho\mathbf{I} + \eta\left(\nabla\mathbf{v} + \left(\nabla\mathbf{v}\right)^{T}\right)\right] + \mathbf{F} \tag{5.7}$$

In the equations, ρ and η are the density and viscosity of the fluid phase, $\mathbf{v}$ are $\mathbf{I}$ are the velocity and momentum vectors of the fluid, and $\mathbf{F}$ is the vector of external forces which influence

the flow field. The equation of the dynamic component mass balance is shown in Eq. 5.8 assuming that only conductive and convective mass transport are present within the unit.

$$\frac{dc_i}{dt} = \mathbf{u}\nabla c_i - \nabla\left(D_i \cdot c_i\right) \tag{5.8}$$

In the equations, c_i is the concentration of the i-th component species, and D_i refers to the isotropic diffusion coefficient of the i-th species in the investigated medium. The physical parameters of the fluid were taken to be the same as pure water at 25 °C. The diffusion coefficient of methylene blue at 25 °C was determined to be $0.38 \cdot 10^{-9}\ m\ s^{-2}$ [166]. Initial and boundary conditions for the modeling procedure are summarized in Table 5.3. The boundary conditions were all assumed to be uniform at the boundaries.

TABLE 5.3: Inlet and boundary conditions of the CFD simulation

Phenomenon	State	Initial conditions	Boundary conditions
Laminar flow	Steady	$\mathbf{v} = \mathbf{0}$	Inlet velocity of 0.17 $m\ s^{-1}$ Outlet pressure of 1 bar
MB component mass balance	Dynamic	$c_{MB} = 0$	Inlet concentration 0.1 $mol\ m^{-3}$

The balance equations have been solved using Newton's method for dynamic and the PARDISO algorithm for steady state calculations. The computational mesh has been refined by observing the computational cost of the simulations and the relative error of the mass balance within the system. The relative error of the mass balance (ϵ) within the system was calculated according to Eq. 5.9 where $\dot{m}$ is the mass flow rate as the inlet and outlet boundaries.

$$\epsilon = \frac{\int_{t=0}^{\infty} |\dot{m}_{x=0} - \dot{m}_{outlet}|\, dt}{\int_{t=0}^{\infty} |\dot{m}_{x=0}|\, dt} \tag{5.9}$$

Three triangular mesh variations have been tested with different element sizes and differing numbers of mesh elements. The element size parameters as well as computation time for the steady-state momentum balance assuming laminar single-phase flow and relative error of MB component mass balance displayed in Table 5.4.

TABLE 5.4: Parameters of the tested mesh configurations and relative error terms (CPU type: Intel(R) Xeon(R) CPU E5620 @ 2.40GHz, Memory speed: 800 MHz)

Mesh identifier	Min. element size [mm]	Max. element size [mm]	ϵ	Computation time [h]
M1	$8 \cdot 10^{-2}$	17	$6 \cdot 10^{-2}$	0.17
M2	$2 \cdot 10^{-2}$	13	$2.2 \cdot 10^{-2}$	0.3
M3	10^{-3}	7	$1.7 \cdot 10^{-2}$	0.35

Mesh M3 has been chosen for the investigations since it provided adequately accurate estimates based on the ϵ value at the cost of a reasonable increase in calculation time. The results of the mesh independence investigations are also visualized in Fig. 5.5 to facilitate understanding of the selection.

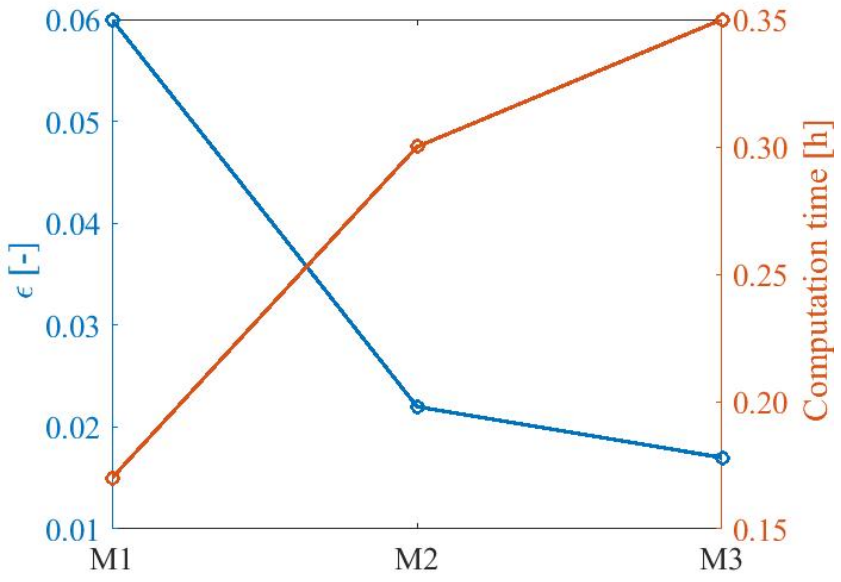

FIGURE 5.5: Results of the mesh independence investigation within the system

The approximate velocity field $[m\ s^{-1}]$ calculated through CFD for the investigated tank geometry is showcased in Fig. 5.6.

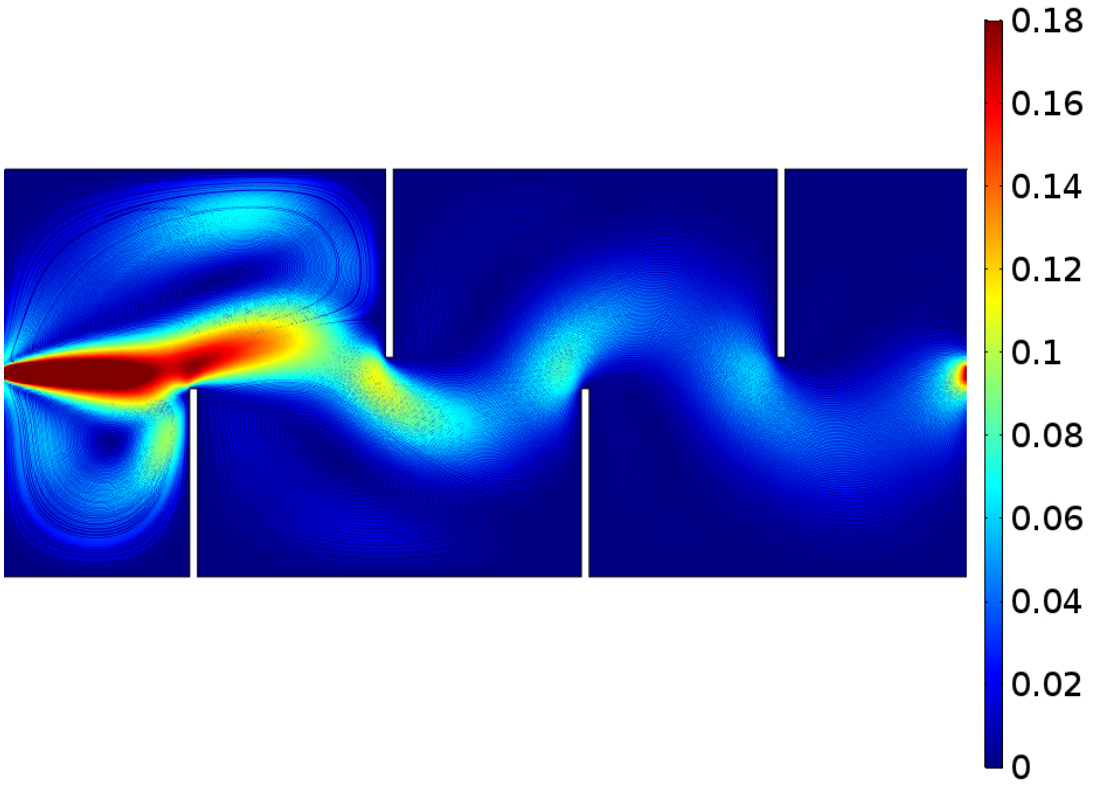

FIGURE 5.6: Steady state velocity field within the tank [$m\ s^{-1}$]

From the velocity field, it can be inferred that zones with strong circulation appear before the first baffle and between the first and second baffle indicating a greater degree of mixing and possibly increased expectancy of residence time within the unit. The intermediate baffles between the first and last baffle create subsequent circulation zones within the unit but with the decrease of the flow velocity across the tank, the recirculation tendency fades. To validate the results of the CFD model we show Fig. 5.7 which displays the RTD function of the investigated geometry for both CFD and experimental cases.

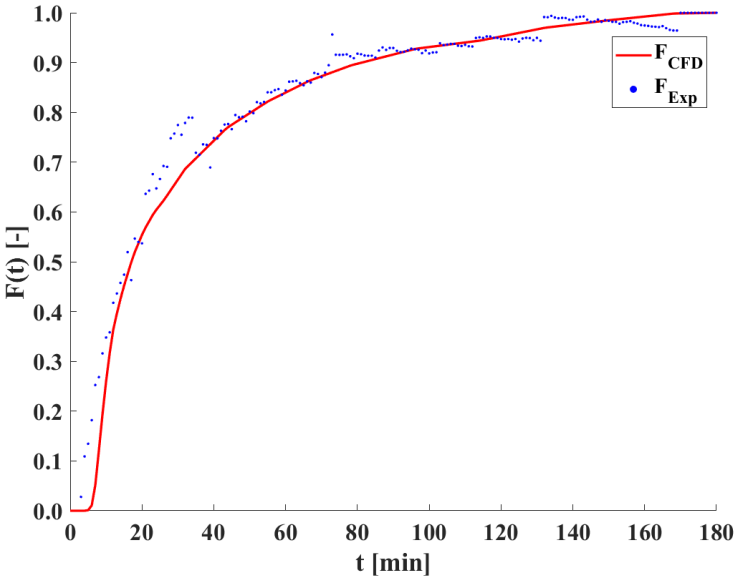

FIGURE 5.7: RTD function of the unit for both experimental and CFD cases

The figure displays that disregarding the experimental noise present, the CFD model accurately approximates the tendency of the system behavior. It must also be noted that the non-monotonous tendency of the experimental RTD results can be attributed to disturbances in the measurement, such as changes within external light conditions, which influenced the registered dye intensity. Preliminary filtering and outlier removal was not performed on these points which lead to the uneven evolution of the RTD function with locally decreasing trends. In order to quantify the differences between the model and the experimental findings, the standard deviation and expectancy of the residence time were calculated. The results for both CFD and experimental results are displayed in Fig. 5.8.

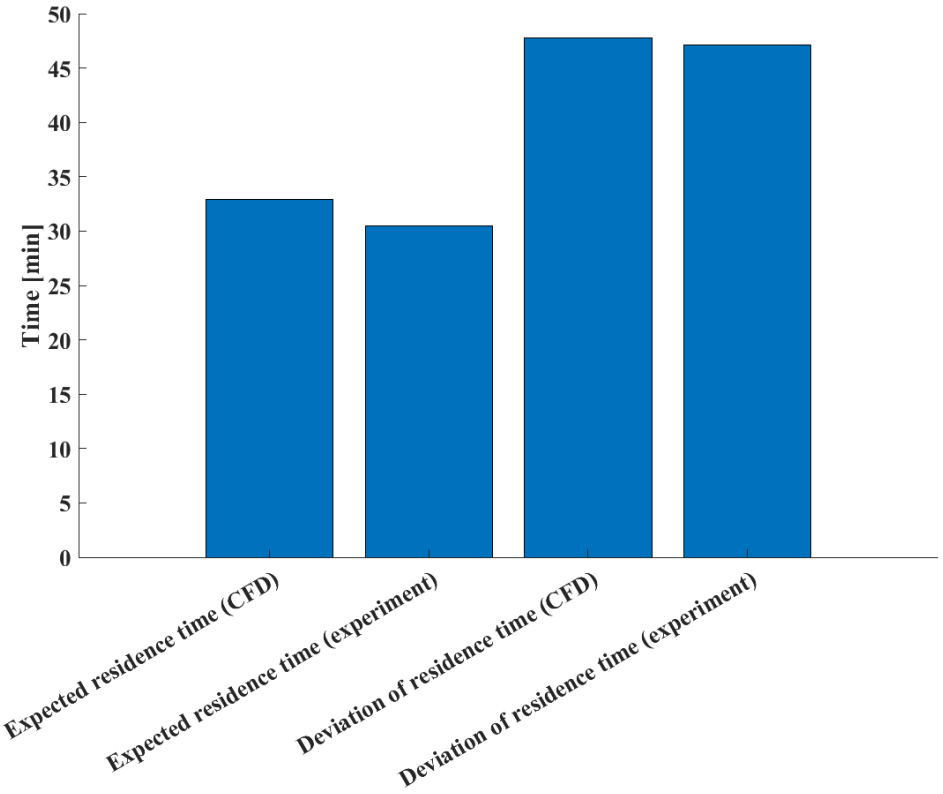

FIGURE 5.8: Expectancy and deviation of residence time for both CFD and experimental results

The absolute difference between modeled and experimental expectancy and standard deviation of residence time were compared to their experimental values, in this case the relative difference between the two was between 2 and 3 %. Based on the results, the CFD model is capable of accurately capturing the system's characteristics and is used as a basis for further CM structure identification.

5.5.3 CM model identification and results

After the CFD results have been acquired, the results were processed using MATLAB R2020b. The obtained velocity field within the unit is shown in Fig. 5.9, with a 10 times scaling of vector magnitude, to show vector trajectory and mixing conditions. The figure reinforces the conclusions drawn from Fig. 5.6, a strong unidirectional PRF-like flow can be seen between the inlet and outlet, the magnitude of the velocity vectors slowly declines as a function of the tank longitude due to the presence of baffles. The baffles in turn create circulation zones with more intense mixing conditions, though the intensity of these zones (velocity magnitude)

decreases after each baffle. The middle of the circulation zones as well as the edges of the unit generally show the presence of dead volumes.

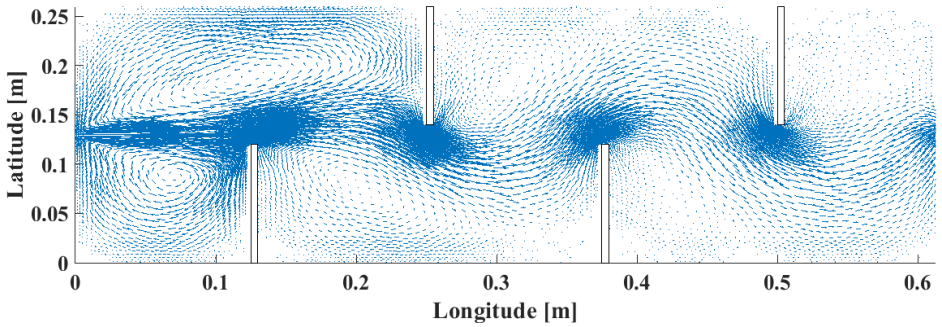

FIGURE 5.9: Velocity vector field within the observed unit (scaling factor of 10)

Before any further calculations were made, the distribution of velocity magnitude values within the unit have been studied. The distribution function of the magnitude values is shown in Fig. 5.10. The distribution shows tendencies of an exponential distribution function, with an expectancy of 0.025 $m\ s^{-1}$, outlier velocity magnitudes at around 0.35 $m\ s^{-1}$ can be observed. A theoretical exponential distribution has been fitted to the data and used for outlier detection, with values being labeled as outliers which were above the 99 % threshold of possible values for the distribution. These outliers have been normalized to a maximum velocity magnitude of 0.17 $m\ s^{-1}$, the same as the inlet velocity, as they could be observed near the outlet and were the result of numerical error within the CFD calculations.

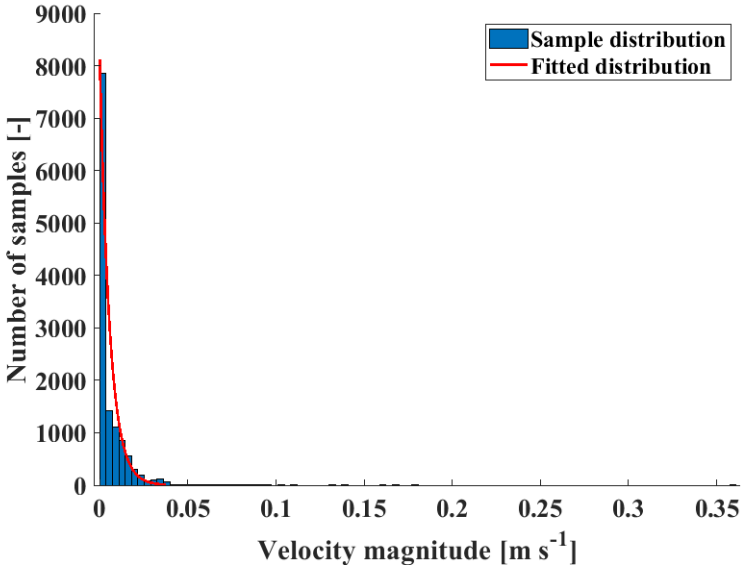

FIGURE 5.10: Distribution of velocity vector magnitudes within the unit

After outlier adjustment the geometry of the system has been partitioned into elementary cell (EC) units in which characteristics of the flow field were investigated, these ECs were chosen to be rectangular. To choose the number and therefore size of the ECs sensitivity analysis has been conducted. The minimum number of individual velocity vectors within each EC (among all possible ECs) as well as the cumulative sum of velocity variance scores within the ECs have been investigated as a function of EC latitude and longitude. These results are shown in Fig. 5.11.

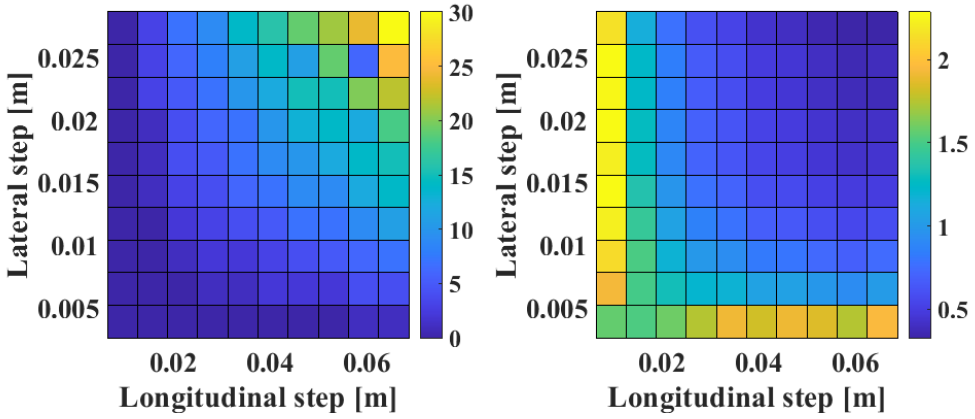

FIGURE 5.11: Minimum number of velocity samples within an EC and cumulative variance of velocity vectors within ECs as function of EC length and height

The results show that as the size of rectangular EC units increases the minimum number of velocity vectors within ECs also steadily increases, on the other hand the cumulative variance of velocity vectors within ECs decreases. The optimal EC size was chosen based on two criteria:

- each EC should hold a minimum of 2 velocity vectors for statistical evaluation
- cumulative variance should not change significantly if smaller ECs are chosen

Based on these two demands rectangular ECs with a longitude of 0.025 m and latitude of 0.010 m have been chosen as at these values the minimal vector number within ECs was 3 (in case of smaller ECs this number was 0 or 1), and the change of cumulative variance was not significant as the point was near the ankle of the cumulative variance plot. This resulted in a $25 \cdot 25$ grid with 625 individual ECs.

After partitioning the observed space into ECs the statistical measures characterizing the velocity vectors within individual ECs have been observed. These were:

- the expectancy of velocity magnitude within each EC
- the variance of the velocity vector components within the ECs
- the skewness of velocity vector components within ECs

The three metrics within the EC grid can be seen in Fig. 5.12. To make them comparable with each other, the results for the individual ECs have been scaled between 0 and 1.

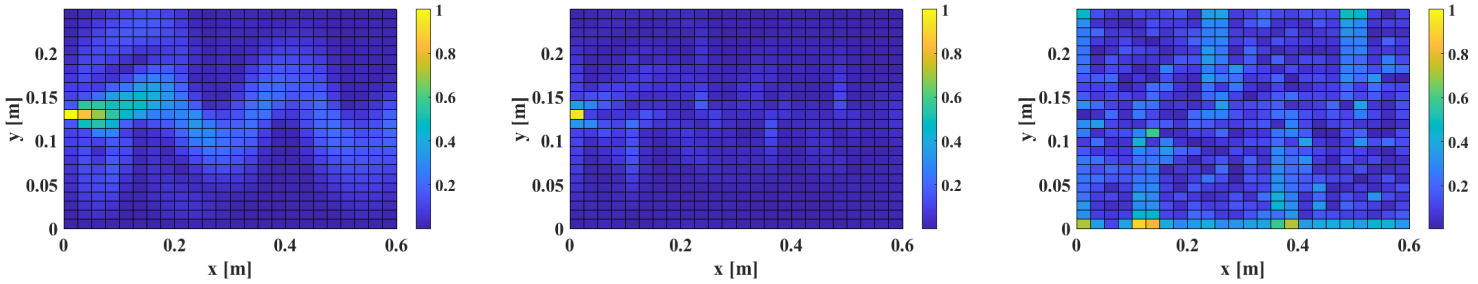

FIGURE 5.12: Scaled values of expectancy (**left**), variance (**middle**) and skewness (**right**) of velocity vectors within the observed ECs

Additionally, the three metrics have been plotted in their representative 3D state space. The distribution of said values is shown in Fig. 5.13.

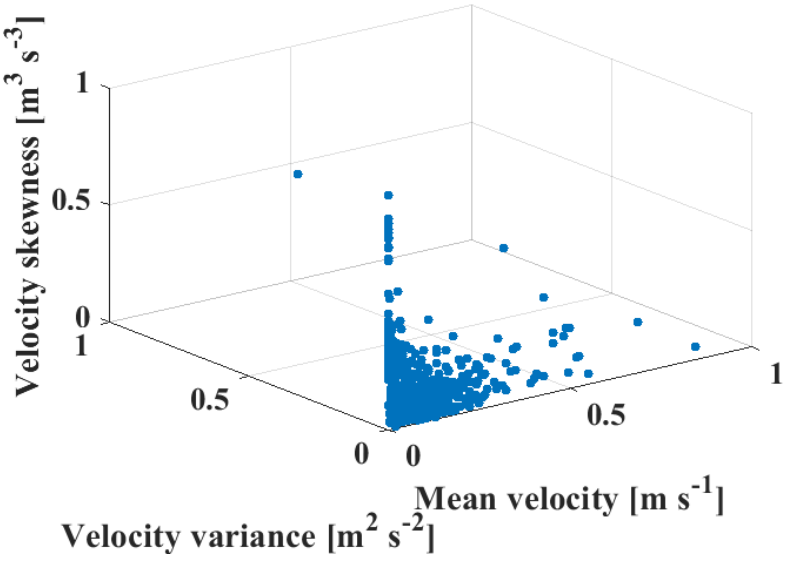

FIGURE 5.13: Statistic metrics within the ECs in state space

It can be seen that while there is a distinct distribution of the statistic variables, the distribution is not widespread. Due to areas with exceptionally high variance in their velocity vector

components and mean velocity vector magnitude (observable mostly near the inlet and outlet) the scores of most samples are dwarfed. This was also taken into account while formulating fuzzy membership functions for the inference system later on. Since the magnitude, direction and density of the vectors are all based on the attributes of the local velocity field within the tank, key observations can be derived from them about the local flow characteristics within the unit, using the logic proposed as follows.

ECs with PFR behavior contain velocity vectors which are unidirectional, therefore they will have a high mean velocity value, while those that contain circular flow with varying vector directions will have generally lower mean velocity values. In contrast, variance will increase within ECs that have strong circular flow with velocity vectors pointing in various directions. Dead volumes are zones with exceptionally low mean velocity magnitudes and are approximated as CSTR units.

The following general rules were established:

- In areas where the flow holds PFR characteristics, the velocity vectors are mostly unidirectional with little variance in their magnitude. The magnitude of the velocity vectors is relatively large compared to the magnitude of the inlet velocity, their skewness is also low.
- In areas where circular flow is present that holds CSTR characteristics, the directional components of the velocity vectors hold higher variance. The magnitude of the velocity vectors in these areas are varying, but they are comparable to the magnitude of the inlet velocity.
- In areas where little to no flow is present "a.k.a." dead volumes, the magnitude of the velocity vectors is negligible compared to the inlet velocity and their skewness is high.

Based on these rules, the flow characteristics within a certain volume of the system can be categorized into one of the idealized flow model types. To do this, the established rules were integrated into a fuzzy logic classifier as explained in Subsection 5.4.1. In case of our system, the numeric inputs of the inference system were the statistic measures within the individual ECs, denoted as $\mathbf{x}$. The numeric features were associated with sets of linguistic labels using monotonic sigmoid membership functions ($S_{j,i}$, $j = 1,...,s$ and $i = 1,...,\Xi_j$), the form of which are shown in Eq. 5.10.

$$S_{i,j} = \begin{cases} \frac{1}{1+e^{-\left(\frac{x_i-a}{b}\right)}}, & \text{if the state membership increases as } x_j \text{ increases} \\ 1 - \frac{1}{1+e^{-\left(\frac{x_i-a}{b}\right)}}, & \text{if the state membership decreases as } x_j \text{ increases} \end{cases} \tag{5.10}$$

Parameters a and b define the spread of the fuzzy membership degrees in the linguistic categories of the inputs as a function of the numerical inputs features. In case of the three possible input features (mean velocity, variance of velocity components, skewness of velocity components) two linguistic classes were defined in each instance which are $K = \{high,\ low\}$. These states are used to describe whether the mean value, variance and skewness of velocity vectors within an EC are high or low compared to the maximum value of the respective attribute within the system.

The possible output classes are contained in the set $S_{cl} = \{PFR,\ CSTR,\ Dead\ volume\}$. After the defuzzification process, the expert system returns crisp values characterizing the degree of PFR, CSTR and dead volume characteristics within each EC. These numbers are also derived from sigmoid discriminant functions related to the output classes. The a and b parameters of the membership functions are displayed in Table 5.5.

TABLE 5.5: Parameters of the fuzzy membership functions

Feature	Low		High	
	a	b	a	b
Velocity expectancy	0.01	0.05	0.03	0.2
Velocity component variance	0.01	0.05	0.02	0.2
Velocity component skewness	0.02	0.1	0.03	0.3
Dead volume	0.02	0.4	0.02	0.6
CSTR	0.02	0.42	0.02	0.55
PFR	0.02	0.4	0.03	0.67

Using the implemented fuzzy classifier, the flow characteristics of the ECs were characterized. The identified degree of PFR, CSTR and dead volume behavior within the unit are shown in Fig. 5.14.

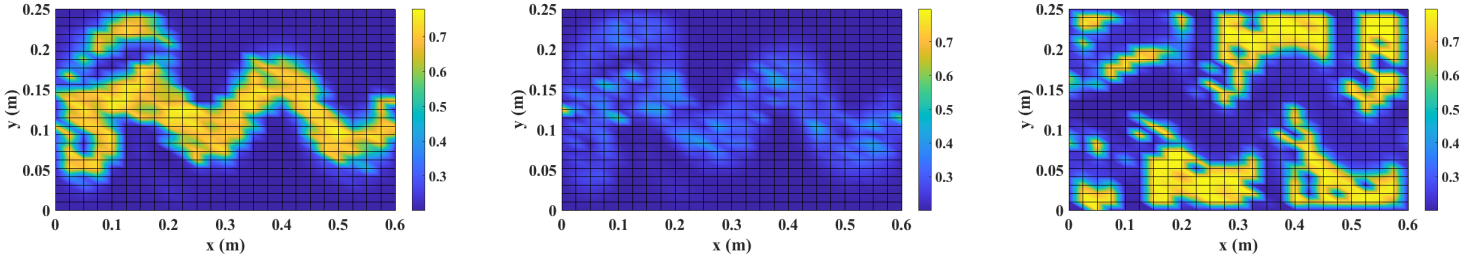

FIGURE 5.14: Idealized tendencies (PFR-**left**, CSTR-**middle** and dead volume-**right**) of ECs as derived from the fuzzy inference system

The results show that the algorithm accurately describes the tendencies observed in the velocity vector field data. The inlet and outlet are connected by a relatively large, plug flow like zone. Stirred areas can be observed at the edges of the PFR zones, where great changes in the local velocity field can be observed. These are especially prominent in the two zones before the first two baffles, where circulation flow is present. Dead volumes are dominant in the middle of circulation zones and after the first two baffles, where flow with high velocity magnitude is not present apart from the plug flow in the middle.

Alternatively, the individual EC characteristics are represented in state space in Fig. 5.15.

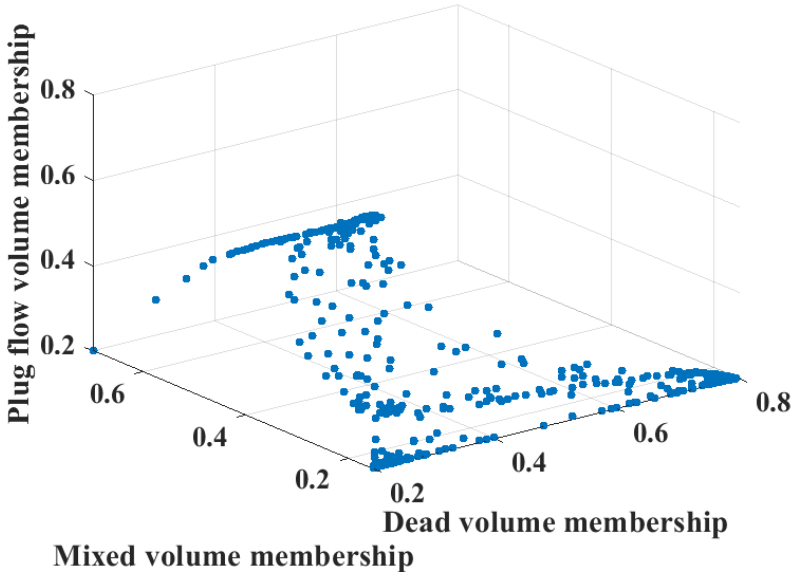

FIGURE 5.15: Idealized tendencies of ECs showcased in state space

Finally, the inferred crisp flow characteristic types within the unit are shown in Fig. 5.16

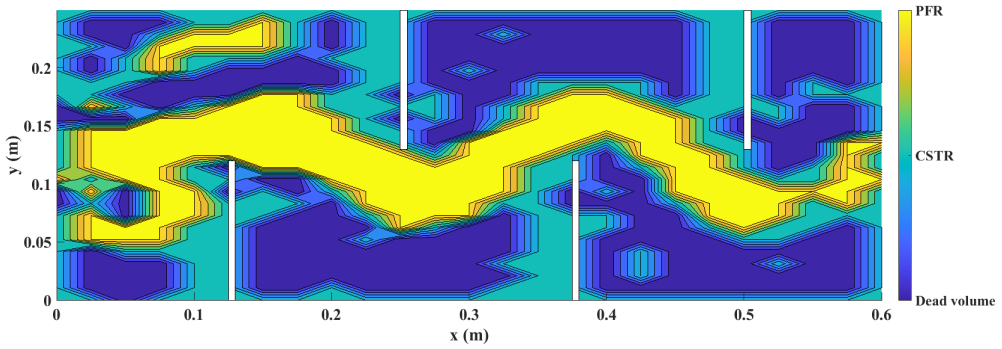

FIGURE 5.16: Contour plot of the identified CM structure

The flow structure derived as a result of classification shows great resemblance when compared with the velocity field of the system. The PFR section in the middle of the unit can be seen clearly, the circulation zones before the first two baffles show strong CSTR tendencies with dead zones at the center of the vortices. Continuing from there, the CSTR tendency fades gradually and the other zones between baffles are dominated by dead zones with weak mixing at the edges of the unit. The distribution of ECs in regard to the identified idealized flow characteristics is shown in Fig. 5.17. The results show that the geometry is dominated by stirred areas, followed by dead volumes, which is in accordance with the results of Fig. 5.6.

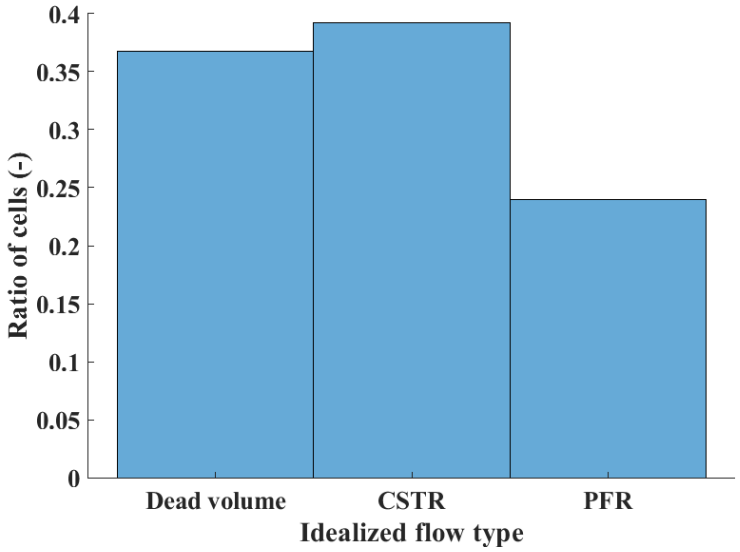

FIGURE 5.17: Distribution of the ECs in regard to their identified idealized flow characteristics

After this, the CM model structure was established, the system was decomposed into a network of seven units to approximate the real system's flow behavior. These include one PFR unit connecting the input and output, two continuous stirred units ($CSTR_1 - CSTR_2$) before

the first two baffles and four dead volume units ($D_1 - D_4$), which could be identified from Fig. 5.14. The chosen partition is showcased in Fig. 5.18 with red lines denoting the boundaries of the identified compartments.

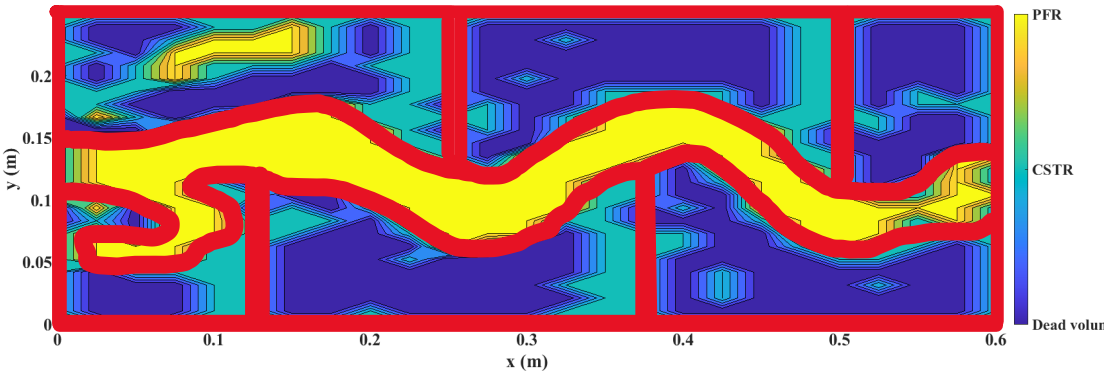

FIGURE 5.18: Partitioning of the observed volume based on idealized flow behavior

The volumes of the units were calculated from the associated number of ECs for each zone. The volume of these ECs is given in Table 5.6.

TABLE 5.6: Volumes of the identified CM network units

EC unit	Volume $[m^3]$
PFR	0.0029
CSTR1	0.0016
CSTR2	0.0034
D1	0.0013
D2	0.0013
D3	0.0013
D4	0.00066

To model the PFR unit and properly include recirculation behavior in the system, the PFR unit was approximated using a TIS model with five CSTR units ($TIS_1 - TIS_5$) with uniform volume. The structure of the EC connections is shown using a directed connectivity graph in Fig. 5.19.

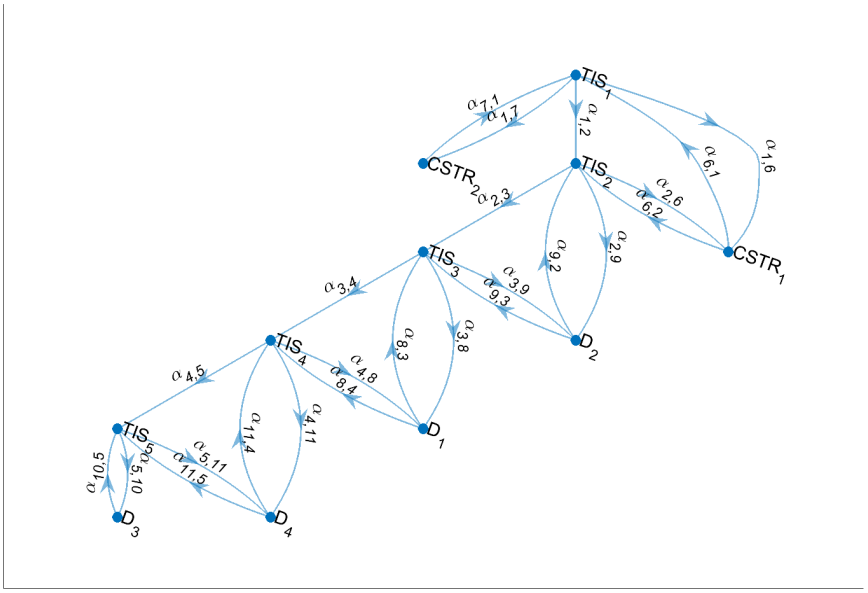

FIGURE 5.19: Connections and structure of the CM network used to approximate system behavior

Zones are linked through flow distributor and mixer units. The main flow between input and output represented by the TIS is connected to each other flow domain and also isolates them from each other together with the walls. Therefore, it sits at the center of the graph, the ratio of flow distributed from each unit to their neighboring units is described by the quantity $\alpha_{i,j} \in [0,1]$, where $i, j = 1,...,11$ are the indices of the connected unit number in the order of TIS, $CSTR$ and finally D compartments. The flow entering the neighboring flow domains reenters the main PFR flow using a mixer unit.

The values of $\alpha_{i,j}$ have been found using a constrained optimization procedure in MATLAB. The network of idealized units has been implemented in the form of a system of differential equations as per Equations 5.1-5.4 with the volumes described in Table 5.6 and operating conditions such as the inlet volumetric flow taken from Table 5.2. A quadratic objective function, $Objective(\alpha)$ for the optimization, has been defined as per Eq. 5.11, where n is the sample number for the simulated time period. Applied equality constraints come in the form of Eq. 5.12 for finding $\alpha_{i,j} \in [0,1]$.

$$Objective(\alpha) = \sum_{i=1}^{n} \left(F_{i,EXP} - F_{i,CM}\right)^2 \tag{5.11}$$

$$\alpha \cdot \mathbf{A} = \mathbf{1} \tag{5.12}$$

The equality constraint matrix **A** defines that the sum of flow ratios exiting any unit in the CM model must add up to exactly one to satisfy mass balance within the system. The system of ODEs has been solved using the Rosenbrock method for stiff differential equations, in parallel the optimization algorithm used for finding α that minimized $O(\alpha)$ was the method of interior points. The optimization lead to the following scores for α, shown in Table 5.7.

TABLE 5.7: Optimized α values of the CM structure

TIS units	α	Value	CSTR units	α	Value	D units	α	Value
TIS_1	$\alpha_{1,2}$	0.21	$CSTR_1$	$\alpha_{6,1}$	0.78	D_1	$\alpha_{8,3}$	0.46
	$\alpha_{1,6}$	0.01					$\alpha_{8,4}$	0.54
	$\alpha_{1,7}$	0.78				D_2	$\alpha_{9,2}$	0.73
TIS_2	$\alpha_{2,3}$	0.37					$\alpha_{9,3}$	0.27
	$\alpha_{2,6}$	0.61				D_3	$\alpha_{10,5}$	1
	$\alpha_{2,9}$	0.02						
TIS_3	$\alpha_{3,4}$	0.94		$\alpha_{6,2}$	0.22			
	$\alpha_{3,8}$	0.01						
	$\alpha_{3,9}$	0.05						
TIS_4	$\alpha_{4,5}$	0.96						
	$\alpha_{4,8}$	0.03						
	$\alpha_{4,11}$	0.01						
TIS_5	$\alpha_{5,10}$	0.998	$CSTR_2$	$\alpha_{7,1}$	1	D_4	$\alpha_{11,4}$	0.31
	$\alpha_{5,11}$	0.002					$\alpha_{11,5}$	0.69

The optimization results in regard to the RTD functions are shown in Fig. 5.20.

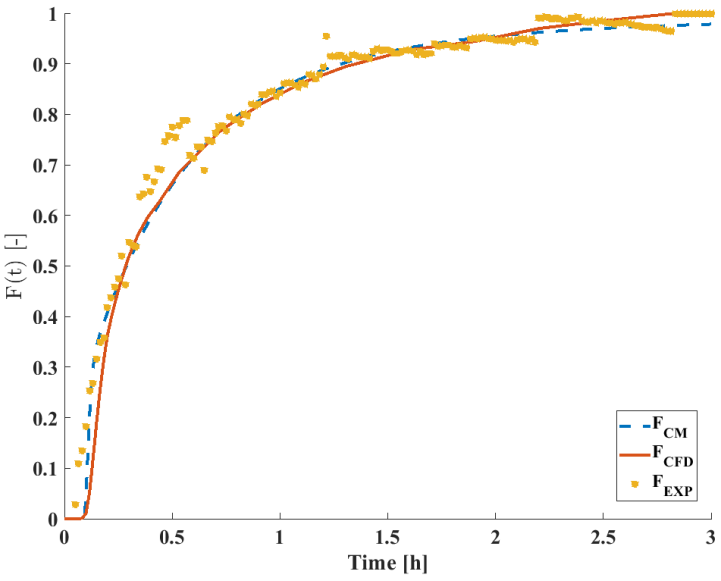

FIGURE 5.20: Comparison of RTD functions for optimized CM, CFD models and experimental results

It can be seen that the three results strongly align, the optimized CM model provides a reasonably good approximation of both the CFD model and experimental findings. And while the CFD model's calculations require around 32 minutes of computation time, the optimized CM model's simulation concludes in 42 seconds, resulting in a 97.8 % reduction in calculation time.

To evaluate the model's applicability under different operating conditions, the RTD function generated by the CFD simulator and CM was observed under differing inlet velocity magnitudes. Three cases have been tested, with a difference of 20 % in inlet velocity compared to its steady-state value at which the model was trained. The resulting RTD functions can be seen in Fig. 5.21.

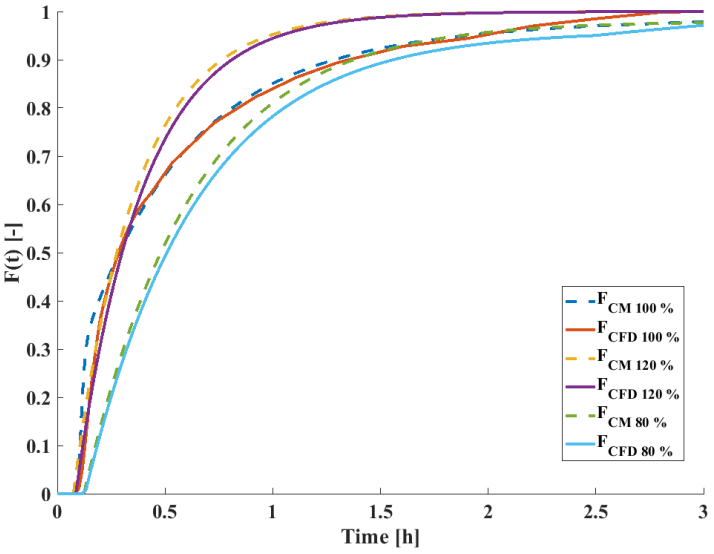

FIGURE 5.21: Comparison of RTD functions under different inlet velocity magnitudes compared to the training case

It can be seen that the model performs well both for the steady-state training data and for the higher inlet velocity case. Larger errors can only be observed in the case with decreased velocity compared to the training case (80 % of the training case inlet velocity) where the CM predicts faster dynamics for the system than the CFD model. To evaluate the results quantitatively, the mean squared prediction error between CFD and CM RTD functions was calculated. The results are displayed as a function of change within the inlet velocity compared to the training case in Fig. 5.22.

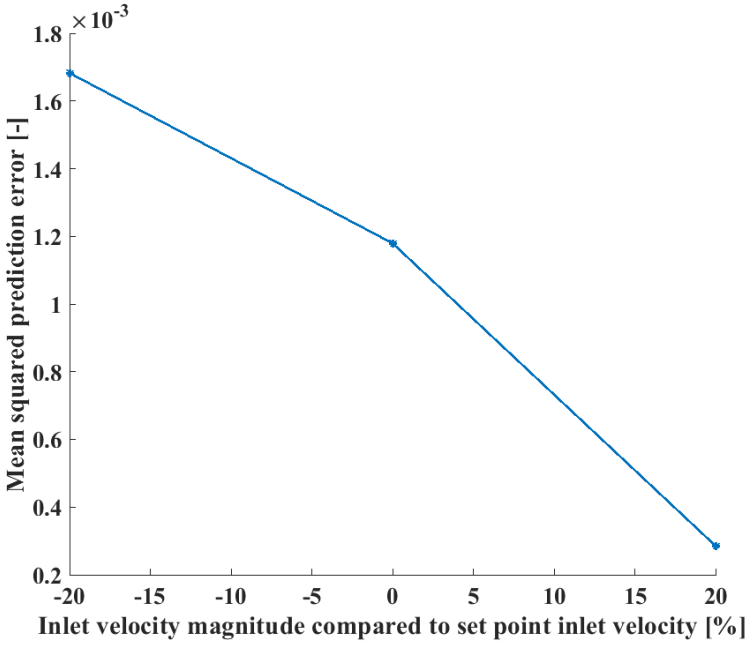

FIGURE 5.22: Mean squared prediction error of the CM compared to the CFD as a function of inlet velocity change compared to the training case

The results show that the applicability of the CM increases for higher velocity magnitudes, while worse performance is expected at lower inlet velocity values. This trend can be attributed to the change of flow tendency and stronger non-ideal flow behavior (dominant laminar flow patterns) however the difference between the mean squared predicted error scores at different velocity magnitudes is not significant enough to clearly draw conclusions. Regardless, the results show a decent applicability of the model in the ± 20 % range of the training inlet velocity. When extrapolating outside these boundaries, especially at lower inlet velocities, new identification of CM structure and flow parameters may be required. This however can be performed under negligible computation time (scale of seconds for this problem) if the velocity field data and RTD function are available.

5.5.4 Fault detection using the compartment model

In the final stage, I wish to showcase the CM's capabilities for training FD methods. As the CM is a reduced model of the system, it can provide approximations for the real system's behavior. Using the CM, operational data for the unit has been generated, and used for the development of a DPCA supervision model. An observation time frame of 3000 hours with 100 step input changes in the inlet concentration was used to observe the system through the

CM model, times were tuned based on the time constant of the system. Five measurement points along the main flow path were assumed, where through sensors the concentration was evaluated. The position of these measurement points are shown in Table 5.9.

TABLE 5.8: Locations of measurement points for system supervision

Measurement point number	Longitudinal position	Lateral position
1	0 mm	130 mm
2	160 mm	130 mm
3	320 mm	130 mm
4	480 mm	130 mm
5	625 mm	130 mm

The data of these measurement points, which include both inlet and outlet boundaries, were used to establish the DPCA model using the procedure described in Section 4.4. The optimal lag number was chosen as one, while the number of retained principal components was chosen as two based on autocorrelation plots and the algorithm of Ku et al. [56]. The results of the algorithm are shown from Fig. 5.24 to Fig. 5.25.

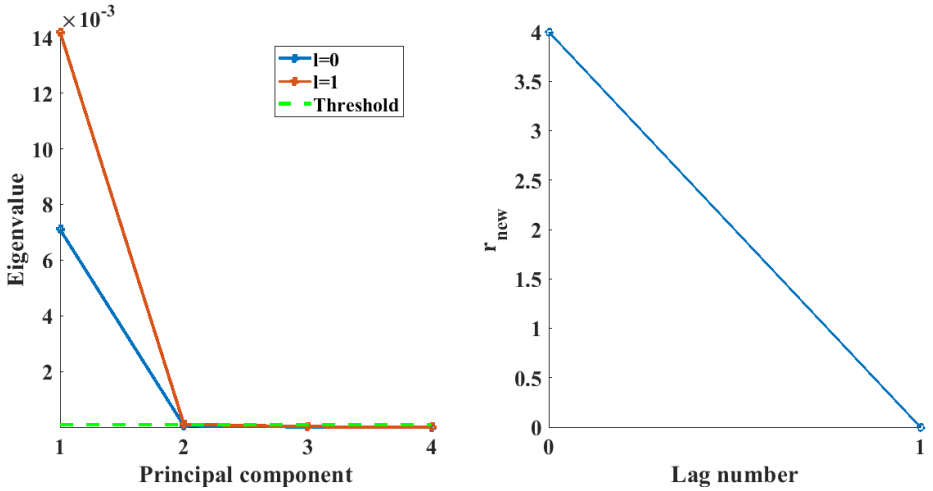

FIGURE 5.23: Scree plot of DPCA transform (**left**) and number of linear relationships (**right**) between variables as function of lag number

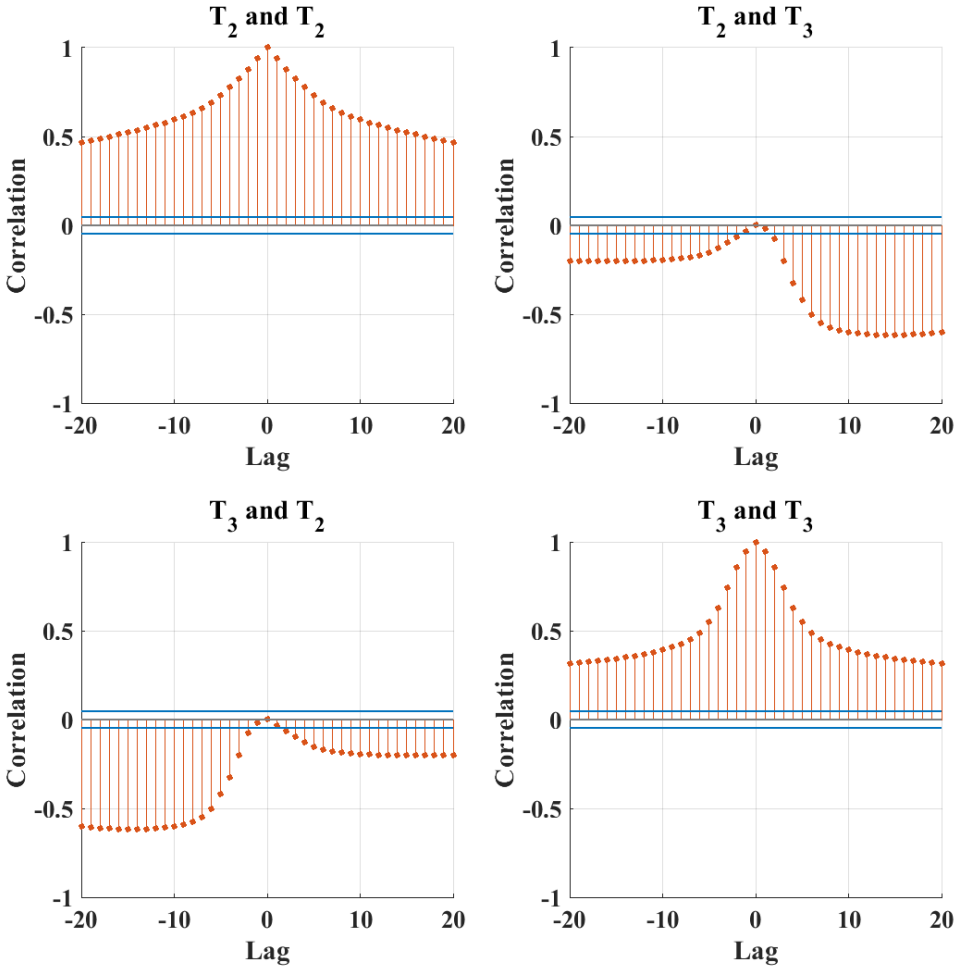

FIGURE 5.24: Autocorrelation plot of DPCA training data for lag value zero

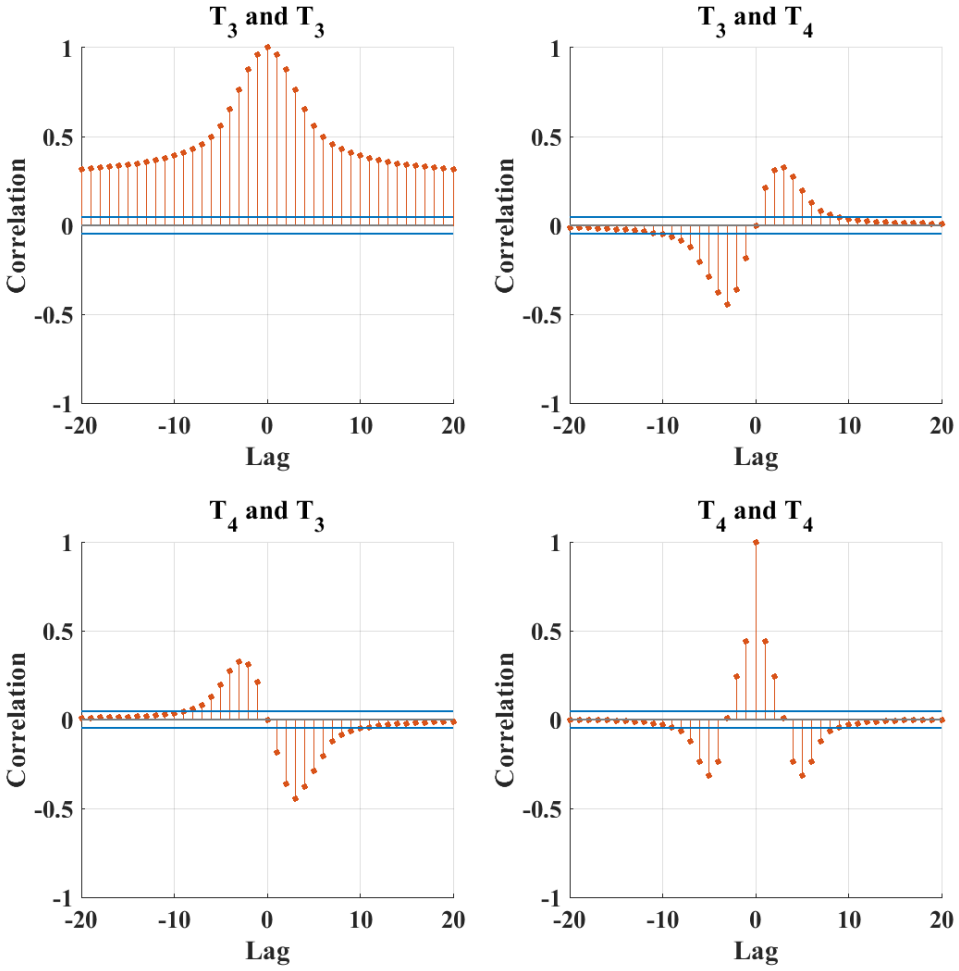

FIGURE 5.25: Autocorrelation plot of DPCA training data for lag value one

To validate the model's performance, a data set of set point changes was generated using the CFD model. The results of the concentration changes within the measurement points are shown in Fig. 5.26.

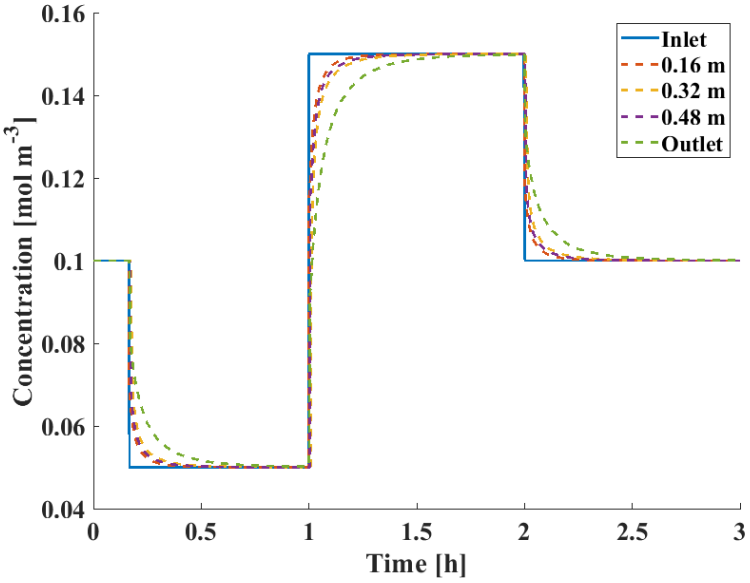

FIGURE 5.26: Validation CFD data for FD under normal operation circumstances

The inlet concentration data, which is the boundary condition of the system, is shown with a continuous line while concentration values of interior and outlet boundary points are represented using dashed lines. It can be observed that in each case concentration values reach the steady state equaling the inlet concentration values. In case of the outlet, this is the most delayed response. To test the FD capabilities of the DPCA established using data generated by the CM model, a fault signal has been introduced into the system as a failure in the input concentration control. The fault signal as well as the faulty system response compared to the normal steady state shown in Fig. 5.26 can be seen in Fig. 5.27. The sudden spikes as well as the random noise are due to the numerical errors of the CFD solver.

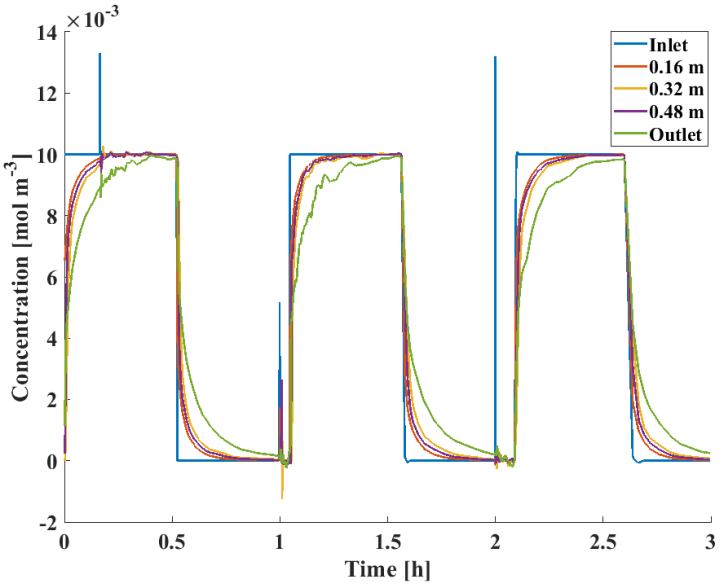

FIGURE 5.27: Fault signal at the inlet and fault response of the system compared to the normal steady state response shown in Fig. 5.26

The Q statistic as well as the resulting alarm signal of the observations are shown in Fig. 5.28.

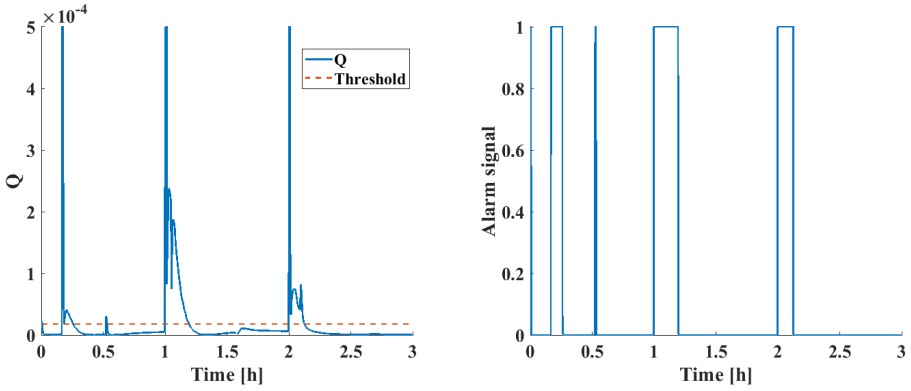

FIGURE 5.28: Q statistic (**left**) of the testing CFD data and alarm responses (**right**)

The results show that while the FD method can successfully identify the onset of faults, the values of the Q statistic diminish after the fault responses reach their steady state values. In this case, this resulted in a MAR score of 0.32 and FAR score of 0. In order to compare the FD capabilities of the DPCA model trained using the CM results, another model was trained using CFD results. The alternative DPCA model was trained and evaluated with the same observation time of 3000 hours and 100-step input steady state change input signals but with data generated by the CFD simulator.

After completing the training, the structures of the two DPCA models were established, and their FD capabilities for a training data set containing 1000 fault signals were compared. The computation time for data generation, FAR, MAR metrics and model structures are displayed in Table 5.9.

TABLE 5.9: Comparison of DPCA models generated from CM and CFD with respect to model structure, computational load and FD metrics for 1000 fault signals (CPU type: Intel(R) Xeon(R) CPU E5620 @ 2.40GHz, Memory speed: 800 MHz)

Characteristics	DPCA based on CM	DPCA based on CFD
Computation time	0.73 h	14.5 h
DPCA lag number	1	2
DPCA PC number	2	2
FAR	0.014	0.002
MAR	0.38	0.22

The results show that while the DPCA generated using the CM model showed degenerated performance in terms of MAR (increase of 0.16 compared to original CFD data trained DPCA) yet the decrement in computational time for training data generation is significant (decrease of 95 % compared to CFD). It may also be argued that more rigorous training of fuzzy inference system through data-based techniques (maximum likelihood estimation methods, etc.) might lead to even more accurate approximation and better FD performance.

5.5.5 Conclusion

During the course of this chapter, an algorithm for creating compartment models (CM) from results obtained through CFD simulators has been presented. The goal was to facilitate data generation and potentially highlight critical areas for sensor placement during FD method development. It was expected that the method could be used to train FD methods with reduced computational load but still provide acceptable FAR and MAR scores compared to more rigorous, first principle models with higher computational load.

The proposed algorithm consist of two phases. In the first phase, the CM structure of the object is defined. For these investigations, the steady state velocity field of the system is utilized. The system was partitioned into elementary cells (EC) in which the local velocity field

was investigated. By analyzing the direction and magnitude of local velocity vectors within the ECs through fuzzy logic, a set of rules was established which were used to categorize the behavior of individual ECs and correlate these ECs to units with idealized behavior. Using the results, the parameters of a CM model to approximate the dynamics of a mixing tank were fitted through optimization based on experimental results.

The method showed greatly reduced computational load for estimating dynamic system behavior compared to CFD methods (computation time was reduced by 95 %). The model was used to train a DPCA FD method for the observed mixing tank. The performance of the FD technique trained using the CM results was used to supervise the system behavior estimated by CFD techniques. The results indicate that the method had good performance for the CFD results, through which it can be inferred that the reduced model proved accurate enough for developing the FD technique in a computationally more efficient manner.

Chapter 6

Conclusion

The research described in the dissertation presents the possible challenges present in Fault Detection (FD) and Isolation (FDI) and provides insights and solutions for select research questions of interest. The dissertation explores the current methods of FD and FDI and contextualizes their shortcomings and strengths in chapter 2, with a strong emphasis on multivariate statistical process monitoring (MSPM) techniques. Three issues were tackled, which include:

- The development of isolation methods for MSPM techniques
- The integration of process risk into FD to minimize false alarm rate
- Developing reduced models to train FD methods for distributed parameter systems in a computationally efficient manner

In chapter 3 a fault isolation technique based on trajectory similarity metrics was developed to supplement the FD method of dynamic principal component analysis (DPCA). The algorithm was tested using a benchmark problem concerning a three tank system. The method proved to be robust in its isolation capabilities, indicated by its F_1 score, which was tested under a broad range of different operating conditions. Its performance was characterized by a macro averaged F_1 score of about 0.75 even under 30 % change in the input variables compared to the steady state where the model was established. This score was well above 0.99 for operating point changes of under 20 % compared to the normal steady state.

In chapter 4 the possibility of combining risk assessment techniques and FD methods for alarm management was explored. A Bayesian network (BN) was developed using failure

mode and effect analysis (FMEA) as a basis. Through the BN, and a DPCA FD method, associated risks of process abnormalities were identified, and a risk priority number was introduced to categorize the severity of failures. High risk failures were signaled by alarms, which were used to alert operators of the need to act immediately. Failures identified through FD but not critical from the perspective of process safety were signaled by warnings only. In this way, a hierarchy between abnormalities was established to support operators in prioritizing tasks and reducing the probability of alarm floods. The applicability of the method has been showcased using the three tank benchmark problem and a model of a dehydrogenation reactor in the hydrogen storage technology.

In chapter 5 the FD problem in distributed parameter systems (DPS) was explored. The data acquisition problem for training data-based FD methods was observed from the perspective of the chemical industry, where spatio-temporal behavior of systems can be characterized using e.g. computational fluid dynamics (CFD) methods. These techniques require significant computational loads, making their use for obtaining training data or real time system supervision impractical. As an alternative, an algorithm was proposed to generate computationally less exhaustive compartment models (CM) using the CFD methods' results. CMs were established using steady state velocity field data within the units by applying fuzzy logic-based inference. The developed CMs were used to approximate the spatio-temporal distribution of process variables in a laboratory scale mixing tank. Residence time distribution was used to characterize the system behavior and evaluate the goodness of both the CFD model and CM. Subsequently, the CM was used to generate training data for training a DPCA FD method for the unit. CFD methods were also used to generate training data, and a CFD-based DPCA model was also established. The performance of the two models for FD was compared, and it was found that the CM-based DPCA could be established with a 95 % decrease in computation time compared to the DPCA based on the CFD model at a cost of a 16 % increase in missed alarm rate. Based on the results, the method was found suitable for system supervision due to the slight deterioration of FD capabilities but with a significant decrease of computational load.

Chapter 7

Thesis points and scientific contribution

In the chapters of the dissertation, the theoretical and practical findings were showcased and conclusively evaluated. In this section, I will give a summary about my research work pertaining to the topic of system supervision through the use of multivariate statistical techniques in the form of thesis points. To accentuate the scope of the work, the relevant conference publications and scientific papers of the author are summarized. These are organized comprehensively, encompassing both results which contribute to specific established thesis points and other research directions not included in the dissertation. The results are listed and comprised in the following item list.

1. **I developed a methodology to enable fault isolation in dynamical systems using trajectory distance metrics and justified its applicability under a wide range of operating conditions within dynamic systems. [85]**

    1.1 I used dynamic principal component analysis as a base fault detection method to analyze system behavior and pinpoint abnormalities in technological units. I fine-tuned the method for various operating states of the system and evaluated the accuracy of the model.

1.2 I recorded characteristic dynamic behavior of the system under different faults and observed trajectory data of fault responses in state space. I explored the dissimilarity of the fault trajectories and drew conclusions about the isolability of fault types.

1.3 I utilized the discrete Fréchet distance metric to compare new fault signals to the established fault library for fault isolation. I observed the isolation capabilities of the method under a wide scope of differing operation conditions. I concluded that the method was able to accurately distinguish the faults under operating conditions in the ± 20 % interval compared to their steady state values, with a macro averaged F_1 score of above 0.99.

- **Related papers**
  - Tarcsay, B. L., Bárkányi, Á., Chován, T., & Németh, S. (2022). A Dynamic Principal Component Analysis and Fréchet-Distance-Based Algorithm for Fault Detection and Isolation in Industrial Processes. Processes, 10(11), 2409.

2. **I confirmed that a methodology combining risk assessment with fault detection techniques for risk-based system supervision could be successfully applied to minimize superfluous alarm rates in technological systems [105, 136].**

2.1 I developed a framework for combining Bayesian networks with failure mode and effect analysis and the results of dynamic principal component analysis for risk-based fault detection.

2.2 I developed a modified, dynamic risk priority number which utilizes missed alarm rate of failures evaluated through dynamic principal component analysis, failure probability based on Bayesian networks and expert knowledge to characterize risk level of process states.

2.3 I utilized the modified risk priority number to categorize process abnormalities into classes which warrant alarms and those which only warrant warnings. Through these classes, the operators' ability to judge whether a process failure requires immediate response or not is increased. Through the use of a case study of both a three tank benchmark system and a dehydrogenation reactor, I concluded that the alarm rate was decreased by 20 – 30 % alleviating the pressure alarm floods exert on operators.

- **Related papers**
  - Tarcsay, B. L., Bárkányi, Á., Németh, S., Chován, T., Lovas, L., & Egedy, A. (2024). Risk-Based Fault Detection Using Bayesian Networks Based on Failure Mode and Effect Analysis. Sensors, 24(11), 3511.
  - Bárkányi, Á., Tarcsay, B. L., Lovas, L., Mérő, T., Chován, T., & Egedy, A. (2024). Future of hydrogen economy: simulation-based comparison of LOHC systems. Clean Technologies and Environmental Policy, 26(5), 1521-1536.

3. **I proved that compartment models can be used to generate data to train fault detection algorithms at reduced computational cost while retaining acceptable performance of the fault detection method [137, 138, 139].**

   3.1 I investigated the methods of developing compartment models using the results of computational fluid dynamics methods in a rigorous manner.

   3.2 I utilized fuzzy logic to describe the transport phenomena in a complex system through a network of idealized models and accurately approximate system responses. I validated a compartment model and computational fluid dynamics model using experimental data obtained through a laboratory scale mixing tank.

   3.3 I utilized the compartment model to develop a fault detection scheme for the mixing tank and compared its fault detection performance with a fault detection scheme based on data gathered from computational fluid dynamics methods. I found that the fault detection scheme based on the compartment model could be established with 95 % less computational time than the one based on computational fluid dynamics at a cost of an increase of 16 % in missed alarm rate metrics and negligible false alarm rate metric increase. I concluded that the method could be used to accurately approximate the spatio-temporal system responses and used to train fault detection methods with acceptable performance at a significantly decreased computational cost.

   - **Related papers**
     - Tarcsay, B. L., Bárkányi, Á., Chován, T., & Németh, S. (2021). Development of Compartment Models for Diagnostic Purposes. Hungarian Journal of Industry and Chemistry, 49(1), 47-58.

  - Tarcsay, B. L., Bobek-Nagy, J., & Egedy, A. (2022). Experimental and modeling based dead-volume detection for externally stirred tanks. Chemical Engineering Communications, 209(6), 1-15.
  - Tarcsay, B. L., Németh, S., Chován, T., & Bárkányi, Á. (2022). Development of CFD based Compartment Models for Analysing High Risk Processes. Chemical Engineering Transactions, 91, 487-492.

Finally, I would like to also provide a list of papers published during my PhD studies but not included in my thesis material, shown below.

- Other scientific publications not related to thesis points during the doctoral research
  - Tarcsay, B. L., Németh, S., Chován, T., & Bárkányi, Á. (2021). Hybrid Fault Detection Method for a Distillation Unit. Chemical Engineering Transactions, 88, 391-396.
  - Tóth, P., Tarcsay, B. L., Kovács, Z., Ionescu, D. T., Németh, S., & Domokos, E. (2023). Assessment of the correlation between the nutrient load from migratory bird excrement and water quality by principal component analysis in a freshwater habitat. Environmental Science and Pollution Research, 30(24), 66033-66049.
  - Kaman, A., Balogh, L., Jakab, M., Meszlenyi, A., Tarcsay, B. L., & Egedy, A. (2023). The Effect of 3D Printing Process Parameters on Nylon Based Composite Filaments: Experimental and Modelling Study. Chemical Engineering Transactions, 100, 481-486.
  - Kámán, A., Balogh, L., Tarcsay, B. L., Jakab, M., Meszlényi, A., Turcsán, T., & Egedy, A. (2024). Glass Fibre-Reinforced Extrusion 3D-Printed Composites: Experimental and Numerical Study of Mechanical Properties. Polymers, 16(2).
  - Zsinka, V., Tarcsay, B. L., & Miskolczi, N. (2024). Determination of Kinetic and Thermodynamic Parameters of Biomass Gasification with TG-FTIR and Regression Model Fitting. Energies, 17(8), 1875.

Appendix A

Employed performance metrics for FD and FDI method evaluation

During my dissertation, fault detection and fault isolation prowess had to be tested. Fault detection accuracy can be evaluated using the FAR and MAR metrics, for which the calculation methods are shown in Eq. A.1 and Eq. A.2 [167].

$$FAR = \frac{FN}{TP + FN} \tag{A.1}$$

$$MAR = \frac{FP}{TN + FP} \tag{A.2}$$

The variables FN, TP, FP and TN, respectively, refer to:

- Samples incorrectly classified as faults under normal operating conditions (FN-False Negative).
- Samples correctly classified under normal operating conditions (TP-True Positive).
- Samples incorrectly classified as normal under abnormal operating conditions (FP-False Positive).
- Samples correctly classified under abnormal operating conditions (TN-True Negative).

at the end of an abnormality detection process.

Since the isolation step of FDI is basically a classification procedure linking detected faults to a specific group of previously known root causes, general performance scores of classification methods may be used to evaluate the isolation performance. The most common performance metrics include classification accuracy, recall, sensitivity and the F_1 metric [168]. The F_1 metric shows the harmonic mean of a classifiers recall (R) and precision (P) ability and is one of the most widely used and thorough methods for evaluating classification performance. Equations A.3, A.4 and A.5 show the method for calculating P, R and F for a multi-class classification problem where $c = 1, 2, ..., C$ such that C is the total number of distinct labels [168] .

$$P_c = \frac{\sum_{c=1}^{C} TP_c}{\sum_{c=1}^{C} TP_c + FP_c} \tag{A.3}$$

$$R_c = \frac{\sum_{c=1}^{C} TP_c}{\sum_{c=1}^{C} TP_c + FN_c} \tag{A.4}$$

$$F_{1,c} = \frac{2P_cR_c}{P_c + R_c} \tag{A.5}$$

Appendix B

The three tank benchmark problem

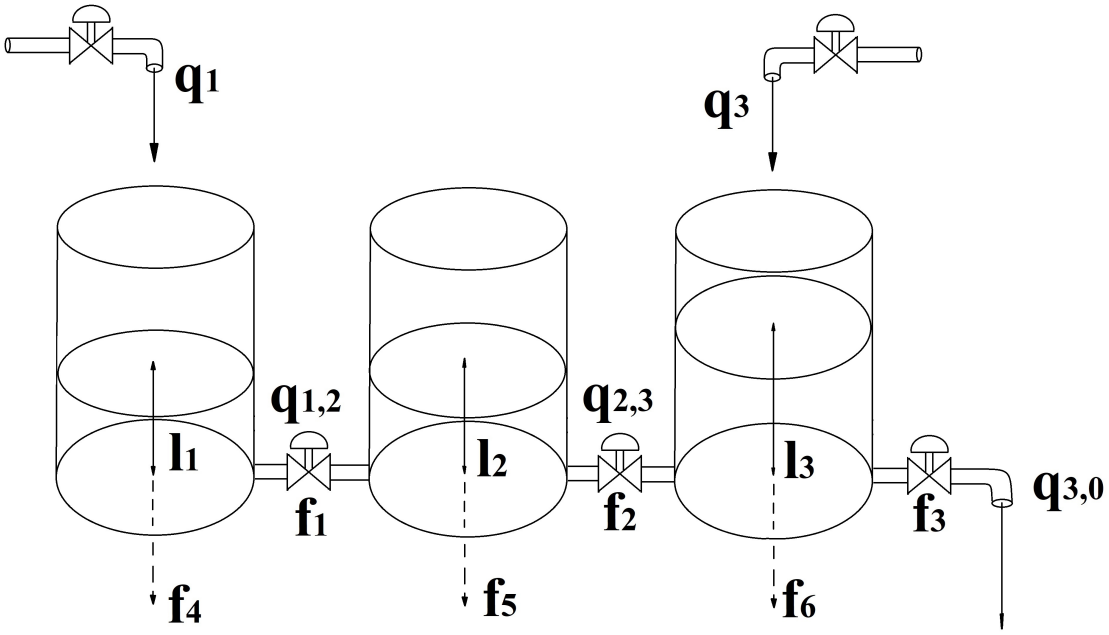

FIGURE B.1: Scheme of the investigated three tank system [98]

The investigated system contains three interconnected cylindrical tanks in series with uniform cross section S. The outlet position of each tank is located at the bottom of the respective tank. Connections between the tanks are possible though flow within the cylindrical pipes connecting them which all have cross section S_n. Inlet flow rates q_1 and q_3 are controlled through externally operated inlet valves.

The three measurable outputs of the system are the liquid levels in each tank (l_1, l_2, l_3), while the measurable inputs that influence the levels are the inlet flow rates in the first and last tank

(q_1, q_3). Flow rates between the tanks are denoted by $q_{i,j}$, where i and j are indices of the connected tanks or the outside (0), respectively. The flow rates between tanks are dependent on the liquid level within each tank as well as the outflow coefficient $\mu_{i,j}$ which is a function of the valve position of the pipe segment.

Six possible faults within the system have been taken into account to validate the method. The first three involve the decrement of the outflow coefficients in each pipe segment (f_1, f_2, f_3) that can be caused by build-up of sediment within the pipe segment or malfunction of the control valve. The latter three are the presence of leakages within each tank (f_4, f_5, f_6).

To gather data about the system behaviour under various normal and irregular operating conditions, the first principle model of the system was established. The system of differential equations governing the liquid level within each tank is shown in Eq. B.1, provided that the cross sections of each tank are unchanged during the observation.

$$\begin{aligned}
\frac{dl_1}{dt} &= \frac{1}{S}\left(q_1 - q_{1,2} - q_{1,f}\right) \\
\frac{dl_2}{dt} &= \frac{1}{S}\left(q_{1,2} - q_{2,3} - q_{2,f}\right) \\
\frac{dl_3}{dt} &= \frac{1}{S}\left(q_3 + q_{2,3} - q_{3,0} - q_{3,f}\right)
\end{aligned} \tag{B.1}$$

Flow rates between tanks were calculated according to the set of equations described in Eq. B.2 based on Torricellis law.

$$\begin{aligned}
q_{i,j} &= \mu_{i,j} S_n \operatorname{sgn}\left(l_i - l_j\right) \sqrt{2g \mid l_i - l_j \mid}, && i \neq 3 \\
q_{3,0} &= \mu_{3,0} Sn \sqrt{2g l_3} \\
q_{i,f} &= f_{i+3} \mu_f S_f \sqrt{2g l_i}
\end{aligned} \tag{B.2}$$

For the calculation of volumetric flow exiting the tank due to leakages $(q_{i,f})$, the fault signals f_{i+3} are assumed to be binary signals with value one if leakage is present within the tank and value of zero otherwise.

To obtain data about the system under normal operating conditions, simulations have been conducted with the model. A steady-state for the system has been chosen, and changes have been made to the input variables (the inlet flow rates) to assess the changes within water level in the tank. The acquired data were utilized thereafter to establish the DPCA transformation.

The operational parameters of the observed steady-state as well as the constructional parameters of the tank and parameters of possible faults are displayed in Table B.1.

TABLE B.1: Operational and constructional parameters of the investigated system.

$\boldsymbol{q_1}\,[\mathrm{m^3 s^{-1}}]$	$\boldsymbol{q_2}\,[\mathrm{m^3 s^{-1}}]$	$\boldsymbol{\mu_{1,2}}\,[-]$	$\boldsymbol{\mu_{2,3}}\,[-]$	$\boldsymbol{\mu_{3,0}}\,[-]$
1.5×10^{-4}	1.5×10^{-4}	0.5	0.5	0.6
$\boldsymbol{\mu_f}\,[-]$	$\boldsymbol{S}\,[\mathrm{m^2}]$	$\boldsymbol{S_p}\,[\mathrm{m^2}]$	$\boldsymbol{S_f}\,[\mathrm{m^2}]$	$\boldsymbol{l_{i,0}}\,[\mathrm{m}]$
0.6	1.5×10^{-2}	5×10^{-5}	5×10^{-5}	0

Bibliography

[1] Web of science. https://www.webofscience.com/wos/woscc/basic-search. Accessed: 2023-12-16.

[2] Google patents. https://patents.google.com/. Accessed: 2024-08-03.

[3] Venkat Venkatasubramanian, Raghunathan Rengaswamy, Kewen Yin, and Surya N Kavuri. A review of process fault detection and diagnosis: Part i: Quantitative model-based methods. *Computers & chemical engineering*, 27(3):293–311, 2003.

[4] Edward Broughton. The bhopal disaster and its aftermath: a review. *Environmental Health*, 4(1):1–6, 2005.

[5] Joseph Isimite and Philip Rubini. A dynamic hazop case study using the texas city refinery explosion. *Journal of loss prevention in the process industries*, 40:496–501, 2016.

[6] Efthimia K Mihailidou, Konstantinos D Antoniadis, and Marc J Assael. The 319 major industrial accidents since 1917. *International review of chemical engineering*, 4(6):529–540, 2012.

[7] Peter JM Sonnemans and Patrick MW Körvers. Accidents in the chemical industry: are they foreseeable? *Journal of Loss Prevention in the Process Industries*, 19(1):1–12, 2006.

[8] Venkat Venkatasubramanian, Raghunathan Rengaswamy, Surya N Kavuri, and Kewen Yin. A review of process fault detection and diagnosis: Part iii: Process history based methods. *Computers & chemical engineering*, 27(3):327–346, 2003.

[9] Venkat Venkatasubramanian, Raghunathan Rengaswamy, and Surya N Kavuri. A review of process fault detection and diagnosis: Part ii: Qualitative models and search strategies. *Computers & chemical engineering*, 27(3):313–326, 2003.

[10] Janos Gertler. Analytical redundancy methods in fault detection and isolation-survey and synthesis. *IFAC Proceedings Volumes*, 24(6):9–21, 1991.

[11] EL Ding, H Fennel, and SX Ding. Model-based diagnosis of sensor faults for esp systems. *Control engineering practice*, 12(7):847–856, 2004.

[12] Ron J Patton and Jie Chen. A review of parity space approaches to fault diagnosis. *IFAC Proceedings Volumes*, 24(6):65–81, 1991.

[13] EYEY Chow and Alan Willsky. Analytical redundancy and the design of robust failure detection systems. *IEEE Transactions on automatic control*, 29(7):603–614, 1984.

[14] Janos Gertler. *Fault detection and diagnosis in engineering systems*. CRC press, 2017.

[15] Hamed Tolouei and Mahdi Aliyari Shoorehdeli. Nonlinear parity approach to sensor fault detection in ph neutralization system. In *2017 Iranian Conference on Electrical Engineering (ICEE)*, pages 889–894. IEEE, 2017.

[16] Abdel Aitouche, Quan Yang, and B Ould Bouamama. Fault detection and isolation of pem fuel cell system based on nonlinear analytical redundancy: An application via parity space approach. *The European Physical Journal-Applied Physics*, 54(2):23408, 2011.

[17] V Krishnaswami and G Rizzoni. Nonlinear parity equation residual generation for fault detection and isolation. *IFAC Proceedings Volumes*, 27(5):305–310, 1994.

[18] Majid Ghaniee Zarch and Mahdi Aliyari Shoorehdeli. Generalization of parity space to fault detection based on takagi-sugeno fuzzy models for non-linear dynamic systems. *Expert Systems*, 35(1):e12228, 2018.

[19] Sing Kiong Nguang, Ping Zhang, and Steven X Ding. Parity relation based fault estimation for nonlinear systems: An lmi approach. *International Journal of Automation and Computing*, 4:164–168, 2007.

[20] Yosr Garbouj, Talel Zouari, and Moufida Ksouri. Parity space method for mode detection of a nonlinear switching system using takagi–sugeno modeling. *International Journal of Fuzzy Systems*, 21(3):837–851, 2019.

[21] Ying Zheng, Huajing Fang, and Hua O Wang. Takagi-sugeno fuzzy-model-based fault detection for networked control systems with markov delays. *IEEE Transactions on Systems, Man, and Cybernetics, Part B (Cybernetics)*, 36(4):924–929, 2006.

[22] Ron J Patton and Jie Chen. Observer-based fault detection and isolation: Robustness and applications. *Control Engineering Practice*, 5(5):671–682, 1997.

[23] George Zames. Feedback and optimal sensitivity: Model reference transformations, multiplicative seminorms, and approximate inverses. *IEEE Transactions on automatic control*, 26(2):301–320, 1981.

[24] Maiying Zhong, Ting Xue, and Steven X Ding. A survey on model-based fault diagnosis for linear discrete time-varying systems. *Neurocomputing*, 306:51–60, 2018.

[25] Maiying Zhong, Steven X Ding, James Lam, and Haibo Wang. An lmi approach to design robust fault detection filter for uncertain lti systems. *Automatica*, 39(3):543–550, 2003.

[26] Steven X Ding. *Model-based fault diagnosis techniques: design schemes, algorithms, and tools*. Springer Science & Business Media, 2008.

[27] Andres Marcos, Subhabrata Ganguli, and Gary Balas. Application of h-infinity fault detection and isolation to a boeing 747-100/200 aircraft. In *AIAA guidance, navigation, and control conference and exhibit*, page 4944, 2002.

[28] Steven X Ding. Data-driven design of model-based fault diagnosis systems. *IFAC Proceedings Volumes*, 45(15):840–847, 2012.

[29] Ying Yang, Steven X Ding, and Linlin Li. On observer-based fault detection for nonlinear systems. *Systems & Control Letters*, 82:18–25, 2015.

[30] PM Frank, G Schrier, and E Alcorta Garcia. Nonlinear observers for fault detection and isolation. In *New Directions in nonlinear observer design*, pages 399–422. Springer, 2007.

[31] Xiaodong Zhang, Marios M Polycarpou, and Thomas Parisini. Fault diagnosis of a class of nonlinear uncertain systems with lipschitz nonlinearities using adaptive estimation. *Automatica*, 46(2):290–299, 2010.

[32] Abdul Qayyum Khan, Muhammad Abid, and Steven X Ding. Fault detection filter design for discrete-time nonlinear systems—a mixed h_-/h_∞ optimization. *Systems & Control Letters*, 67:46–54, 2014.

[33] Christodoulos Keliris, Marios M Polycarpou, and Thomas Parisini. A robust nonlinear observer-based approach for distributed fault detection of input–output interconnected systems. *Automatica*, 53:408–415, 2015.

[34] Linlin Li, Steven X Ding, Jianbin Qiu, Ying Yang, and Dongmei Xu. Fuzzy observer-based fault detection design approach for nonlinear processes. *IEEE Transactions on Systems, Man, and Cybernetics: Systems*, 47(8):1941–1952, 2016.

[35] T Muller, Nicolas Réhault, and Tim Rist. A qualitive modeling approach for fault detection and diagnosis on hvac systems. 2013.

[36] Paul M Frank. Fault diagnosis in dynamic systems using analytical and knowledge-based redundancy: A survey and some new results. *automatica*, 26(3):459–474, 1990.

[37] EJ Henley. Application of expert systems to fault diagnosis. In *AIChE annual meeting, San Francisco, CA*, 1984.

[38] DN Batanov and Zhuang Cheng. An object-oriented expert system for fault diagnosis in the ethylene distillation process. *Computers in Industry*, 27(3):237–249, 1995.

[39] J Zhang and PD Roberts. Process fault diagnosis with diagnostic rules based on structural decomposition. *Journal of Process Control*, 1(5):259–269, 1991.

[40] Wayne R Becraft and PL Lee. An integrated neural network/expert system approach for fault diagnosis. *Computers & chemical engineering*, 17(10):1001–1014, 1993.

[41] Carlos Rojas-Guzman and Mark A Kramer. Comparison of belief networks and rule-based expert systems for fault diagnosis of chemical processes. *Engineering Applications of Artificial Intelligence*, 6(3):191–202, 1993.

[42] Nizar Chatti, Belkacem Ould-Bouamama, Anne-Lise Gehin, and Rochdi Merzouki. Signed bond graph for multiple faults diagnosis. *Engineering Applications of Artificial Intelligence*, 36:134–147, 2014.

[43] Nizar Chatti, Belkacem Ould-Bouamama, Anne-Lise Gehin, and Rochdi Merzouki. Merging bond graph and signed directed graph to improve fdi procedure. In *2013 European Control Conference (ECC)*, pages 1457–1462. IEEE, 2013.

[44] Yong-Kuo Liu, Guo-Hua Wu, Chun-Li Xie, Zhi-Yong Duan, Min-Jun Peng, and Meng-Kun Li. A fault diagnosis method based on signed directed graph and matrix for nuclear power plants. *Nuclear Engineering and Design*, 297:166–174, 2016.

[45] Erika Echavarria, Tetsuo Tomiyama, H Huberts, and G Van Bussel. Fault diagnosis system for an offshore wind turbine using qualitative physics. In *Proc. EWEC*. Citeseer, 2008.

[46] Yu Hen Hu and Jeng-Neng Hwang. Handbook of neural network signal processing, 2002.

[47] Frank Rosenblatt et al. *Principles of neurodynamics: Perceptrons and the theory of brain mechanisms*, volume 55. Spartan books Washington, DC, 1962.

[48] Seongmin Heo and Jay H Lee. Fault detection and classification using artificial neural networks. *IFAC-PapersOnLine*, 51(18):470–475, 2018.

[49] Venkat Venkatasubramanian, Ravi Vaidyanathan, and Y Yamamoto. Process fault detection and diagnosis using neural networks—i. steady-state processes. *Computers & Chemical Engineering*, 14(7):699–712, 1990.

[50] S Rajakarunakaran, P Venkumar, D Devaraj, and K Surya Prakasa Rao. Artificial neural network approach for fault detection in rotary system. *Applied Soft Computing*, 8(1):740–748, 2008.

[51] Michele Basseville, Igor V Nikiforov, et al. *Detection of abrupt changes: theory and application*, volume 104. prentice Hall Englewood Cliffs, 1993.

[52] Walter Andrew Shewhart. Control of quality of manufactured product. 1929.

[53] SW Roberts. Control chart tests based on geometric moving averages. *Technometrics*, pages 239–250, 1959.

[54] Alexander Kalmuk, Oleg Granichin, Olga Granichina, and Mingyue Ding. Detection of abrupt changes in autonomous system fault analysis using spatial adaptive estimation of nonparametric regression. In *2016 American Control Conference (ACC)*, pages 6839–6844. IEEE, 2016.

[55] Sotiris Bersimis, John Panaretos, and Stelios Psarakis. Multivariate statistical process control charts and the problem of interpretation: a short overview and some applications in industry. *arXiv preprint arXiv:0901.2880*, 2009.

[56] Wenfu Ku, Robert H Storer, and Christos Georgakis. Disturbance detection and isolation by dynamic principal component analysis. *Chemometrics and intelligent laboratory systems*, 30(1):179–196, 1995.

[57] Aurélie Bellemans, Gianmarco Aversano, Axel Coussement, and Alessandro Parente. Feature extraction and reduced-order modelling of nitrogen plasma models using principal component analysis. *Computers & chemical engineering*, 115:504–514, 2018.

[58] Sang Wook Choi, Changkyu Lee, Jong-Min Lee, Jin Hyun Park, and In-Beum Lee. Fault detection and identification of nonlinear processes based on kernel pca. *Chemometrics and intelligent laboratory systems*, 75(1):55–67, 2005.

[59] J Edward Jackson and Govind S Mudholkar. Control procedures for residuals associated with principal component analysis. *Technometrics*, pages 341–349, 1979.

[60] Muhammad Mashuri, Muhammad Ahsan, Muhammad Hisyam Lee, Dedy Dwi Prastyo, et al. Pca-based hotelling's t2 chart with fast minimum covariance determinant (fmcd) estimator and kernel density estimation (kde) for network intrusion detection. *Computers & Industrial Engineering*, 158:107447, 2021.

[61] Herman Wold. Soft modelling by latent variables: the non-linear iterative partial least squares (nipals) approach. *Journal of Applied Probability*, 12(S1):117–142, 1975.

[62] Svante Wold, Arnold Ruhe, Herman Wold, and WJ Dunn, Iii. The collinearity problem in linear regression. the partial least squares (pls) approach to generalized inverses. *SIAM Journal on Scientific and Statistical Computing*, 5(3):735–743, 1984.

[63] Soraya Berbache, Mohamed Faouzi Harkat, and Frédéric Kratz. Sensor fault detection and isolation techniques based on pca. In *2019 international conference on advanced electrical engineering (ICAEE)*, pages 1–7. IEEE, 2019.

[64] Yunbing Huang, Janos Gertler, and Thomas J McAvoy. Sensor and actuator fault isolation by structured partial pca with nonlinear extensions. *Journal of Process Control*, 10(5):459–469, 2000.

[65] Janos Gertler, Weihua Li, Yunbing Huang, and Thomas McAvoy. Isolation enhanced principal component analysis. *AIChE Journal*, 45(2):323–334, 1999.

[66] Steven Ding, Ping Zhang, Eve Ding, Amol Naik, Pengcheng Deng, and Weihua Gui. On the application of pca technique to fault diagnosis. *Tsinghua Science and Technology*, 15(2):138–144, 2010.

[67] Fouzi Harrou, Mohamed N Nounou, Hazem N Nounou, and Muddu Madakyaru. Statistical fault detection using pca-based glr hypothesis testing. *Journal of loss prevention in the process industries*, 26(1):129–139, 2013.

[68] Yining Dong and S Joe Qin. A novel dynamic pca algorithm for dynamic data modeling and process monitoring. *Journal of Process Control*, 67:1–11, 2018.

[69] Rongfu Luo, Manish Misra, and David M Himmelblau. Sensor fault detection via multiscale analysis and dynamic pca. *Industrial & Engineering Chemistry Research*, 38(4):1489–1495, 1999.

[70] Tiago J Rato and Marco S Reis. Defining the structure of dpca models and its impact on process monitoring and prediction activities. *Chemometrics and Intelligent Laboratory Systems*, 125:74–86, 2013.

[71] Rasmus Bro, Karin Kjeldahl, Age K Smilde, and HAL Kiers. Cross-validation of component models: a critical look at current methods. *Analytical and bioanalytical chemistry*, 390:1241–1251, 2008.

[72] Erik Vanhatalo, Murat Kulahci, and Bjarne Bergquist. On the structure of dynamic principal component analysis used in statistical process monitoring. *Chemometrics and intelligent laboratory systems*, 167:1–11, 2017.

[73] Wahiba Bounoua and Azzeddine Bakdi. Fault detection and diagnosis of nonlinear dynamical processes through correlation dimension and fractal analysis based dynamic kernel pca. *Chemical Engineering Science*, 229:116099, 2021.

[74] Chudong Tong, Ting Lan, and Xuhua Shi. Fault detection and diagnosis of dynamic processes using weighted dynamic decentralized pca approach. *Chemometrics and Intelligent Laboratory Systems*, 161:34–42, 2017.

[75] Azzeddine Bakdi and Abdelmalek Kouadri. A new adaptive pca based thresholding scheme for fault detection in complex systems. *Chemometrics and Intelligent Laboratory Systems*, 162:83–93, 2017.

[76] Manish Misra, H Henry Yue, S Joe Qin, and Cheng Ling. Multivariate process monitoring and fault diagnosis by multi-scale pca. *Computers & Chemical Engineering*, 26(9):1281–1293, 2002.

[77] You-Jin Park, Shu-Kai S Fan, and Chia-Yu Hsu. A review on fault detection and process diagnostics in industrial processes. *Processes*, 8(9):1123, 2020.

[78] Uwe Kruger and Grigorios Dimitriadis. Diagnosis of process faults in chemical systems using a local partial least squares approach. *AIChE Journal*, 54(10):2581–2596, 2008.

[79] Qilong Jia and Yingwei Zhang. Quality-related fault detection approach based on dynamic kernel partial least squares. *Chemical Engineering Research and Design*, 106:242–252, 2016.

[80] Sang Wook Choi and In-Beum Lee. Nonlinear dynamic process monitoring based on dynamic kernel pca. *Chemical engineering science*, 59(24):5897–5908, 2004.

[81] Anam Abid, Muhammad Tahir Khan, and Javaid Iqbal. A review on fault detection and diagnosis techniques: basics and beyond. *Artificial Intelligence Review*, 54:3639–3664, 2021.

[82] O Zadakbar, S Imtiaz, and Faisal Khan. Dynamic risk assessment and fault detection using a multivariate technique. *Process Safety Progress*, 32(4):365–375, 2013.

[83] Matthieu Lucke, Moncef Chioua, Chriss Grimholt, Martin Hollender, and Nina F Thornhill. Advances in alarm data analysis with a practical application to online alarm flood classification. *Journal of Process Control*, 79:56–71, 2019.

[84] Jia Cai, Hasan Ferdowsi, and Jagannathan Sarangapani. Model-based fault detection, estimation, and prediction for a class of linear distributed parameter systems. *Automatica*, 66:122–131, 2016.

[85] Bálint Levente Tarcsay, Ágnes Bárkányi, Tibor Chován, and Sándor Németh. A dynamic principal component analysis and fréchet-distance-based algorithm for fault detection and isolation in industrial processes. *Processes*, 10(11):2409, 2022.

[86] Yvon Tharrault, Gilles Mourot, and José Ragot. Fault detection and isolation with robust principal component analysis. In *2008 16th Mediterranean Conference on Control and Automation*, pages 59–64. IEEE, 2008.

[87] Gary R Halligan and S Jagannathan. Pca-based fault isolation and prognosis with application to pump. *The international journal of advanced manufacturing technology*, 55:699–707, 2011.

[88] Fu Xiao, Shengwei Wang, Xinhua Xu, and Gaoming Ge. An isolation enhanced pca method with expert-based multivariate decoupling for sensor fdd in air-conditioning systems. *Applied Thermal Engineering*, 29(4):712–722, 2009.

[89] D Garcia-Alvarez, MJ Fuente, and GI Sainz. Fault detection and isolation in transient states using principal component analysis. *Journal of Process Control*, 22(3):551–563, 2012.

[90] Yue Yu, Min-jun Peng, Hang Wang, Zhan-guo Ma, and Wei Li. Improved pca model for multiple fault detection, isolation and reconstruction of sensors in nuclear power plant. *Annals of Nuclear Energy*, 148:107662, 2020.

[91] Hanli Weng, Sheng Wang, Yi Wan, Xiangning Lin, Zhenxing Li, and Jingguang Huang. Discrete fréchet distance algorithm based criterion of transformer differential protection with the immunity to saturation of current transformer. *International Journal of Electrical Power & Energy Systems*, 115:105449, 2020.

[92] Shize Huang, Xiaolu Yang, Ling Wang, Wei Chen, Fan Zhang, and Decun Dong. Two-stage turnout fault diagnosis based on similarity function and fuzzy c-means. *Advances in Mechanical Engineering*, 10(12):1687814018811402, 2018.

[93] Jingwei Wang, Yun Yuan, Tianle Ni, Yunlong Ma, Min Liu, Gaowei Xu, and Weiming Shen. Anomalous trajectory detection and classification based on difference and intersection set distance. *IEEE Transactions on Vehicular Technology*, 69(3):2487–2500, 2020.

[94] Haozhou Wang, Han Su, Kai Zheng, Shazia Sadiq, and Xiaofang Zhou. An effectiveness study on trajectory similarity measures. In *Proceedings of the Twenty-Fourth Australasian Database Conference-Volume 137*, pages 13–22, 2013.

[95] Han Su, Shuncheng Liu, Bolong Zheng, Xiaofang Zhou, and Kai Zheng. A survey of trajectory distance measures and performance evaluation. *The VLDB Journal*, 29:3–32, 2020.

[96] Yaguang Tao, Alan Both, Rodrigo I Silveira, Kevin Buchin, Stef Sijben, Ross S Purves, Patrick Laube, Dongliang Peng, Kevin Toohey, and Matt Duckham. A comparative analysis of trajectory similarity measures. *GIScience & Remote Sensing*, 58(5):643–669, 2021.

[97] Thomas Eiter and Heikki Mannila. Computing discrete fréchet distance. 1994.

[98] Didier Theilliol, Hassan Noura, and Jean-Christophe Ponsart. Fault diagnosis and accommodation of a three-tank system based on analytical redundancy. *ISA transactions*, 41(3):365–382, 2002.

[99] Miguel A Sainz, Joaquim Armengol, and Josep Vehı. Fault detection and isolation of the three-tank system using the modal interval analysis. *Journal of process control*, 12(2):325–338, 2002.

[100] Birgit Köppen-Seliger, E Alcorta García, and Paul M Frank. Fault detection: Different strategies for modelling applied to the three tank benchmark—a case study. In *1999 European Control Conference (ECC)*, pages 4432–4437. IEEE, 1999.

[101] Daniel Amigo, David Sánchez Pedroche, Jesús García, and José Manuel Molina. Review and classification of trajectory summarisation algorithms: From compression to segmentation. *International Journal of Distributed Sensor Networks*, 17(10):15501477211050729, 2021.

[102] Thomas Devogele, Laurent Etienne, Maxence Esnault, and Florian Lardy. Optimized discrete fréchet distance between trajectories. In *Proceedings of the 6th ACM SIGSPATIAL Workshop on Analytics for Big Geospatial Data*, pages 11–19, 2017.

[103] Alan Saalfeld. Topologically consistent line simplification with the douglas-peucker algorithm. *Cartography and Geographic Information Science*, 26(1):7–18, 1999.

[104] Alejandro J Rojas and Hugo O Garcés. Signal-to-noise ratio based fault detection and identification. *Frontiers in Control Engineering*, 3:806558, 2022.

[105] Bálint Levente Tarcsay, Ágnes Bárkányi, Sándor Németh, Tibor Chován, László Lovas, and Attila Egedy. Risk-based fault detection using bayesian networks based on failure mode and effect analysis. *Sensors*, 24(11), 2024.

[106] O Zadakbar, S Imtiaz, and Faisal Khan. Why risk-based multivariate fault detection and diagnosis? *IFAC Proceedings Volumes*, 46(32):672–677, 2013.

[107] Rym Kanes, Maria Clementina Ramirez Marengo, Hazem Abdel-Moati, Jack Cranefield, and Luc Véchot. Developing a framework for dynamic risk assessment using bayesian networks and reliability data. *Journal of Loss Prevention in the Process Industries*, 50:142–153, 2017.

[108] Hongyang Yu, Faisal Khan, and Vikram Garaniya. Risk-based fault detection using self-organizing map. *Reliability Engineering & System Safety*, 139:82–96, 2015.

[109] Md Tanjin Amin, Faisal Khan, Salim Ahmed, and Syed Imtiaz. Risk-based fault detection and diagnosis for nonlinear and non-gaussian process systems using r-vine copula. *Process Safety and Environmental Protection*, 150:123–136, 2021.

[110] Benjamin Rutt, Umit Catalyurek, Aram Hakobyan, Kyle Metzroth, Tunc Aldemir, Richard Denning, Sean Dunagan, and David Kunsman. Distributed dynamic event tree generation for reliability and risk assessment. In *2006 IEEE Challenges of Large Applications in Distributed Environments*, pages 61–70. IEEE, 2006.

[111] Mohammad Yazdi, Sohag Kabir, and Martin Walker. Uncertainty handling in fault tree based risk assessment: state of the art and future perspectives. *Process Safety and Environmental Protection*, 131:89–104, 2019.

[112] Lefayet Sultan Lipol and Jahirul Haq. Risk analysis method: Fmea/fmeca in the organizations. *International Journal of Basic & Applied Sciences*, 11(5):74–82, 2011.

[113] Huizhi Bao, Faisal Khan, Tariq Iqbal, and Yanjun Chang. Risk-based fault diagnosis and safety management for process systems. *Process Safety Progress*, 30(1):6–17, 2011.

[114] Faisal I Khan and Paul R Amyotte. How to make inherent safety practice a reality. *The Canadian Journal of Chemical Engineering*, 81(1):2–16, 2003.

[115] Terje Aven. Risk assessment and risk management: Review of recent advances on their foundation. *European journal of operational research*, 253(1):1–13, 2016.

[116] Min Hyok Jon, Yun Pyong Kim, and Uk Choe. Determination of a safety criterion via risk assessment of marine accidents based on a markov model with five states and mcmc simulation and on three risk factors. *Ocean Engineering*, 236:109000, 2021.

[117] Naimeh Sadeghi, Aminah Robinson Fayek, and Witold Pedrycz. Fuzzy monte carlo simulation and risk assessment in construction. *Computer-Aided Civil and Infrastructure Engineering*, 25(4):238–252, 2010.

[118] Sohag Kabir and Yiannis Papadopoulos. Applications of bayesian networks and petri nets in safety, reliability, and risk assessments: A review. *Safety science*, 115:154–175, 2019.

[119] Shahrzad Faghih-Roohi, Min Xie, and Kien Ming Ng. Accident risk assessment in marine transportation via markov modelling and markov chain monte carlo simulation. *Ocean engineering*, 91:363–370, 2014.

[120] Philippe Weber, Gabriela Medina-Oliva, Christophe Simon, and Benoît Iung. Overview on bayesian networks applications for dependability, risk analysis and maintenance areas. *Engineering Applications of Artificial Intelligence*, 25(4):671–682, 2012.

[121] Zhongyi Wu, Weidong Liu, and Wenbin Nie. Literature review and prospect of the development and application of fmea in manufacturing industry. *The International Journal of Advanced Manufacturing Technology*, 112:1409–1436, 2021.

[122] Abdelkader Bouti and Daoud Ait Kadi. A state-of-the-art review of fmea/fmeca. *International Journal of reliability, quality and safety engineering*, 1(04):515–543, 1994.

[123] JFW Peeters, Rob JI Basten, and Tiedo Tinga. Improving failure analysis efficiency by combining fta and fmea in a recursive manner. *Reliability engineering & system safety*, 172:36–44, 2018.

[124] Christian Spreafico, Davide Russo, and Caterina Rizzi. A state-of-the-art review of fmea/fmeca including patents. *computer science review*, 25:19–28, 2017.

[125] Alessandro Brun and Matteo Mario Savino. Assessing risk through composite fmea with pairwise matrix and markov chains. *International Journal of Quality & Reliability Management*, 35(9):1709–1733, 2018.

[126] Shubharthi Barua, Xiaodan Gao, Hans Pasman, and M Sam Mannan. Bayesian network based dynamic operational risk assessment. *Journal of Loss Prevention in the Process Industries*, 41:399–410, 2016.

[127] Raziyeh Farmani, Hans Jørgen Henriksen, Dragan Savic, and David Butler. An evolutionary bayesian belief network methodology for participatory decision making under uncertainty: An application to groundwater management. *Integrated environmental assessment and management*, 8(3):456–461, 2012.

[128] Gang Liang and Bin Yu. Maximum pseudo likelihood estimation in network tomography. *IEEE Transactions on Signal Processing*, 51(8):2043–2053, 2003.

[129] I Ben Brahim, Sid-Ali Addouche, A El Mhamedi, and Y Boujelbene. Build a bayesian network from fmeca in the production of automotive parts: diagnosis and prediction. *IFAC-PapersOnLine*, 52(13):2572–2577, 2019.

[130] Pushparenu Bhattacharjee, Vidyut Dey, and UK Mandal. Risk assessment by failure mode and effects analysis (fmea) using an interval number based logistic regression model. *Safety Science*, 132:104967, 2020.

[131] Zhiwei Ji, Qibiao Xia, and Guanmin Meng. A review of parameter learning methods in bayesian network. In *Advanced Intelligent Computing Theories and Applications: 11th International Conference, ICIC 2015, Fuzhou, China, August 20-23, 2015. Proceedings, Part III 11*, pages 3–12. Springer, 2015.

[132] Matthias Niermann, Alexander Beckendorff, Martin Kaltschmitt, and Klaus Bonhoff. Liquid organic hydrogen carrier (lohc)–assessment based on chemical and economic properties. *International Journal of Hydrogen Energy*, 44(13):6631–6654, 2019.

[133] Purna Chandra Rao and Minyoung Yoon. Potential liquid-organic hydrogen carrier (lohc) systems: A review on recent progress. *Energies*, 13(22):6040, 2020.

[134] Muhammad Haris Hamayun, Ibrahim M Maafa, Murid Hussain, and Rabya Aslam. Simulation study to investigate the effects of operational conditions on methylcyclohexane dehydrogenation for hydrogen production. *Energies*, 13(1):206, 2020.

[135] Yasushi Sekine and Takuma Higo. Recent trends on the dehydrogenation catalysis of liquid organic hydrogen carrier (lohc): a review. *Topics in Catalysis*, 64(7-8):470–480, 2021.

[136] Ágnes Bárkányi, Bálint Levente Tarcsay, László Lovas, Tamás Mérő, Tibor Chován, and Attila Egedy. Future of hydrogen economy: simulation-based comparison of lohc systems. *Clean Technologies and Environmental Policy*, 26(5):1521–1536, 2024.

[137] Bálint Levente Tarcsay, Janka Bobek-Nagy, and Attila Egedy. Experimental and modeling based dead-volume detection for externally stirred tanks. *Chemical Engineering Communications*, 209(6):1–15, 2022.

[138] Bálint Levente Tarcsay, Ágnes Bárkányi, János Tibor Chován, and Sándor Németh. Development of compartment models for diagnostic purposes. *Hungarian Journal of Industry and Chemistry*, 49(1):47–58, 2021.

[139] Bálint Levente Tarcsay, Sándor Németh, Tibor Chován, and Ágnes Bárkányi. Development of cfd based compartment models for analysing high risk processes. *Chemical Engineering Transactions*, 91:487–492, 2022.

[140] Maciej Patan and Dariusz Uciński. Optimal activation strategy of discrete scanning sensors for fault detection in distributed-parameter systems. *IFAC Proceedings Volumes*, 38(1):209–214, 2005.

[141] Amir Baniamerian and Khashayar Khorasani. Fault detection and isolation of dissipative parabolic pdes: Finite-dimensional geometric approach. In *2012 American Control Conference (ACC)*, pages 5894–5899. IEEE, 2012.

[142] Michael A Demetriou. A model-based fault detection and diagnosis scheme for distributed parameter systems: A learning systems approach. *ESAIM: Control, Optimisation and Calculus of Variations*, 7:43–67, 2002.

[143] Satadru Dey, Hector E Perez, and Scott J Moura. Robust fault detection of a class of uncertain linear parabolic pdes. *Automatica*, 107:502–510, 2019.

[144] HA Preisig and DWT Rippin. Theory and application of the modulating function method—i. review and theory of the method and theory of the spline-type modulating functions. *Computers & chemical engineering*, 17(1):1–16, 1993.

[145] F Fischer and J Deutscher. Algebraic fault detection and isolation for parabolic distributed–parameter systems using modulation functions. *IFAC-PapersOnLine*, 49(8):162–167, 2016.

[146] F Fischer and J Deutscher. Fault detection for parabolic systems with distributed inputs and outputs using the modulation function approach. *IFAC-PapersOnLine*, 50(1):6774–6779, 2017.

[147] Yun Feng and Han-Xiong Li. Detection and spatial identification of fault for parabolic distributed parameter systems. *IEEE Transactions on Industrial Electronics*, 66(9):7300–7309, 2018.

[148] Zhao-Dong Luo and Han-Xiong Li. Dynamic partial-least-squares-based fault detection for nonlinear distributed parameter systems. *IEEE Transactions on Instrumentation and Measurement*, 73:1–9, 2024.

[149] Maciej Patan and Dariusz Uciński. Configuring a sensor network for fault detection in distributed parameter systems. *International Journal of Applied Mathematics and Computer Science*, 18(4):513–524, 2008.

[150] Maciej Patan and Krzysztof Patan. Optimal observation strategies for model-based fault detection in distributed systems. *International Journal of Control*, 78(18):1497–1510, 2005.

[151] Maciej Patan. A parallel sensor scheduling technique for fault detection in distributed parameter systems. In *Euro-Par 2008–Parallel Processing: 14th International Euro-Par Conference, Las Palmas de Gran Canaria, Spain, August 26-29, 2008. Proceedings 14*, pages 833–843. Springer, 2008.

[152] Thu Hang Vu and Andrew J Deeks. Use of higher-order shape functions in the scaled boundary finite element method. *International Journal for Numerical Methods in Engineering*, 65(10):1714–1733, 2006.

[153] M Ragheb. Computational fluid dynamics. *mragheb Website, Available Online at https://mragheb. com/NPRE*, 20475, 1976.

[154] Muhammad Mubashir Bhatti, M Marin, Ahmed Zeeshan, and Sara I Abdelsalam. Recent trends in computational fluid dynamics. *Frontiers in Physics*, 8:593111, 2020.

[155] Fabrizio Bezzo and Sandro Macchietto. A general methodology for hybrid multizonal/cfd models: Part ii. automatic zoning. *Computers & chemical engineering*, 28(4):513–525, 2004.

[156] Radojka M Savic, Daniël M Jonker, Thomas Kerbusch, and Mats O Karlsson. Implementation of a transit compartment model for describing drug absorption in pharmacokinetic studies. *Journal of pharmacokinetics and pharmacodynamics*, 34:711–726, 2007.

[157] Attila Egedy, Tamás Varga, and Tibor Chován. Compartment model structure identification with qualitative methods for a stirred vessel. *Mathematical and Computer Modelling of Dynamical Systems*, 19(2):115–132, 2013.

[158] Octave Levenspiel. *Chemical reaction engineering*. John wiley & sons, 1998.

[159] Angélique Delafosse, Marie-Laure Collignon, Sébastien Calvo, Frank Delvigne, Michel Crine, Philippe Thonart, and Dominique Toye. Cfd-based compartment model for description of mixing in bioreactors. *Chemical Engineering Science*, 106:76–85, 2014.

[160] Szabolcs Fogarasi, Attila Egedy, Florica Imre-Lucaci, Tamás Varga, and Tibor Chován. Hybrid cfd-compartment approach for modelling and optimisation of a leaching reactor. In *Computer Aided Chemical Engineering*, volume 33, pages 1255–1260. Elsevier, 2014.

[161] Tannaz Tajsoleiman, Robert Spann, Christian Bach, Krist V Gernaey, Jakob Kjøbsted Huusom, and Ulrich Krühne. A cfd based automatic method for compartment model development. *Computers & Chemical Engineering*, 123:236–245, 2019.

[162] Anders Nørregaard, Christian Bach, Ulrich Krühne, Ulrik Borgbjerg, and Krist V Gernaey. Hypothesis-driven compartment model for stirred bioreactors utilizing computational fluid dynamics and multiple ph sensors. *Chemical Engineering Journal*, 356:161–169, 2019.

[163] Dragan Kukolj. Design of adaptive takagi–sugeno–kang fuzzy models. *Applied Soft Computing*, 2(2):89–103, 2002.

[164] Ludmila I Kuncheva. How good are fuzzy if-then classifiers? *IEEE Transactions on Systems, Man, and Cybernetics, Part B (Cybernetics)*, 30(4):501–509, 2000.

[165] Oscar Cordón, Maria José Del Jesus, and Francisco Herrera. A proposal on reasoning methods in fuzzy rule-based classification systems. *International Journal of Approximate Reasoning*, 20(1):21–45, 1999.

[166] Derek G Leaist. The effects of aggregation, counterion binding, and added nacl on diffusion of aqueous methylene blue. *Canadian journal of chemistry*, 66(9):2452–2457, 1988.

[167] Yupeng Li, Weihua Cao, Wenkai Hu, Ying Xiong, and Min Wu. Incipient fault detection for geological drilling processes using multivariate generalized gaussian distributions and kullback–leibler divergence. *Control Engineering Practice*, 117:104937, 2021.

[168] Luis Cuadros-Rodríguez, Estefanía Pérez-Castaño, and Cristina Ruiz-Samblás. Quality performance metrics in multivariate classification methods for qualitative analysis. *TrAC Trends in Analytical Chemistry*, 80:612–624, 2016.